A COMPACT HIGH GAIN DUAL-BAND ANTENNA ARRAY FOR WLAN APPLICATIONS

by

Vian Reynders

Submitted in partial fulfilment of the requirements for the degree
Master of Engineering (Electronic Engineering)

in the

Department of Electrical, Electronic and Computer Engineering
Faculty of Engineering, Built Environment and Information Technology

UNIVERSITY OF PRETORIA

May 2019

SUMMARY

A COMPACT HIGH GAIN DUAL-BAND ANTENNA ARRAY FOR WLAN APPLICATIONS

by

Vian Reynders

Supervisor: Prof. J. Joubert

Co-supervisor: Prof. J. W. Odendaal

Department: Electrical, Electronic and Computer Engineering

University: University of Pretoria

Degree: Master of Engineering (Electronic Engineering)

Keywords: Dual-band, directional antenna, dipole antenna, frequency ratio, wireless local area network (WLAN), radio frequency (RF), mutual coupling.

The continuously growing number of wireless devices and the demand for wireless local area network (WLAN) coverage received a lot of research and design attention during the past decade. The WLAN application is a popular dual-band IEEE standard, which operates in two distinct bands with a large centre frequency ratio. This dissertation presents the design and performance of a compact, high gain, dual-band and directional antenna array meant to be used for such applications. The low band, as stated by the IEEE 802.11b standard, covers the frequency range of 2.400 GHz to 2.484 GHz, and the high band is defined by IEEE 802.11a and starts at 5.150 GHz and stops at 5.850 GHz. The frequency ratio between the centres of the two bands is 2.25:1 and is considered a large ratio.

The antenna array design is based on an existing dual-band antenna configuration. A parametric study was conducted on the antenna configuration features to obtain a detailed understanding of the antenna performance changes in relation to the physical parameters.

The original design was modified to obtain a new sub-array design which can be used in an array for higher gain performance.

The sub-array antenna element consists of one capacitively loaded dipole for the lower 2.4 GHz band and four smaller rectangular dipoles for the high 5.5 GHz band. The low band dipole is fed with a microstrip line whereas the four high band dipoles are fed with a slot line. Four of these sub-array antenna elements are configured into an array for increased gain performance. The final gain of the antenna array was measured as 12 dBi at the 2.4 GHz band and 16 dBi at the 5.5 GHz band. The radiation patterns of both the low and high bands have side lobes 10 dB below the main lobe and front to back lobe ratios of at least 17 dB. The volume of the final antenna is $128 \times 128 \times 12$ mm^3 and is compact compared to other dual-band antenna arrays.

This dissertation is dedicated to my mother and father,
thank you for your love and belief,
with love.

To my beautiful wife,
I am grateful for your support,
"All my love is yours, all my time is ours
All my reckless dreams and all my restless hours",
with all my love.

LIST OF ABBREVIATIONS

CAD	Computer-Aided Design
CCLL	Complementary Capacitively Loaded Loop
CPW	Coplanar waveguide
CRR	Closed Ring Resonator
IEEE	Institute of Electrical and Electronic Engineering
MoM	Method of Moments
RF	Radio Frequency
SRE	Slot Radiating Element
SRR	Split Ring Resonator
TEM	Transverse Electro-Magnetic
VSWR	Voltage Standing Wave Ratio
WiMAX	Worldwide Interoperability for Microwave Access
WLAN	Wireless Local Area Network

TABLE OF CONTENTS

CHAPTER 1 INTRODUCTION

1.1 PROBLEM STATEMENT

1.1.1 The context of the problem

A dual-band antenna is a practical approach to accommodate for the increasing number of users and devices utilising the popular Wireless Local Area Network (WLAN) application. The WLAN application is defined by the IEEE standards 802.11a/b, where IEEE 802.11b specifies the 2.4 GHz band (2.400 to 2.484 GHz) and IEEE 802.11a the 5.5 GHz band (5.150 to 5.850 GHz), as well as the data rates in the two bands [1]. The bandwidth is defined as the frequency range where the reflection coefficient is below -10 dB. The required WLAN bandwidths can be expressed as percentages, where the low band require a 3% bandwidth and the high band a 13% bandwidth. One possible advantage of a dual-band antenna is that when one band experiences an interference the additional band may function normally. The dual-band antenna also allows for complementary functionality and can deal with downlink and uplink of data simultaneously [2].

Typical patch and dipole antennas are single band antennas with less than 5% bandwidth, low gain, and do not use the occupied volume effectively [3]. A variety of printed patch and dipole antenna configurations have been presented in the open literature to either increase the antenna bandwidth or to introduce a second frequency band, e.g.; patch antennas with slot arrangements [4], stacked patch antenna assemblies [5] and capacitive feeding configurations [6].

Various dual-band antenna configurations are presented in the literature that is suited for the WLAN application. The patch antenna configuration requires a modification to the typical patch to create a second band. The dual-band property can be introduced with a U-shaped slot in the patch [4], with shorted slots in the patch [7] or with unusual layups and feeding techniques [8, 9].

The dual-band slot radiating element (SRE) in [10] has high gain in the two bands where a microstrip line is used to feed the slot and the complimentary microstrip stub. The complexity of the SRE structure is increased with the termination of the microstrip line. An eleven-slot antenna consists of two rectangular parallel slots [11]. The eleven-slot configuration complexity is increased with a shorting wall to terminate the inverted face. Compared to dual-band dipole antenna configurations, the dual-band slot antennas have more complex structures.

The dual-band split ring resonating (SRR) antenna [12, 13] and closed ring resonating (CRR) antenna [14, 15] has a very narrow low band and an omnidirectional radiation pattern. The very narrow bandwidth at the lower frequency can make the manufacturing of the antenna expensive as high tolerances and skilled technicians are required to manufacture the antenna. The omnidirectional radiation property of the SRR antenna and CRR antenna cannot be directly compared to a directional antenna gain, so this antenna cannot be used for high gain applications.

The dual-band monopole and dipole antennas without a ground plane has an omnidirectional radiation pattern [16]. The directional dual-band dipole arrays presented in [17] and [18] has high gain compared to the occupied volume of the antenna array. The dual-band dipole configuration presented in [18] is identified as a configuration with potential to be expanded into an array for increased gain.

The printed antenna array configuration of this dissertation is a dual-band dipole design that operates with a large frequency ratio that is suitable for WLAN applications. The two main design characteristics are listed below:

- The configuration is compact in size – the size of the low band radiator is reduced with the use of capacitive loading arms at the low band dipole ends. The sub-array element is a compact array of one low band dipole and four high band dipoles.
- The gain of the antenna is increased by arranging the sub-array elements in an array. The designed sub-array element enables the sub-array to be used in an array with adequate suppression of grating lobes in the high band.

1.1.2 Research gap

The identified research gap is a design solution for a compact, high gain, dual-band and directional antenna where the dual-band feature is within the large frequency ratio ($f_{c2}/f_{c1} > 1.5$). Such a design is presented in this dissertation, for WLAN applications, where the frequency ratio of the two band centres is 2.25. The final antenna array occupies a compact volume of 128 × 128 × 12 mm^3 and achieves a high gain of 12 dBi and 16 dBi at the two respective IEEE 802.11a/b WLAN frequency bands. The combination of the dual-band sub-array elements in an array with high gain in both bands that utilises a total of four low band and sixteen high band dipoles is the contribution of this dissertation. This antenna also has relatively simple structure with an easy to implement feed network and only one input/output connector.

1.2 RESEARCH OBJECTIVE

The research objective is to design a dual-band antenna array. The antenna array should be compact with high gain and it should easy to manufacture. The antenna sub-array should be directional as this design will be implemented as an array of such elements for wall mounted WLAN applications.

1.3 APPROACH

A literature study was first conducted on dual-band antennas. The literature study confirmed that the dual-band property of an antenna can either be achieved with an element that resonates at two distinct frequency bands or a network of single band antennas [18]. As part of the literature study dual-band patch, slot, ring and dipole antennas are compared to each other with specific attention to the gain, complexity and volume of the antennas. A dual-band dipole antenna configuration [18] with the potential to be modified and expanded for use as a high gain antenna array was identified from this literature study.

The different building blocks and relevant parameters of the dipole antenna configuration in [18] were investigated. The identified building blocks are the dipole radiators, the microstrip line, the slot transmission line and the microstrip line to slot line transition. Some array design considerations were also investigated. A parametric study was performed to obtain a better understanding of the various design parameters and their effect on the performance of the antenna.

The dipole antenna configuration in [18] was then modified by adding two more high band elements to the configuration resulting in a new sub-array of one low band and four high band elements. The intention was to use four elements of this sub-array in a larger array to improve the gain. The addition of extra elements would help to suppress grating lobes in the high band as the elements are stacked closer to each other in the array. A feed network was designed to feed the four sub-array elements in the array with equal magnitude and phase over the wide bandwidth.

The sub-array element with the desired dual-band performance was modelled in a simulation environment. Four sub-array elements were arranged in a square 2 × 2 array, and the design was finalized with a full electromagnetic simulation and optimization that includes the feed network. The simulated compact, high gain, dual-band antenna was

manufactured and measured in a compact antenna range. The simulated and measured antenna array results were compared to confirm the validity of the design.

1.4 RESEARCH GOALS

The research goal for this dissertation is to design a compact, high gain and dual-band antenna array; (i) The antenna should be a dual-band antenna for WLAN applications, (ii) the antenna should be compact with a small volume to gain ratio, (iii) the antenna should have higher gain in both bands when compared to dual-band antennas of similar size, and (iv) the antenna should have a simple feeding technique to reduce the complexity of the antenna.

1.5 RESEARCH CONTRIBUTION

The research contribution of the research presented in this dissertation is the design and validation of a compact, high gain and dual-band antenna array for WLAN applications. The array design is kept compact with capacitively loaded low band dipoles in the sub-array elements. Good gain and radiation pattern performance of the array in the high band is achieved by using four high band elements per sub-array.

1.6 OVERVIEW OF STUDY

The layout of the dissertation is as follows;

- Chapter 2 contains the literature study and a summarized comparison of various dual-band antennas. A specific dual-band antenna configuration is identified as an antenna with the potential to be expanded in an array for increased gain performance. Background on the basic building blocks of this identified antenna is also presented in this chapter.
- In Chapter 3 simulation results of the identified antenna element are presented to confirm the published results for this antenna. The important dimensional parameters

of the antenna element are used in a parametric study and a design example is presented to confirm the conclusions made from the parametric study. The antenna element is modified with two additional high band elements to enable the antenna to be arranged in an array. The array spacing of the high band elements are optimised with a spacing experiment to obtain the maximum gain in an array with side lobe levels 10 dB below the main beam magnitude in both the E- and H-planes. The high band elements are also substituted with ports to perform an S-parameter simulation to investigate whether the slot transmission line feed network perform as expected. Finally, the improved sub-array element is assembled in a 2 × 2 array and the simulated results are discussed.

- Chapter 4 contains an experimental verification of the 2 × 2 array. The antenna was manufactured and measured in a compact antenna range at the University of Pretoria. A comparison between the simulated and measured results is presented and discussed.
- In Chapter 5 the performance of the new antenna array design is summarised and some conclusions drawn on the research presented in this dissertation. Potential future research is also identified.

CHAPTER 2 LITERATURE STUDY AND BACKGROUND

2.1 CHAPTER OBJECTIVES

Wireless Local Area Network (WLAN) applications require dual-band antennas, the design of which can be a challenge for antenna designers. Various antenna designs can be considered for these dual-band applications, such as patch, slot, dipole and ring configurations. Printed antenna configurations are compared to each other in terms of size, radiation performance and complexity. An antenna configuration is identified from the comparison study as a potential element that can be used in an array of elements to achieve higher gain. A background study is presented on the building blocks of the identified antenna configuration. The building blocks are the planar dipole antenna, microstrip transmission line, slot transmission line and microstrip line to slot line transition. Array spacing is also important to consider for the suppression of grating lobes.

2.2 WLAN APPLICATIONS

The widely used technology of wireless internet or network access, better known as WLAN, is a wireless local area network managed by the Institute of Electrical and Electronic Engineering (IEEE). The IEEE specifies the frequency bands and data rates for the WLAN application. The standard is labelled the 802.11x standard, and according to the 802.11a and 802.11b standards, the frequency bands which WLAN utilise is 2.400 – 2.484 GHz and 5.150 -5.825 GHz [1].

The low band is also suited for Bluetooth which operate from 2.400 – 2.483 GHz. Bluetooth is a low range low energy technology that is used in many mobile devices [19]. Included in the high-frequency band is the high operating band of Worldwide Interoperability for Microwave Access (WiMAX) at 5.200 – 5.800 GHz utilising the IEEE standard 802.16.

2.3 DUAL-BAND ANTENNAS

The dual-band property of an antenna design can either be achieved with an element that resonates at two distinct frequency bands, or a network of single frequency antennas [1]. A dual-band antenna design can also be categorised into two categories, either a small frequency ratio design ($f_2/f_1 < 1.5$) or a large frequency ratio design ($f_2/f_1 > 1.5$), where f_1 and f_2 are the centre frequencies of the low and high bands respectively. Depending if a large or small ratio is required, the design approach can be somewhat different [5]. The antennas focused on in this literature study are dual-band antennas that operate with a large frequency ratio, specifically dual-band WLAN antennas and dual-band antennas with a similar frequency ratio.

2.3.1 Dual-band patch antennas

Patch antennas typically have a narrow frequency band (<5%) and a low gain (6 dBi) [20]. The standard patch is resonant when the patch length is close to half a wavelength of the excitation frequency. The patch has a pair of opposite radiating edges and a pair of non-radiating edges; the radiating edges are perpendicular to the E-plane. The radiating edges are responsible for the linear polarisation property of the patch antenna. The fields at the pair of radiating edges are of opposite polarity because of the half wavelength characteristic of the patch antenna [3].

The use of a variety of shapes of slots on the patch has been introduced to increase the operating bandwidth of the patch antenna [21, 22]. One such a slot is the U-shaped slot cut in the patch that has been used to increase the frequency bandwidth to as high as 30% for

an air-substrate with a thickness of $0.08\lambda_0$, and more than 20% for material substrates [4]. The U-shaped slot has a capacitive reactance component to help improve the input impedance of the antenna to increase the antenna bandwidth. The U-shaped slot can initiate a second resonant frequency, and a third resonant frequency is also possible by adding a second slot in the patch [4].

The U-shaped slot dual-band patch antenna design can be approached using two methods for the large frequency ratio design. One approach for the large frequency ratio design is to define the total length of the slot to be half wavelength of the desired high band frequency resonant [4]. A somewhat different, but beneficial approach for the large frequency ratio would be to look at the U-shaped slot as a patch on its own inside the slot boundaries. The smaller patch is designed to resonate at the high band frequency, and finally, the width of the slot and the position of the feed is used to improve the matching at the high band for a wider bandwidth [5]. Using this approach, a frequency ratio of 2.2 was obtained with suitable bandwidths, acceptable radiation patterns and gains larger than 6 dBi. At ratios larger the 2.2, the radiation pattern of the high band tends to become unusable as low band higher order modes may be introduced, affecting the high band radiation pattern, resulting in squint. Squint in a dual-band antenna is an undesirable property as the antenna cannot be directed or aligned effectively.

Another patch antenna configuration that consists of shorted slots and an asymmetric coplanar feed network is proposed in [23]. The antenna gain in the low and high bands are 5.1 and 5.5 dBi respectively, and the antenna occupies a volume of $50 \times 70 \times 8$ mm^3. The antenna has the advantage of similar gain levels in the two operating bands.

Other patch antennas that operate with a large frequency ratio typically have a complicated feeding technique, low to medium gain (5 to 7 dBi) or they are larger in size than other dual-band patch antennas [24].

2.3.2 Dual-band slot antennas

The slot radiating element (SRE) presented in [10] is a high gain directional antenna with a measured gain of 9.2 and 10.1 dBi in the respective WLAN bands, and with an simple feeding technique. A microstrip line is used to feed the slot on the bottom of the substrate with a complimentary microstrip stub that is used to couple to the slot. This microstrip line is terminated with a matched load to the ground plane that increases the complexity of the SRE antenna manufacturing. The antenna occupies a volume of 96 × 73 × 14 mm^3. Another dual-band slot antenna, the T-slot antenna proposed in [25], has less than 2 dBi gain, but a compact structure of 50 × 20 × 10 mm^3 that would be ideal for indoor and home WLAN applications.

The eleven-slot antenna with two rectangular parallel slots has a complex structure since a shorting wall is required to terminate the inverted face [11]. The eleven-slot structure, with dimensions 43 × 38 × 4.5 mm^3 has low gain and not enough bandwidth at the 5.5 GHz WLAN resonance. The front to back lobe ratio of the antenna presented in [11] is only 7 dB at the 2.45 GHz resonance, most probably because of the small ground plane that was used.

2.3.3 Dual-band ring antennas

The split ring resonating (SRR) antenna and closed ring resonating (CRR) antenna typically has a very narrow lower band and struggles to operate with the large frequency ratio applications [12, 13]. The SRR antenna also has an omnidirectional radiation pattern so the ring antenna size cannot directly be compared to the above mentioned dual-band antennas. There are cases where the antenna designers achieved the large frequency ratio between the two bands [14, 15]. The gain and size of these antennas [14, 15] are not directly comparable to the previously discussed patch and slot antennas as these antennas do not have ground planes and are omnidirectional.

The antenna presented in [13] consists of four concentric ring structures where three of the rings are SRR and the fourth a CRR. The outer CRR is responsible for the narrow low band at 2.89 GHz, and the inner SRR rings responsible for the three higher bands at 3.61 GHz, 5.29 GHz and 6.51 GHz. The large frequency ratio between the highest and lowest bands has potential for WLAN applications as the ratio can be scaled down for. The very narrow low band can make the manufacturing of the antenna difficult as it would have to be built within fine tolerances to resonate at the desired frequencies. Another ring antenna consisting of three rings, two inner SRRs and a CRR [15], are combined with two monopoles to improve the low band bandwidth. This antenna can potentially be designed to function for indoor WLAN applications because of the radiation performance and low gain.

2.3.4 Dual-band monopole and dipole antennas

A temple tower Kalasam shaped monopole antenna is presented in [26]. The monopole is fed with a coplanar waveguide (CPW) with two vertical slots connected to the CPWs ground. The vertical slots introduce the second resonance to make the antenna a dual-band antenna. The frequency ratio of the proposed antenna is 2 and could probably be extended to 2.25 by decreasing the size of the vertical slots. The antenna has a low gain of 3 dBi at the lower 5 GHz resonance and a gain of 5 dBi at 10 GHz.

A planar triple-band dipole antenna makes use of complementary capacitively loaded loop (CCLL) slots on a wideband bowtie structure to initiate a second and third band [16]. A microstrip to coplanar stripline balun is used to feed the dipole element for improved bandwidth matching over the wide band. The CCLL slots are like the U-shaped slot commonly found on a wide band or dual-band patch antenna, implying or characterising the smaller high band antennas. The design also has an omnidirectional radiation pattern with high gain of 4 dBi for an omnidirectional pattern, at the high 5.5 GHz band. The physical size of the antenna is significantly increased by the balun feed technique that is crucial for the improved bandwidth matching.

A directional bowtie dipole antenna is an example of a dual-band single element antenna, and in this case, the bowtie is loaded with a square loop for dual-band performance [27]. The loaded dipole antenna and wideband balun operate with a large frequency ratio. The balun transforms from microstrip to parallel strip line, allowing the 2.6 – 6.3 GHz and 9.4 – 12.7 GHz bands. The gain of the low band is a constant 7 dBi where the gain increases to 11.5 dBi at the high band. Once again, the balun increases the volume of the antenna, thus illustrating that the wideband performance comes at the price of a physical size of 50 × 50 × 10 mm^3 that is large at these high frequencies.

A somewhat different but effective method to design a dual-band antenna is to use a network to feed two single resonant frequency elements. For the antenna presented in [1], the designer uses the feed network to phase shift the one polarisation with 90º to enable circular polarisation for the antenna array. The dual-band antenna consists of two single resonant frequency elements. The low band is a printed rhombus shaped dipole and the high band a printed rectangular dipole element. The feed network and circular polarization property significantly increases the volume of the antenna array and for an antenna volume of 148 × 148 × 101 mm^3 higher gain for a directional antenna would be expected as the gain at the low 2.4 GHz band is 4 dBi and the gain at the high 5.5 GHz band peaks at 6.5 dBi. The feed network with single resonant frequency elements can without difficulty be used to obtain the desired frequency ratio; one of the more challenging design aspects involve making the feed network wide band.

A low profile directional dual-band array consisting of 16 (4 × 4) low band and 64 (8 × 8) high band dipole elements has high gain, 24 dBi and 18 dBi respectively, is presented in [17]. The array has good radiation patterns as the feed network is weighted for side-lobe suppression. The array of so many elements becomes large (280 × 280 × 12 mm^3) and the structure of the antenna is quite complicated as it consists of 6 layers with probe radiators at different levels of the structure.

The compact directional antenna in [18] is a planar dual-band antenna that contains one low band and two high band dipoles for WLAN applications. The single frequency dipole

antennas are connected and fed with a microstrip and slot line combination. The low band dipole is fed with an open ended microstrip line that capacitively couples through to the second half of the low band dipole. The microstrip line is also used to create a transition from the microstrip line to a slot line. The slot line is used to feed the two high band dipole antennas. The configuration is placed above a ground plane to produce a directional antenna. The antenna gain is 7.5 dBi at the low 2.4 GHz band and 9.5 dBi at the high 5.5 GHz band. The volume of the antenna is $43 \times 26 \times 12$ mm^3 and is compact for the gain and frequency ratio performance. The top and side views of this antenna is displayed in Figure 2.1 and 2.2 respectively.

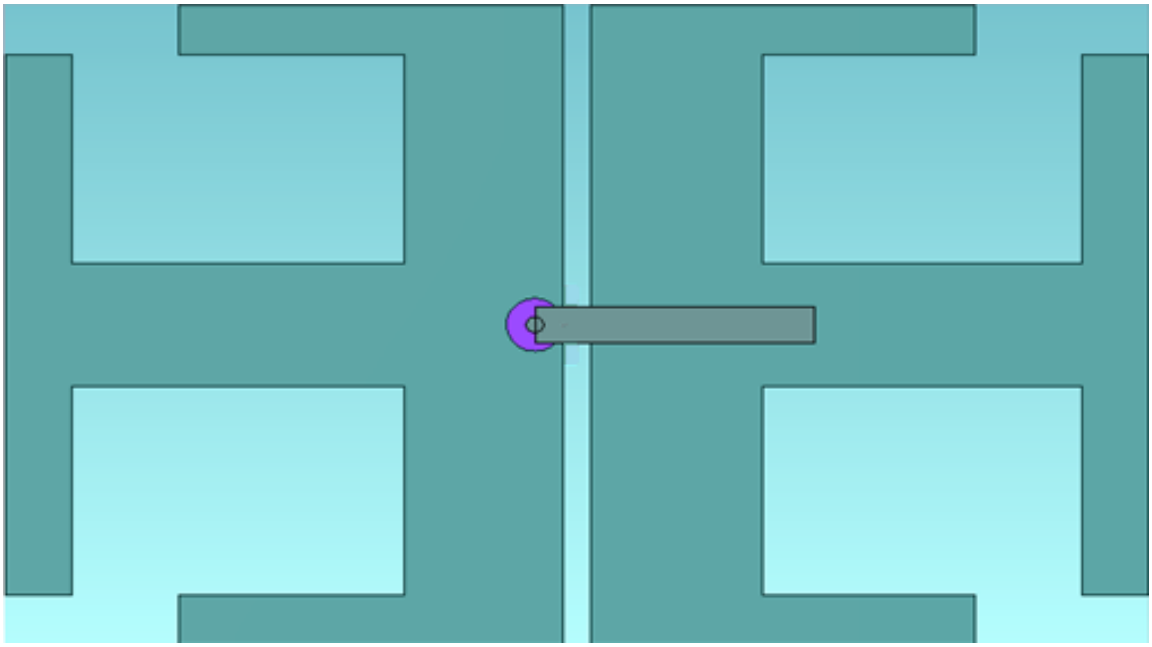

Figure 2.1. Top view of the compact dual-band directional antenna. (Transparent substrate)

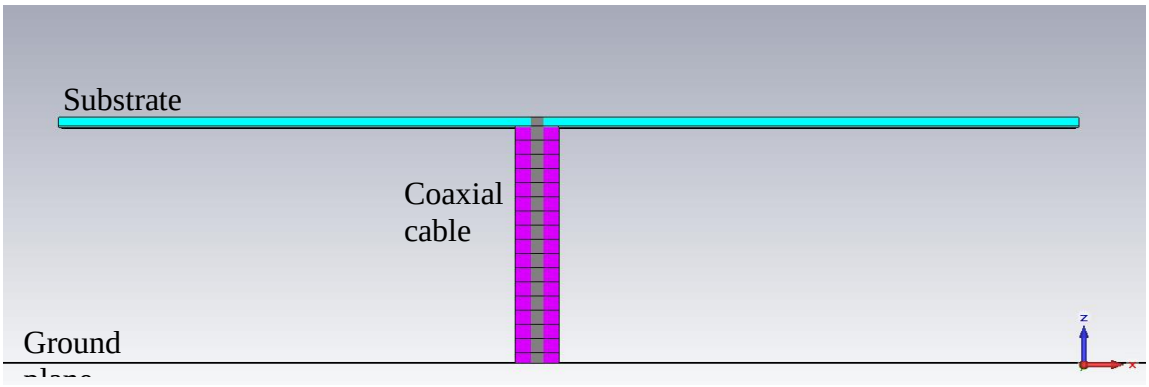

Figure 2.2. Side view of the compact dual-band directional antenna.

2.3.5 Performance comparison of dual-band antennas

Table 2.1 compares the important performance and physical characteristics of the dual-band antennas discussed in this section.

Table 2.1. Performance comparison of antennas discussed in section 2.2.

Ref	Frequency band (GHz)			Gain (dBi)		Volume (mm^3)
	Low band	High band	f_2/f_1	Low band	High band	$L \times W \times H$
Patch antennas						
[21]	2.37 – 2.53	3.6 – 3.7	1.50	8.4	4.4	38 ×38 × 4.5
[23]	2.4 – 2.5	5.15 – 5.85	2.25	5.1	5.5	53 × 49 × 11
[24]	2.4 - 2.5	5.15 – 5.85	2.25	3.5	8.2	Not available
Slot antennas						
[10]	2.4 – 2.5	5.15 – 5.85	2.25	9.2	10.1	96 × 73 × 14
[25]	2.4 – 2.5	5.15 – 5.85	2.25	0.5	1.8	50 × 20 ×10
[11]	2.4 – 2.5	5.25 – 5.8	2.25	3	5	42 × 38 × 4.5
Ring antennas						
[14]	2.7 – 2.9	5.1 – 6.8	2.13	1.2	1.5	27 × 26 × 1.6

[15]	1.3 – 2.3	2.8 – 5.1	2.19	Not available		27 × 32 1.6
Monopole & Dipole antennas						
[16]	2.2 – 2.8	5 – 6	2.20	1.3	4.5	78.5 × 70 × 0.8
[27]	2.7 – 6.3	9.4 – 12.7	2.46	7	11.5	51 × 51 × 18
[1]	2.3 – 2.8	4.3 – 6	2.02	3.5	6	148 × 148 × 101
[17]	2.36 – 2.5	5.1 – 5.9	2.26	24	18	280 × 280 × 12
[18]	2.39 – 2.51	4.4 – 6.5	2.22	7.5	9.5	43 × 26 × 12

The antennas listed in Table 2.1 were all considered in terms of a gain versus volume trade-off, and usability as an element to be utilised in an array configuration. The antennas presented in [10], [17] and [18] has the highest gains in the two frequency bands. The antenna presented in [18] occupies the smallest volume between the three high gain antenna configurations.

The compact planar dipole configuration from [18] is considered the best in terms of volume and gain for dual-band antennas and has the potential to be expanded into an array for increased gain performance in the two bands. A background study was conducted on the building blocks of the antenna configuration in [18]. The antenna configuration building blocks were identified as the dipole radiators, the microstrip line, the slot line, and the microstrip to slot line transition. Another important aspect that was investigated was array spacing.

2.4 BASIC DIPOLE ANTENNA CHARACTERISTICS

The centre fed half-wave dipole antenna commonly consists of a pair of wire conductors and is well known for its omnidirectional radiation pattern with a theoretical maximum gain of 1.64 (2.15 dBi). The far field radiation pattern is generally shaped as a toroid (doughnut) with no power radiated in the direction of the wire ends. The two separate halves of the dipole antenna are quarter wavelengths of the design frequency with opposite

polarities, meaning the dipole has a balanced input. The current distribution of the half-wave dipole antenna is a cosine distribution along the length of the dipole with its maximum in the centre of the dipole and zeros at the wire ends. The dipole antenna has a linear polarisation, with the polarisation parallel with the direction of the dipole wires. The dipole antenna is mainly used in the vertical polarisation position due to its radiation pattern properties [3].

The standard wire dipole antenna is typically a narrow band antenna, but with the use of a variety of different wire thicknesses or printed shapes the bandwidth can be increased or the physical size can be decreased. A printed dipole antenna has the capability for broader bandwidth performance and better surface efficiency than a printed microstrip antenna. An example of an improved bandwidth dipole antenna is a biconical dipole antenna [28]. The bow tie configuration makes use of triangular shaped arms to improve the bandwidth to 37% [28]. The use of matching networks together with the dipole arms has shown to increase the bandwidth performance up to 56% [29].

2.4.1 Dipole in front of a ground plane

A printed dipole antenna on a substrate can be designed to function as a directional antenna by introducing a ground plane underneath the antenna. Different aspects of the printed antenna have been studied, such as the effect of the dielectric constant of the substrate and the spacing between the ground plane and the dipole. Carefully choosing these two characteristics, an impedance bandwidth of 25% was achieved in [30]. The optimum distance between the ground plane and the dipole is a quarter of a wavelength of the design frequency to ensure optimum directivity and positive superposition. By adding such a ground plane the gain is more than doubled to 7.5 dBi as the radiation directions are limited because of the ground plane. The input impedance of a dipole in front of a perfect electrical conducting (PEC) ground plane is affected by the presence of the ground plane. The method of images can be used to explain this occurrence [31]. Figure 2.3 displays the centre fed dipole antenna parallel to a perfectly conducting infinite ground plane and also the associated image dipole. The dipole antenna parallel to the ground plane and its image

is an odd mode dipole array because the dipole and the image are out of phase. The input impedance of the halfwave dipole change as the dipole interacts with the image (ground plane).

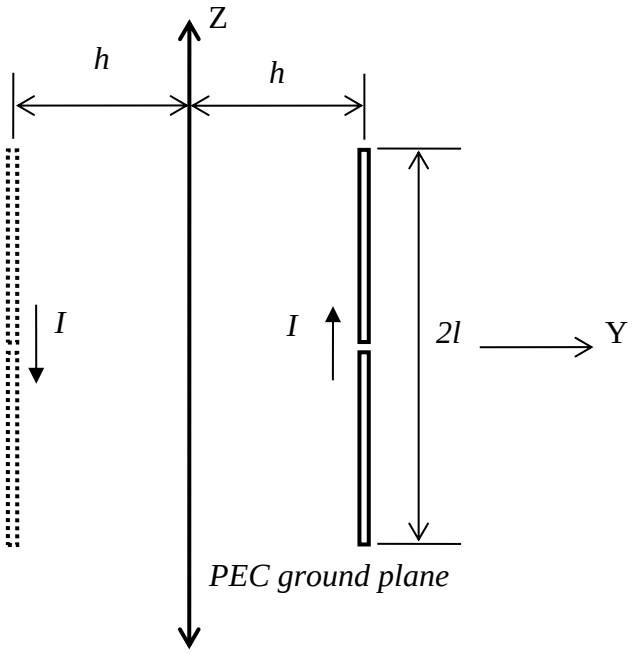

Figure 2.3. Dipole and image of dipole on either side of the infinite PEC ground plane.

The odd mode two element input impedance of the dipole array (dipole and image) is $Z_{11} - Z_{12}$. The mutual impedance, Z_{12}, approaches the self-impedance, Z_{11}, as the dipole moves closer to the ground plane. The input impedance is a function of the distance between the dipole and the ground plane and decreases as the dipole moves closer to the ground plane (h decreases). The maximum directivity of the beam is in the direction of Y when $h \leq \lambda_0/4$. The following equation can be used to calculate the directivity for the case where $h \leq \lambda_0/4$ [31];

$$directivity = \frac{4\eta sin^2(2\pi h/\lambda_0)[1 - cos(kl)]^2}{\pi(R_{11} - R_{12})} \tag{2.1}$$

where h is the distance between the dipole and the ground plane, $2l$ the total length of the dipole, and R_{11} and R_{12} the real self- and real mutual impedances of the dipole in front of a ground plane. The phase change constant, k, is defined as radians per unit length ($k =$

$2\pi/\lambda$), and eta (η) as the impedance of free space that is 376.7 Ω. From equation 2.1 the directivity of a halfwave dipole that is $\lambda_0/4$ above a ground plane can be calculated as 7.5 dBi, with the beam peak perpendicular to the ground plane [31].

2.4.2 Capacitively loaded dipole

The capacitive loading of a dipole antenna can be used to decrease the physical length of the dipole antenna. The decreased length can be advantageous to achieve a smaller antenna that resonates at the same frequency. The electrical length of the radiator remains the same and the loading is done with a perpendicular conductor at the dipole arm end. An additional advantage of the capacitive loading is that the configuration has two more parameters that can be used to optimise the dipole for improved bandwidth. Figure 2.4 shows a planar dipole and two capacitively loaded dipole antennas that is designed to resonate at 2 GHz. The reflection coefficients of the three dipole antenna configurations are displayed in Figure 2.5.

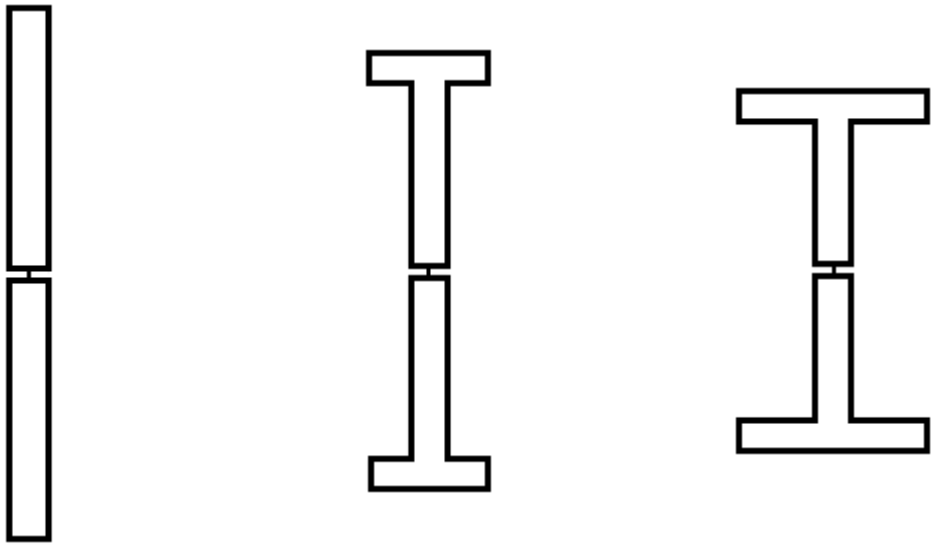

(a) Planar dipole

(b) Planar capacitively loaded dipole

(c) Planar capacitively loaded dipole

Figure 2.4. Three planar dipole configurations.

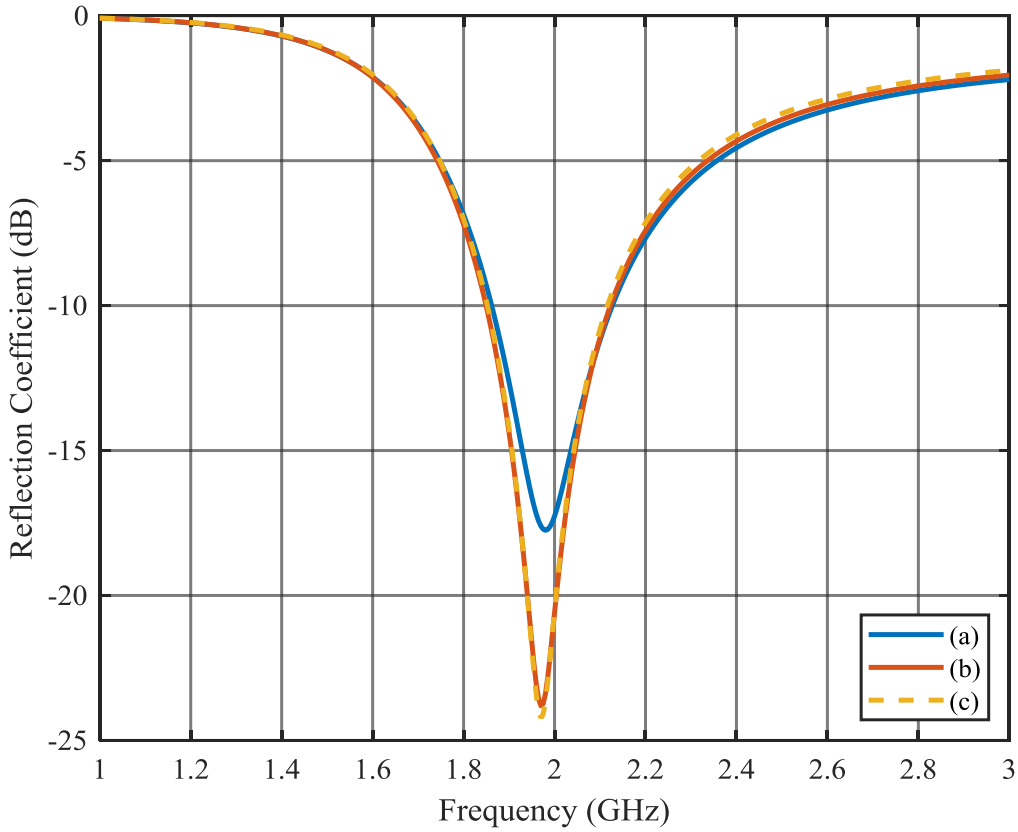

Figure 2.5. Reflection coefficient comparison of the three dipole configurations of Figure 2.4.

The three dipole configurations in Figure 2.4 resonate at 2 GHz. The vertical length of the planar dipole in (a) is 67 mm. The vertical length of the dipole configuration with the shorter capacitive loading arms in (b) is 51 mm and the vertical length of the dipole configuration with the longer capacitive loading arms in (c) is 41 mm. From this example, it is clearly evident that a shorter capacitively loaded dipole can be used to resonate at the design frequency.

2.5 MICROSTRIP TRANSMISSION LINE

The microstrip line is a popular planar transmission line because of the simplicity of the design and implementation. The impedance of the microstrip transmission line is primarily determined from the dielectric constant of the substrate, the thickness of the substrate and the strip line width. The dielectric constant of the substrate and the substrate thickness are

usually fixed design parameters, so the width of the strip line can then be used as the primary design parameter to realise required microstrip line impedances. The substrate holds most of the field lines between the strip conductor and the ground plane and cannot support a pure transverse electro-magnetic (TEM) wave. The mode of transmission in microstrip lines are quasi TEM transmission [3]. The characteristic impedance of the microstrip line can be calculated as

$$Z_0 = \begin{cases} \frac{60}{\sqrt{\epsilon_e}} ln\left(\frac{8d}{W} + \frac{W}{4d}\right), & \text{for } W/d \leq 1 \\ \frac{120\pi}{\sqrt{\epsilon_e}[W/d + 1.393 + 0.667ln(W/d + 1.444)]}, & \text{for } W/d \geq 1 \end{cases} \quad (2.2)$$

where W is the strip width, d the substrate thickness and ϵ_e the effective dielectric constant. The effective dielectric constant is defined as

$$\epsilon_e = \frac{\epsilon_r + 1}{2} + \frac{\epsilon_r - 1}{2}\left[\frac{1}{\sqrt{1 + 12\left(\frac{d}{W}\right)}} + 0.04\left(1 - \left(\frac{W}{d}\right)\right)^2\right] \quad (2.3)$$

where ϵ_r is the dielectric constant of the substrate.

The microstrip line in the dipole configuration from [18] has two functions. In the low band the microstrip line is used to feed the low band dipole via proximity coupling, and in the high band a microstrip to slot line transition is used to feed the high band dipoles.

2.6 SLOT TRANSMISSION LINE

A slot transmission line consists of a thin slot in a planar conductor. The slot line has electric fields extending across the slot and the magnetic fields perpendicular to the slot line. The wavelength of the slot line is shorter than the same frequency free space wavelength as the dielectric substrate with a higher permittivity closely confines the fields

in the substrate. The guide wavelength of the slot line transmission line can be calculated using [3]

$$\frac{\lambda_0}{\lambda_g} = \sqrt{\frac{2}{\epsilon_r + 1}} \tag{2.4}$$

where λ_0 is the is the free space wavelength, λ_g the guide wavelength and ϵ_r the relative permittivity of the substrate. Substrates with a relative permittivity lower than 9.8 are known as low permittivity substrates. The characteristic impedance varies with a change in frequency because of the non TEM nature of the slot line mode [32 - 34]. The following equation can be used to determine the characteristic impedance when $0.0015 \leq w/\lambda_g \leq 0.075$ [34]:

$$\begin{aligned} Z_0 = 60 + 3.69 sin\left[\frac{(\epsilon_r - 2.22)\pi}{2.36}\right] + 133.5 ln(10\epsilon_r)\sqrt{\frac{w}{\lambda_g}} \\ + 2.81[1 - 0.011\epsilon_r(4.48 + ln\epsilon_r)]\left(\frac{w}{d}\right) ln\left(\frac{100d}{\lambda_g}\right) \\ + 131.1(1.028 - ln\epsilon_r)\sqrt{\frac{d}{\lambda_g}} \\ + 12.48(1 + 0.18 ln\epsilon_r)\frac{{}^{w}/_{d}}{\sqrt{\epsilon_r - 2.06 + 0.85\left({}^{w}/_{d}\right)^2}} \end{aligned} \tag{2.5}$$

where *w* is the slot line width and *d* the substrate height.

The characteristic impedance of the slot line against frequency is calculated from equation (2.4) and shown in figure 2.6. The dielectric constant of the substrate used in the equation is 2.2, the slot line width 1 mm, and the substrate height as 0.5 mm.

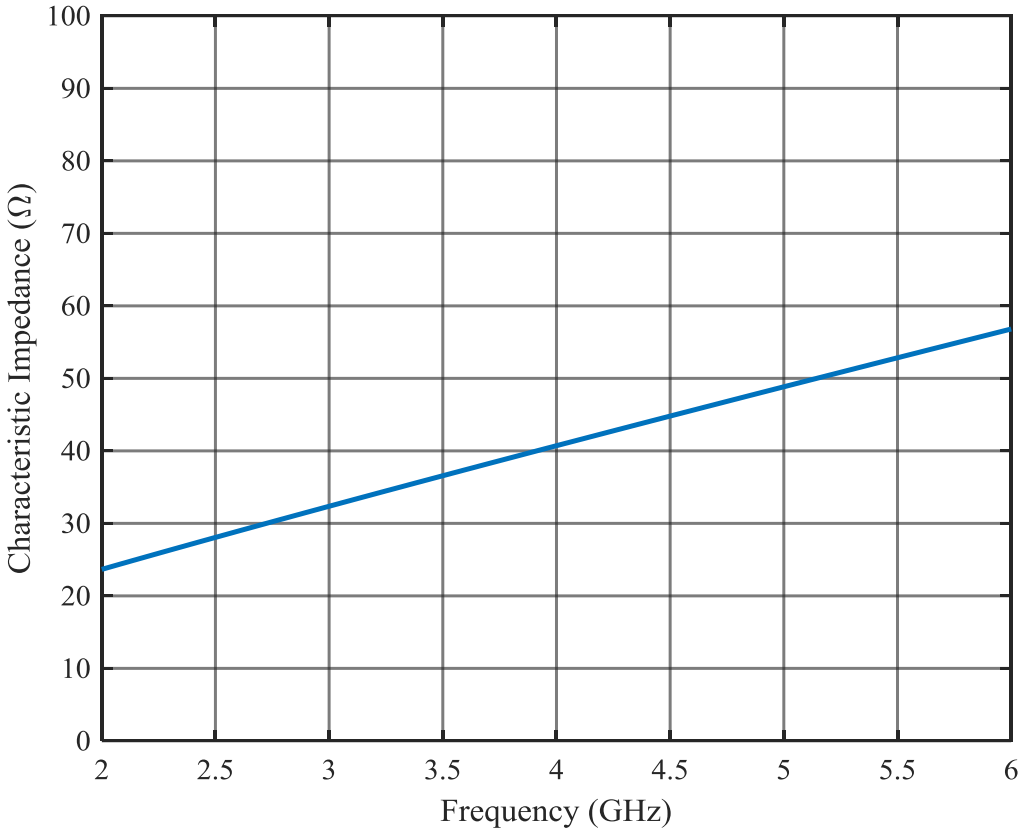

Figure 2.6. The characteristic impedance of the slot line.

From figure 2.6 it is visible that the characteristic impedance of the slot line is matched at the high frequency band for the chosen slot line parameters.

2.7 MICROSTRIP TO SLOT LINE TRANSITION

The microstrip to slot line transition is a popular transition tool used in a range of microwave applications such as filters, mixers, phase shifters and dipole antennas. The microstrip to slot line transition is inherently a broadband transition method where the insertion loss of the transition increases with increasing frequency. The increasing insertion loss is due to the radiation loss of the slot line and the impedance change with the higher frequencies [35].

The dipole configuration from [18] utilises a microstrip line virtual short (with quarter wavelength open microstrip line) to slot line transition. One advantage of this transition type is that the transition offers improved frequency flatness compared to other transition

types. The virtual short with quarter wave open microstrip line of the transition produces a less complex structure as the need for a via to short the microstrip line is removed. The slot line is used to feed the two planar dipoles at the ends of the slot line.

2.8 ANTENNA ARRAY DESIGN CONSIDERATIONS

An antenna array is a combination of multiple antenna elements that are specifically spaced to enhance the radiation performance by increasing the gain and can also be used to suppress grating lobes. The array can consist of similar or different antenna elements. The array gain is increased as the number of elements is increased, which causes a decrease in the main beamwidth making the antenna more directional.

To preserve the radiated power in the boresight direction of the array, thus avoiding grating lobes, the spacing between the elements should be less than one wavelength. The elements in the array experience some impedance characteristic changes because of the physical presence of the adjacent elements and is known as mutual coupling. Mutual coupling excites currents on adjacent elements that affect the element input impedance as well as radiation characteristics. Elements with surface waves such as planar antenna elements are more susceptible to mutual coupling compared to cavity antennas such as horn antennas. The substrate properties, thickness and dielectric constant, can also influence the mutual coupling between adjacent planar elements. A thicker substrate would contain the surface waves more densely compared to a thinner substrate, with the effect of decreased mutual coupling effect. Similar effects would be present for a substrate with a higher dielectric constant. The effects of mutual coupling become stronger as the elements are more closely spaced to each other. The affects that the increased mutual coupling can have are a bandwidth shift or an increased reflection coefficient at the design frequency [31].

2.9 SUMMARY

The literature study on the various dual-band antennas showed that; (i) the dual-band patch antennas has lower gain compared to the other antennas, (ii) dual-band slot antennas have

more complex structures, and (iii) dual-band ring antennas have very narrow impedance bandwidths in the low band and low gain due to their omnidirectional radiation patterns. From the literature study a dual-band dipole configuration [18] was identified as an antenna with the potential for further improvement. Some background was provided on the various building blocks of the identified antenna.

CHAPTER 3 DUAL-BAND ARRAY DESIGN

3.1 CHAPTER OBJECTIVES

In this chapter the identified antenna configuration from [18] is further investigated and expanded to obtain a new sub-array element, which is then used in a 2 × 2 dual-band array. The first investigation is to study the dual-band antenna and use the configuration in a parametric study to determine what parameters are responsible for what performance characteristics. The conclusions from the parametric study are then used in a design example to illustrate a general design approach. The dipole configuration from [18] is then modified to enable the configuration to be incorporated into an array. The spacing of the elements in the array is also considered to obtain desirable radiation patterns and gain. The simulated results of the sub-array element and a 2 × 2 array are also presented in this chapter.

3.2 DUAL-BAND DIPOLE CONFIGURATION

The dual-band antenna from Quan et al. [18] is studied in detail. The results in [18] are reproduced and a parametric study is performed to have a better understanding of the operation of the dual-band antenna. Figure 3.1 shows the top view of the dipole layout which consists of two conducting layers, where the microstrip is the top layer on top of the substrate and the second layer is the two dipole configurations on the bottom of the substrate (the substrate is transparent in Figure 3.1). Figure 3.2 shows the side view of the antenna.

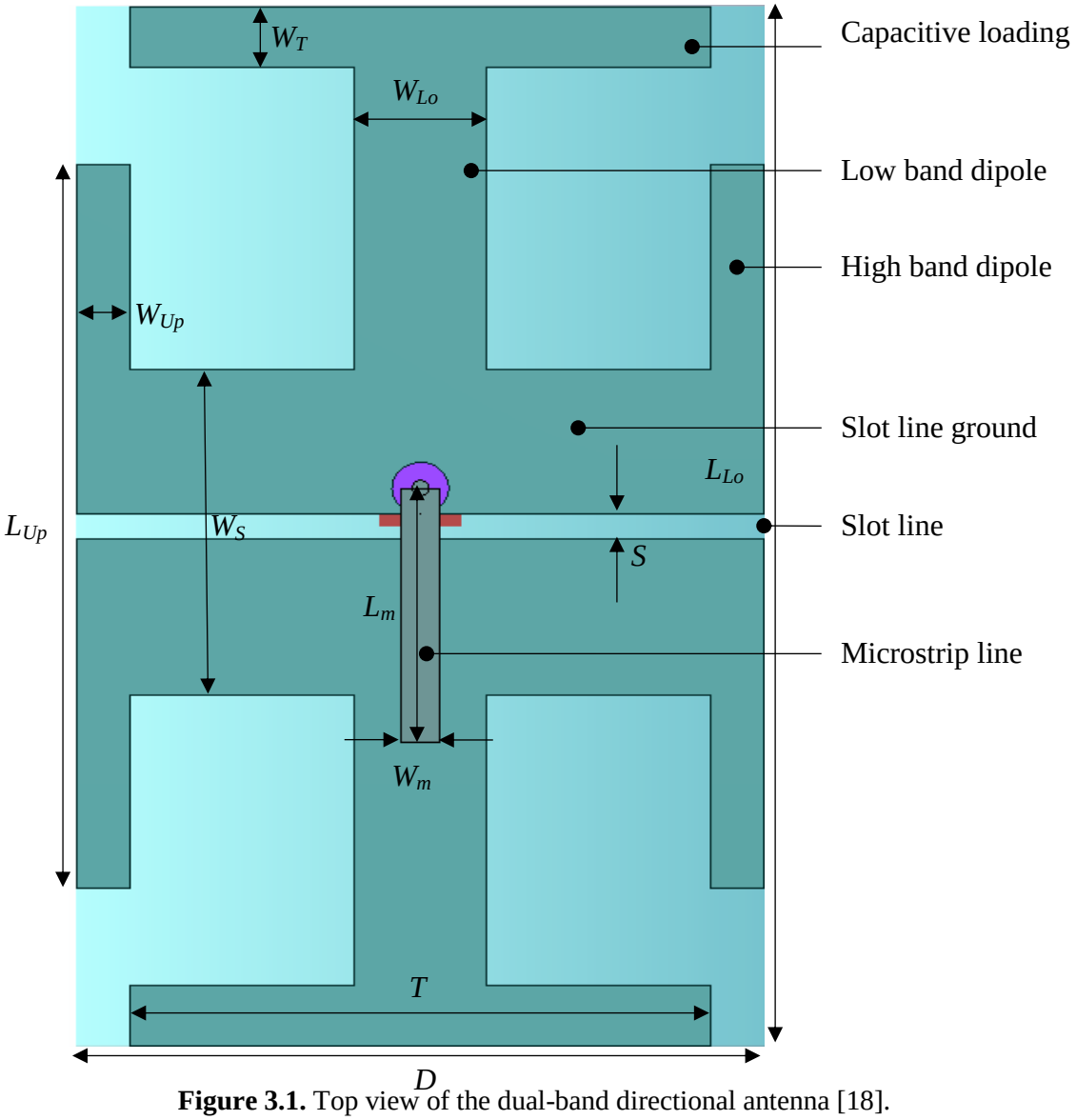

Figure 3.1. Top view of the dual-band directional antenna [18].

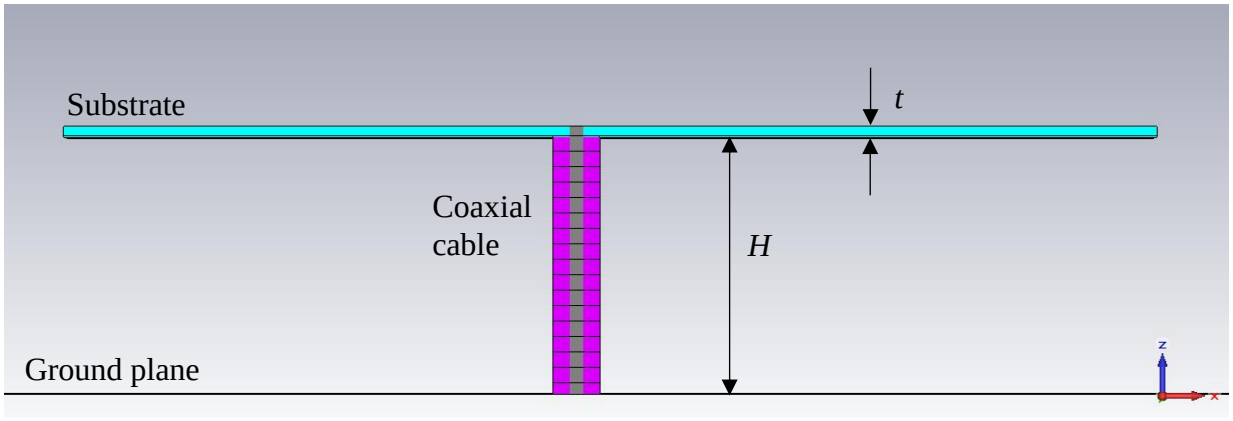

Figure 3.2. Side view of the dual-band directional antenna [18].

Table 3.1. Parameters and dimensions of the original design [18].

Parameter	Dimension	Parameter	Dimension
Length of low band dipole (L_{Lo})	43 mm	Width of slot line ground (W_S)	13 mm
Length of high band dipole (L_{Up})	30 mm	Slot line width (S)	1 mm
Length of the microstrip feed line (L_m)	10.5 mm	Width of the microstrip feed line (W_m)	1.5 mm
Width of the antenna (D)	26 mm	Width of low band dipole (W_{Lo})	5 mm
Capacitive loading parameter (T)	22 mm	Width of high band dipole (W_{Up})	2 mm
Height (H)	12 mm	Capacitive loading width (W_T)	2.5 mm
Thickness of the substrate (t)	0.5 mm		

The compact dual-band antenna consists of a dipole configuration on a substrate and a ground plane. The substrate used is the thin low loss Rogers RT/Duroid 5880 (t = 0.5 mm) with a relative dielectric constant (ϵ_r) of 2.2 and dissipation factor (tan δ) of 0.0009. The dipole configuration is printed on the bottom side of the substrate facing the ground plane. The printed dipole configuration consists of a compact capacitive loaded dipole responsible for the low band and a pair of smaller rectangular dipoles responsible for the high band. On the top face of the substrate, a microstrip line is used to feed the low band

dipole and form part of a microstrip to slot line transition to feed the high band dipole pair. The antenna is fed with a 0.085" (50 Ω) coaxial cable. The ground plane is used as a reflector to make the radiation patterns of the printed dipole design directional.

Figure 3.3 shows the simulated reflection coefficient of the dipole configuration from [18]. Two full-wave electromagnetic software simulators, CST Microwave Studio [36] and Feko [37], were used to simulate the results from [18]. The CST Microwave Studio time domain solver performed the analysis quicker compared to the frequency domain FEKO Method of Moments (MoM) solver. The CST Microwave Studio simulator was used for the majority of simulations in this chapter.

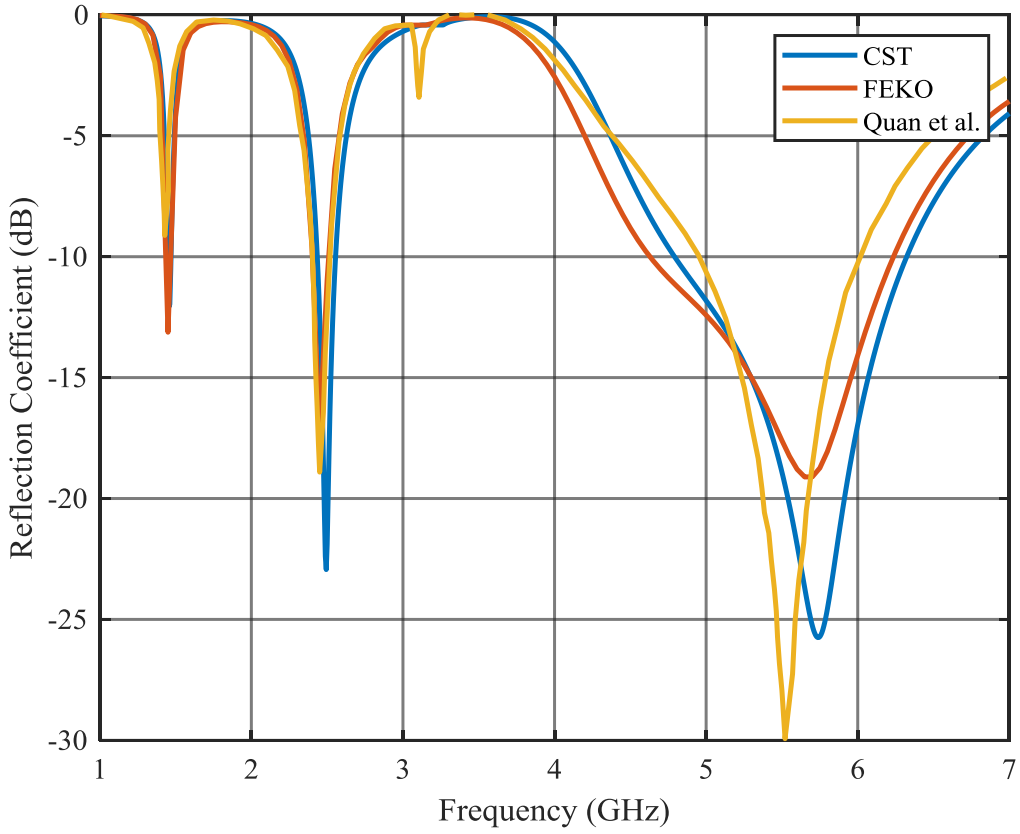

Figure 3.3. The simulated reflection coefficient results of CST Microwave Studio and FEKO.

The results obtained by simulating the dual-band antenna correspond well with the results presented by Quan *et al*. [18] in the low band. The high frequency band simulated by Quan *et al*. is narrow compared to the CST and FEKO results. Minor deviations between the

CST and FEKO results are visible in Figure 3.3 at the high band. The CST result has a lower reflection coefficient level at the two WLAN bands. The dual-band property is visible with a narrow resonance at 2.45 GHz and a broad resonance centred at 5.5 GHz.

The simulated realised gain against frequency is displayed in Figure 3.4. The peak gain of the antenna is simulated as 7.1 dBi in the low band and 9.8 dBi in the high band. The corresponding values as published in [18] are 7.8 dBi and 9.9 dBi. The radiation patterns are presented in Figure 3.5a and b, and Figure 3.6a and b.

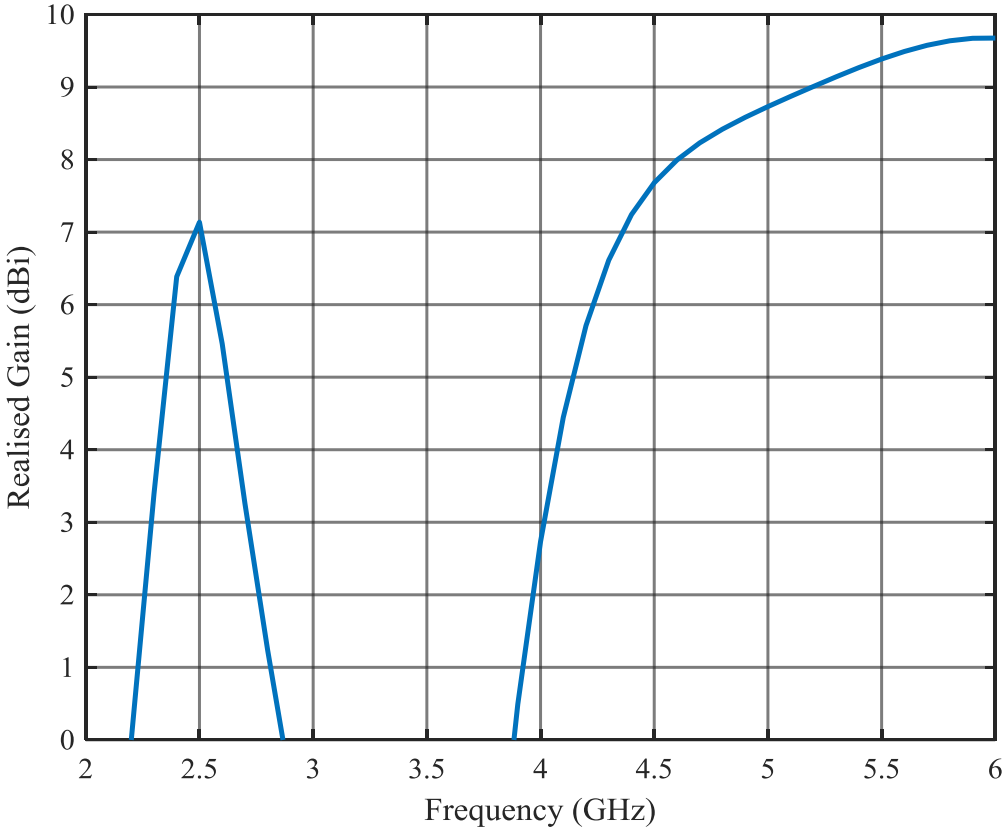

Figure 3.4. The simulated realised boresight gain.

The radiation patterns at the low 2.45 GHz band and high 5.5 GHz band have good radiation performance with the antenna energy directed in the boresight direction.

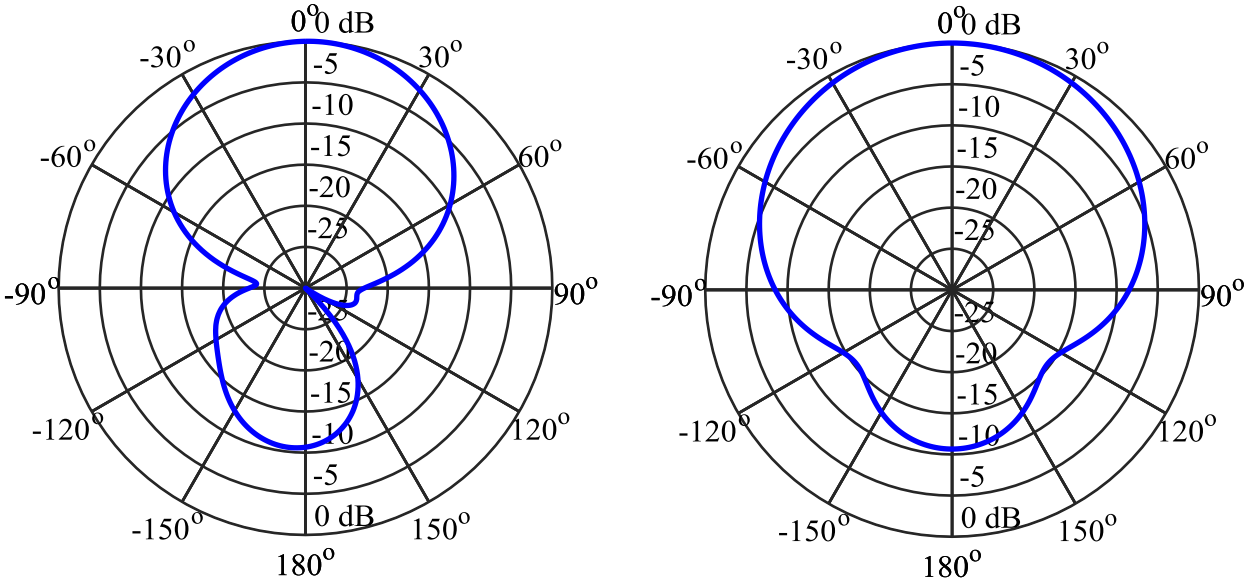

(a) (b)

Figure 3.5. Normalised radiation pattern at 2.45 GHz.

(a) *E*-plane (b) *H*-plane

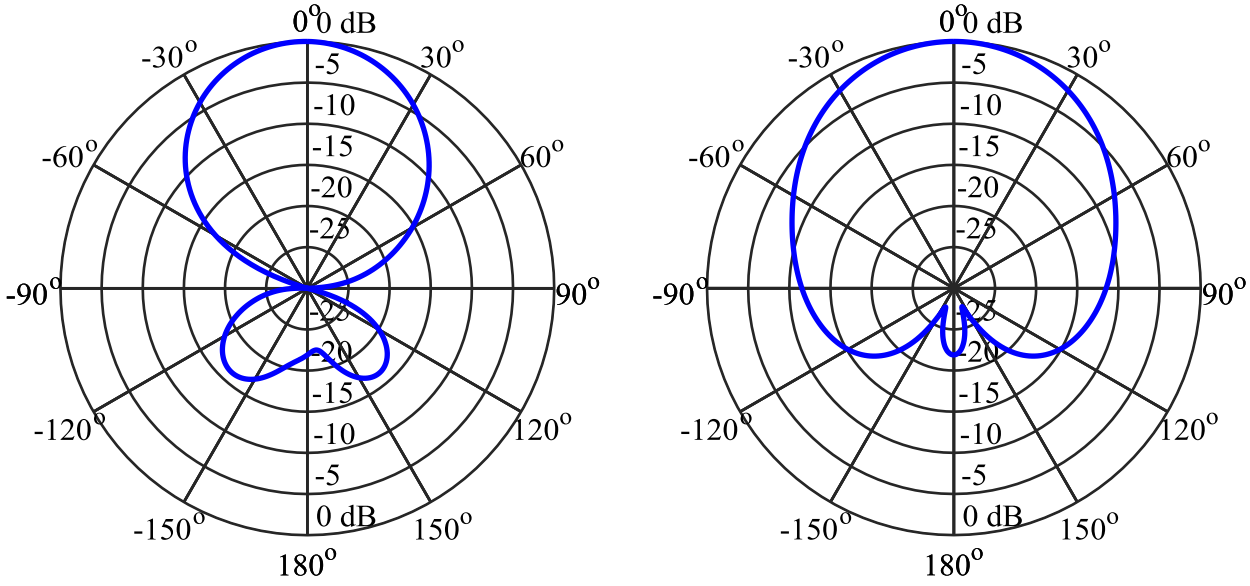

(a) (b)

Figure 3.6. Normalised radiation pattern at 5.5 GHz.

(a) *E*-plane (b) *H*-plane

The simulated results of the printed dipole antenna from [18] indicated a low band centred at 2.48 GHz with a bandwidth of 4.9%, and a high band that is centred at 5.55 GHz with a 27.5% bandwidth. The bandwidth is defined as the frequency range were the reflection coefficient is below -10 dB for the respective band. The radiation pattern performance of the two bands are directional with the peak gain directed in the boresight direction. The simulated frequency ratio is 2.23, and the antenna is suitable as a dual-band WLAN antenna.

3.3 PARAMETRIC STUDY

The goal of the parametric study is to investigate the effects of the important physical parameters of the antenna element. The reflection coefficient of the antenna is evaluated as the dipole configuration is altered and the radiation pattern performance is evaluated as the spacing between the high band elements is changed. The intended outcome is to identify parameters that can be optimised to increase the bandwidth of the antenna configuration and to alter the frequency ratio between the two bands.

The parameters identified to have an influence on the low band performance are the length of the low band dipole, L_{Lo}, the capacitive loading parameter, T, the width of the low band dipole, W_{Lo}, and the length of the microstrip feed line, L_m. The parameters identified as critical for the high band performance are the length of the high band dipole, L_{Up}, the slot line width, S, the width of the antenna, D, and the width of the slot line ground, W_S.

3.3.1 Length of low band dipole (L_{Lo})

The first parameter that is investigated in the parametric study is the length of the large capacitively loaded dipole, parameter L_{Lo} of **Figure 3.1**. The length of the low band dipole is mainly linked to the centre frequency of the low band. Figure 3.7 displays the results of the parameter sweep from 37 mm up to 53 mm. The black dashed line represents the reflection coefficient of the primary design.

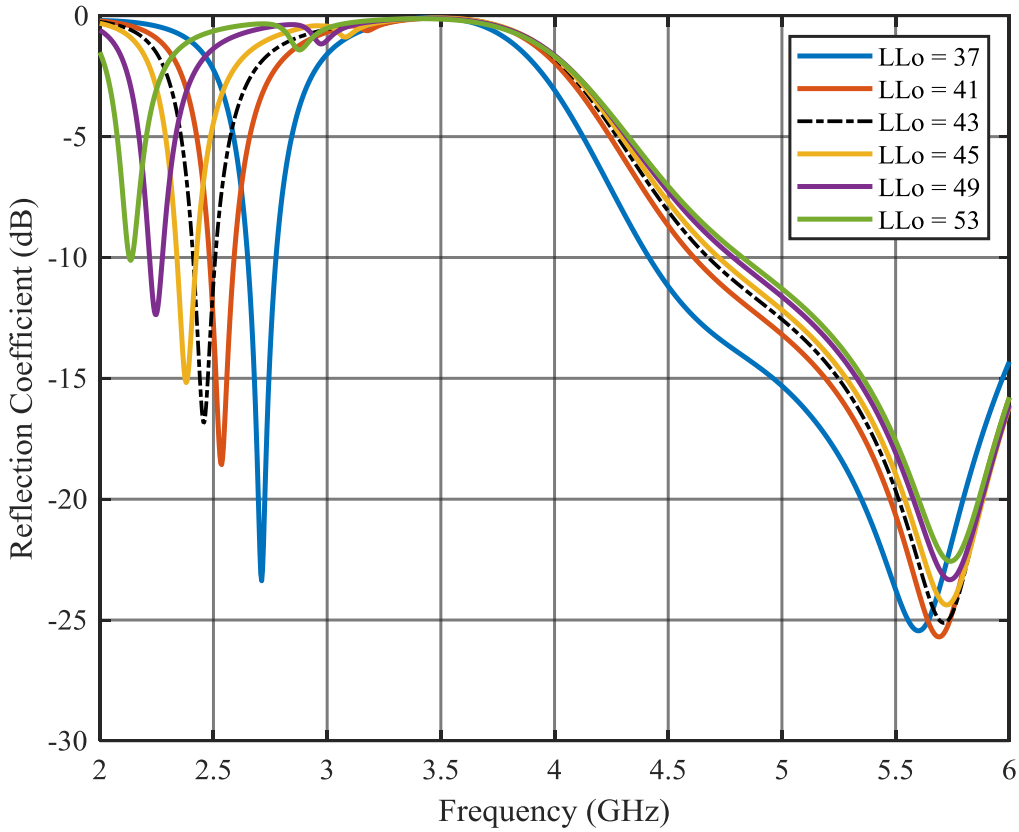

Figure 3.7. Reflection coefficient for different values of the low band dipole length.

The length of the low band dipole is responsible for the resonating frequency of the low band. The best matching of the low band dipole also occurred for the shortest length of the low band dipole.

3.3.2 Length of high band dipole (L_{Up})

The next parameter that is stepped through a range of values is the length of the two high band dipoles, parameter L_{Up}. The two high band dipoles are responsible for the high frequency resonant band. Figure 3.8 displays the reflection coefficient as L_{Up} is stepped from 20 mm to 36 mm. The black dashed line represents the reflection coefficient of the primary design.

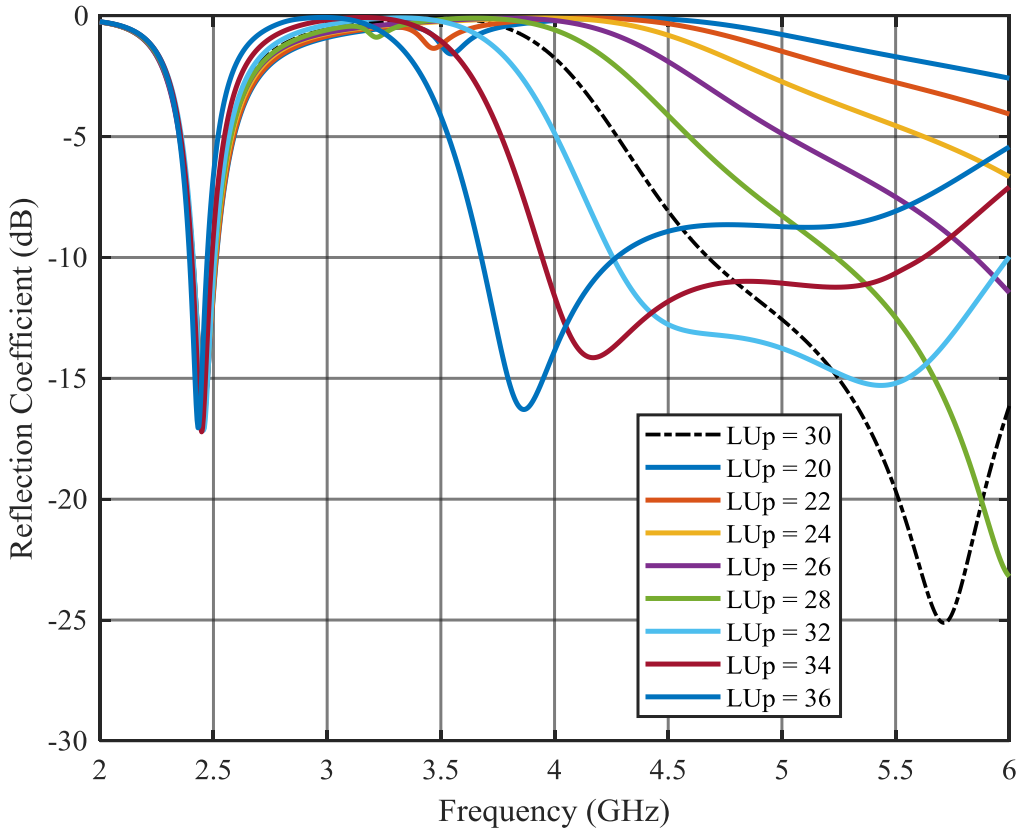

Figure 3.8. Reflection coefficient for different values of the high band dipole length.

The reflection coefficient of the low band remains unchanged for the change of the high band dipole length. The high band resonance changes significantly with the different lengths of the high band dipole pair. The shorter lengths of the high band dipole move the resonance to a higher frequency where the longer high band dipoles resonate at lower frequencies. The length of the high band dipole, L_{Up}, can be used to determine the resonant frequency of the high band.

3.3.3 Length of the microstrip feed line (L_m)

The microstrip feed line is stepped from 8.5 mm up to 12.5 mm. The length of the microstrip line determines the quarter wavelength virtual short frequency for the microstrip line to slot line transition. The reflection coefficient of the stepped microstrip feed line

length is displayed in Figure 3.9. The black dashed line represents the reflection coefficient of the primary design.

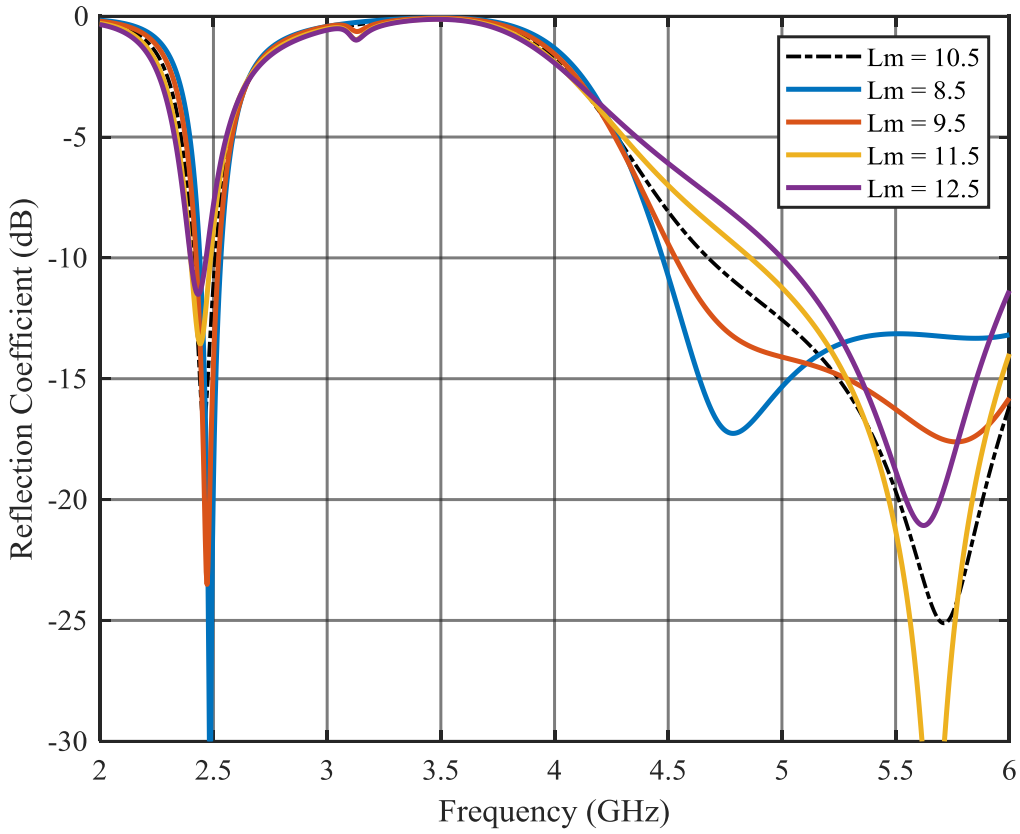

Figure 3.9. Reflection coefficient for different values of the microstrip feed line length.

The microstrip feed line length influences the matching of the high band. The position of the low band can be considered unchanged with the length of the microstrip feed line parameter study. The microstrip feed line length parameter should be optimised to obtain the best matching at both the frequency bands.

3.3.4 Slot line width (*S*)

The slot line width parameter, *S*, is primarily determines the characteristic impedance of the slot line that feeds the high band dipoles. The slot line width is also the feed gap between the low band dipole arms and can also influence the low band performance. Figure 3.10 displays the reflection coefficient as the slot line width is stepped from 0.5 mm

up to 2 mm. The black dashed line represents the reflection coefficient of the primary design.

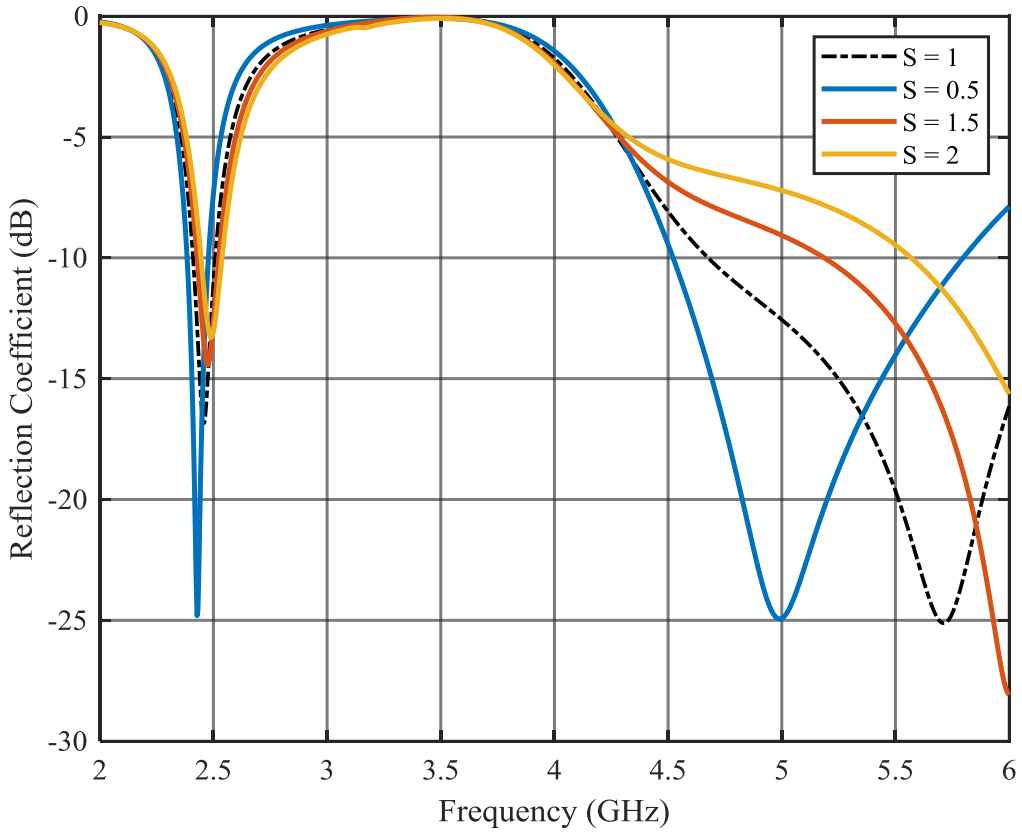

Figure 3.10. Reflection coefficient for different values of the slot line width.

The steps in the width of the slot separating the dipole polarities had a significant influence on the high band as well as the frequency ratio between the two bands. The resonating frequency of the low band remained virtually unchanged. Thus, parameter *S* can be used to alter the resonating high band frequency and the frequency ratio of the design.

3.3.5 The capacitive loading parameter (*T*)

The capacitive loading for the low band dipole is used to keep the design as compact as possible. A basic half wavelength dipole design for 2.5 GHz would mean the antenna should be approximately 60 mm in total length, but the capacitive loading reduces the

overall length to 43 mm. The electrical length of the radiator remains the same and the loading is achieved with a perpendicular conductor at each of the dipole arm ends.

The loading parameter step is expected to influence the low band as the electrical length of the low band dipole is altered. Figure 3.11 illustrates the reflection coefficient changes as the capacitive loading arms are stepped from 4 mm up to 26 mm. The black dashed line represents the reflection coefficient of the primary design.

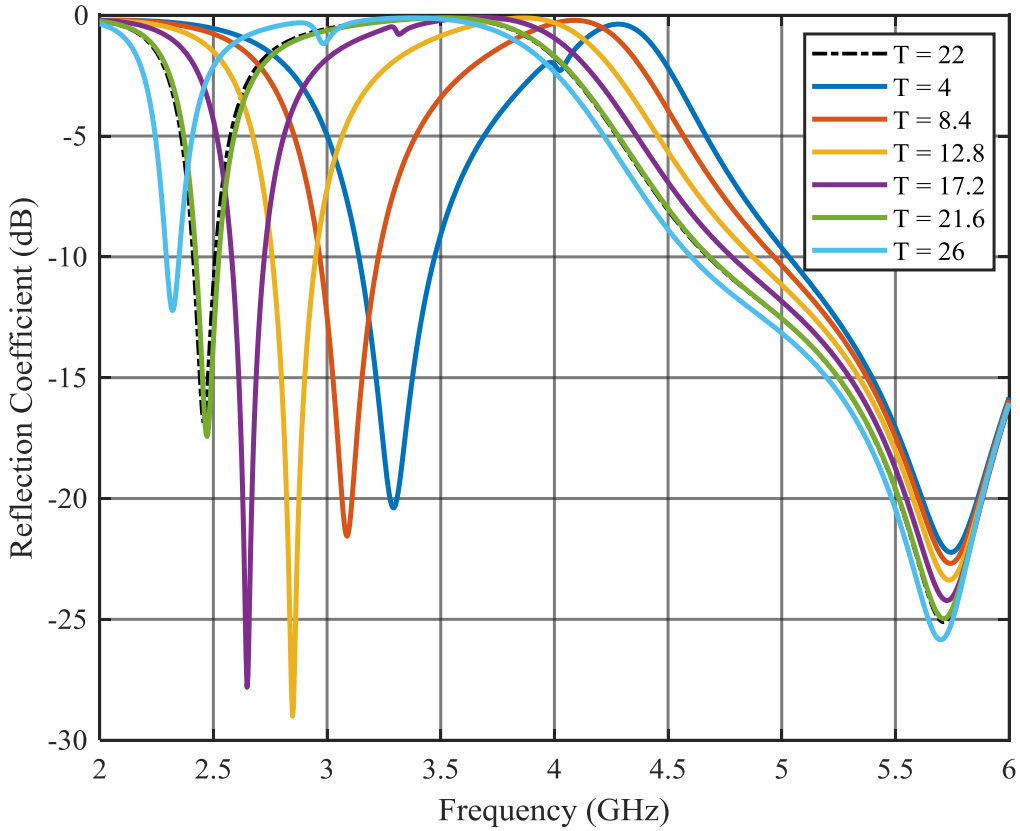

Figure 3.11. Reflection coefficient for different values of the capacitive loading length.

The capacitive loading parameter, *T*, can be used to primarily alter the low band resonant frequency. As T increases the low band centre frequency shifts lower and the bandwidth is reduced. The high band centre frequency is higher for the shorter lengths of the capacitive loading arms.

3.3.6 Width of the antenna (*D*)

The total width of the antenna is stepped from 22 mm to 30 mm, changing the length of the slot line, slot line ground and the spacing between the two high band dipoles. A change in the radiation pattern and the reflection coefficient is expected for the high band. The resulting reflection coefficient results are displayed in Figure 3.12. The radiation patterns are displayed in Figures 3.13 to 3.15.

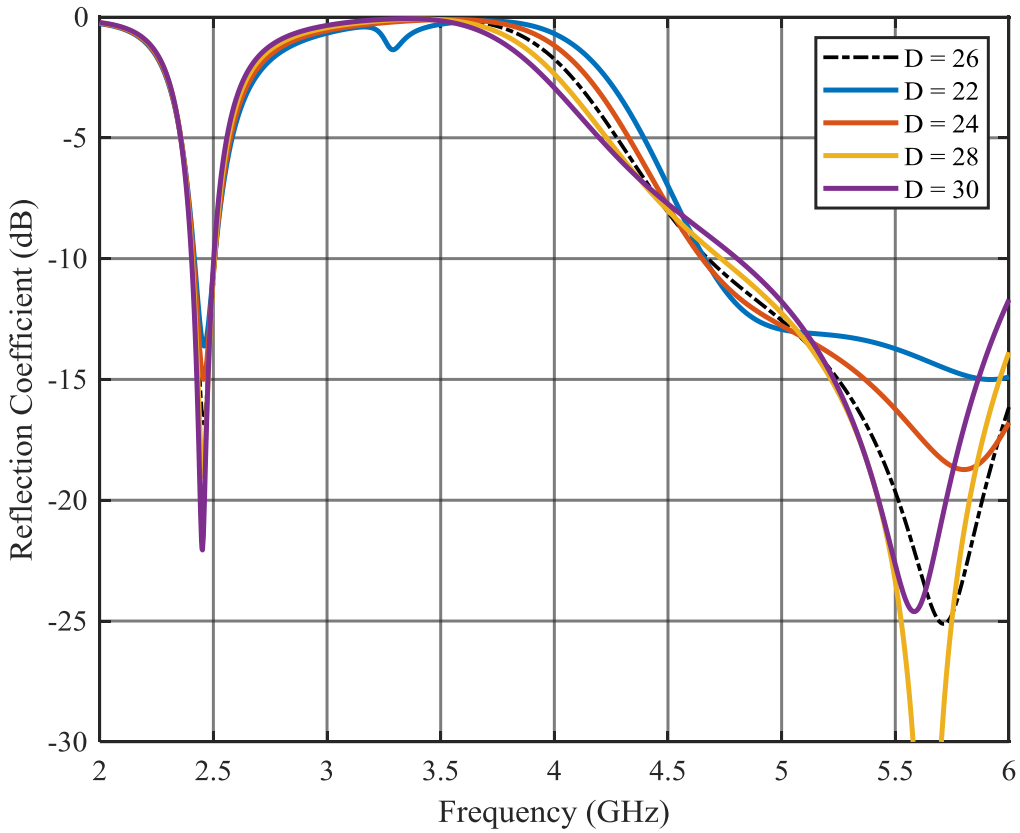

Figure 3.12. Reflection coefficient for different values of the antenna width.

The variation in width of the antenna had an insignificant influence on the bandwidths of the two bands. The changing width, *D*, had a small effect on the *E*-plane of the radiation pattern and more noticeable influence on the *H*-plane radiation patterns as the compact antenna becomes more directional as the parameter *D* is increased. A 1.5 dBi gain increase is observed when the antenna width is changed from 22 mm up to 30 mm.

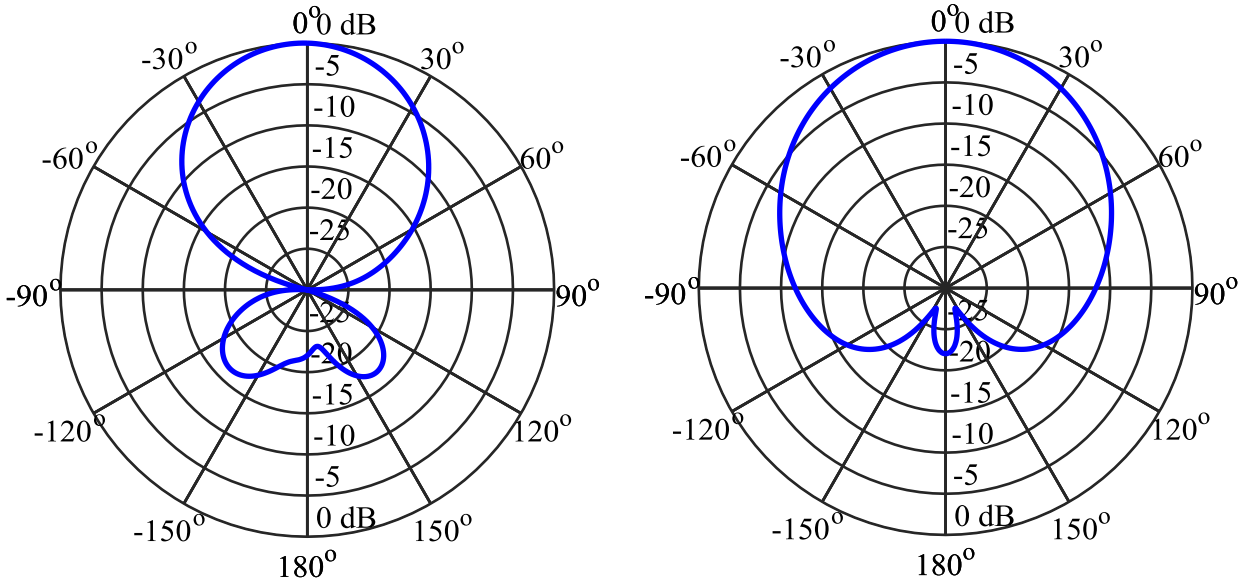

Figure 3.13. Normalised high band radiation pattern as D = 22 mm.

(a) *E*-plane. (b) *H*-plane.

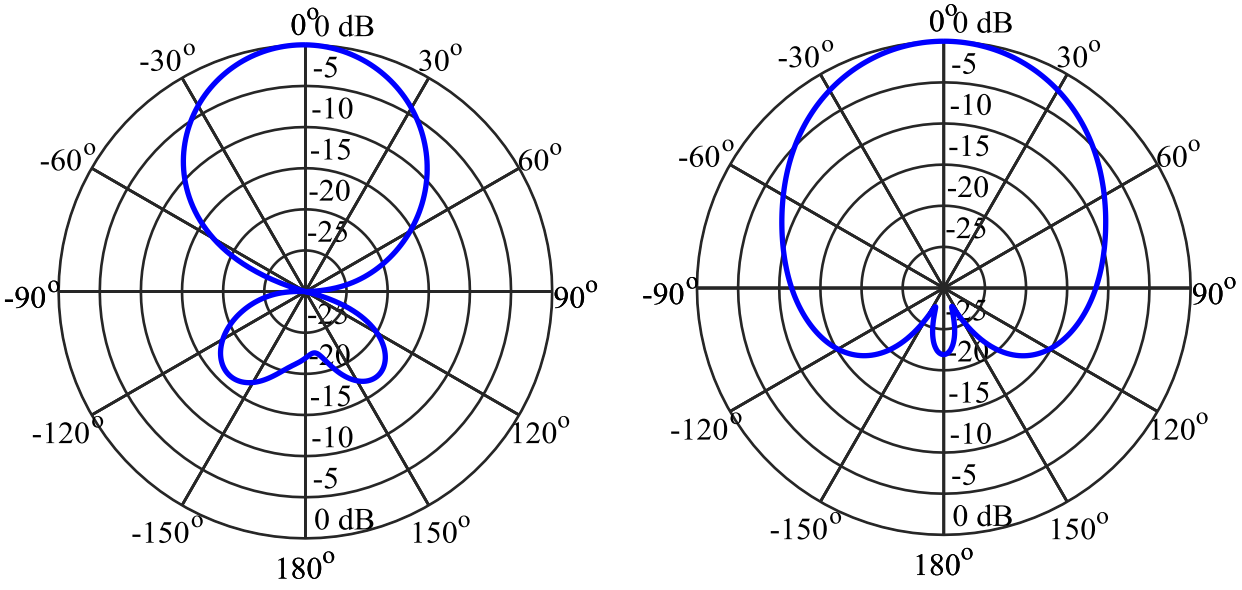

Figure 3.14. Normalised high band radiation pattern as D = 26 mm.

(a) *E*-plane. (b) *H*-plane.

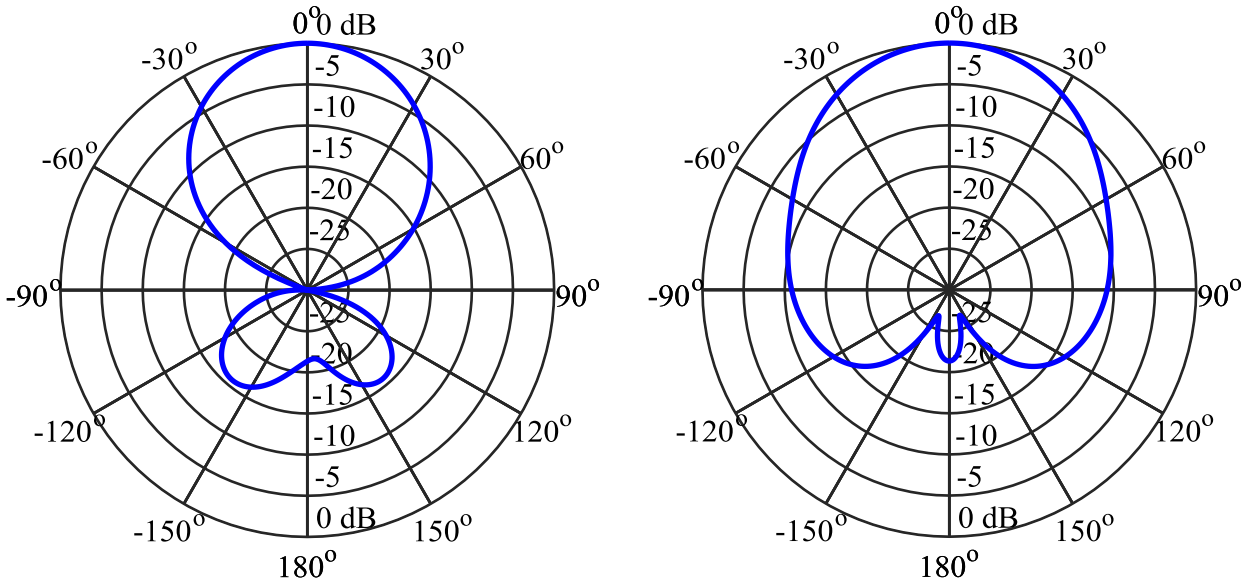

Figure 3.15. Normalised high band radiation pattern as D = 30 mm.

(a) *E*-plane. (b) *H*-plane.

3.3.7 Width of the slot line ground (W_S)

The width of the slot line ground, parameter *Ws*, is stepped from 9 mm up to 17 mm and the results are displayed in Figure 3.16. This parameter changes the width of the slot line ground. The slot line ground width is expected to have a larger influence on the high band performance as the width will influence the slot line impedance that feeds the high band dipoles. The slot line ground width can also influence the low band, as the length of the element is decreased as the ground width is increased. The black dashed line represents the reflection coefficient of the primary design.

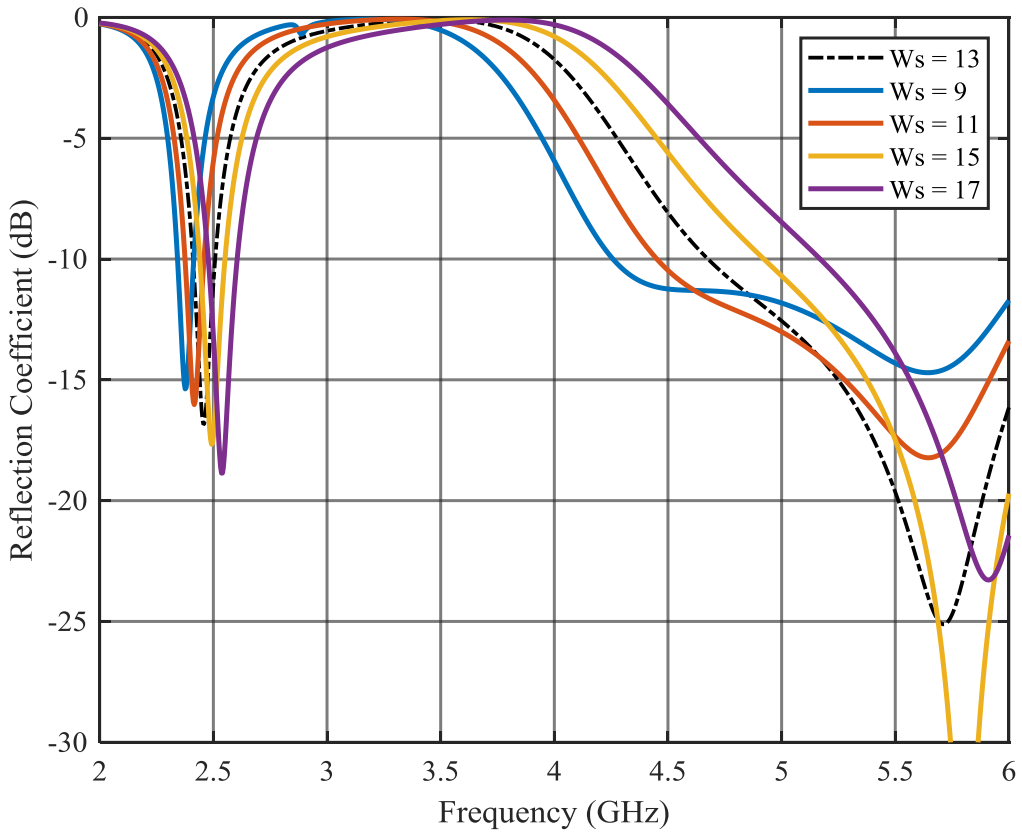

Figure 3.16. Reflection coefficient for different values of the slot line ground width.

This parameter had a more noticeable effect on the high band. The slot line ground width can be used to optimise the bandwidth in the high band, and has a small influence on the low band resonating frequency.

3.3.8 Width of low band dipole (W_{Lo})

The low band dipole width is stepped from 3 mm up to 7 mm. It is anticipated that the low band will be affected to a larger extent than the high band. The reflection coefficient results are displayed in Figure 3.17. The black dashed line represents the reflection coefficient of the primary design.

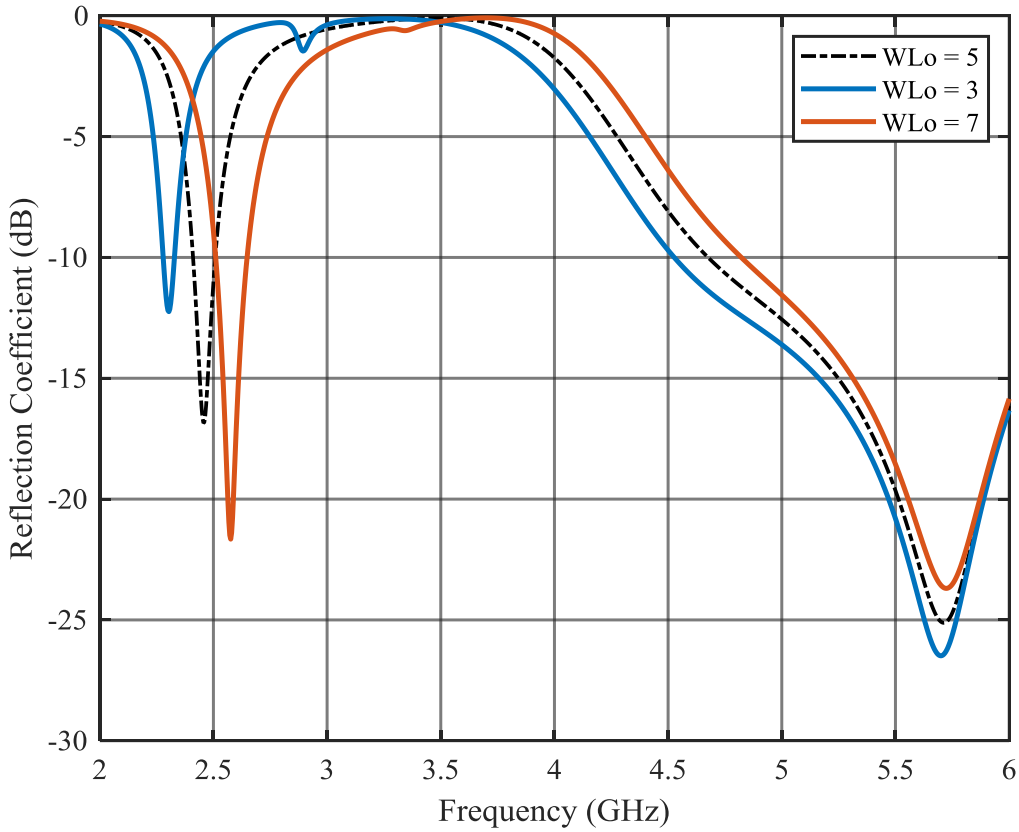

Figure 3.17. Reflection coefficient for different values of the low band dipole width.

The low band dipole width had a larger than expected influence on the low band centre frequency which shifted to a higher frequency for the larger widths. The wider low band dipole also had a broader bandwidth.

3.3.9 Parametric study conclusion

The parametric study conducted on the printed dipole antenna provided valuable insight into what parameters are responsible for what performance characteristics. The length of the capacitively loaded low band dipole, L_{Lo}, and the capacitively loading parameter, T, primarily determines the low band resonating frequency. The length of the high band dipole, L_{Up}, and the length of the microstrip feed line, L_m, determines the resonating frequency of the high band resonance. The width of the antenna, D, that is the H-plane array spacing between the two high band dipoles can be used to improve the high band

radiation patterns in the *H*-plane. The slot line width, *S*, controls the slot line impedance which can be optimised to increase the high band matching. The width of the connection between the dipole configuration, W_S, and the width of the low band dipole, W_{Lo}, can be optimised for wider bandwidth matching at both bands.

3.4 DESIGN EXAMPLE

A design example is presented in three steps to illustrate how knowledge obtained from the parametric study can be used to design for a general dual-band requirement. The new design example proposed is for a dual-band antenna where the low band is centred at 900 MHz with a 10% bandwidth. The high band is centred at 1.8 GHz with a 20% bandwidth. This dual-band example has a frequency ratio of 2. The design example is assumed to be implemented on Roger RT/Duriod 5880 substrate with a thickness of 0.5 mm and dielectric constant of 2.2.

3.4.1 Step 1. Dipole layout

The lengths of the two dipoles are calculated as their corresponding electrical half wavelengths. The effects of the thin low permittivity substrate are ignored in the calculation of the dipole antenna electrical length. The lengths are calculated with the following equation:

$$\frac{\lambda_0}{2} = \frac{c}{2f_c} \tag{3.1}$$

where λ_0 is the free space wavelength (m), c is the speed of light (m/s) and f_c is the frequency (Hz). The length of a dipole required to resonate at 900 MHz is 167 mm. The 1.8 GHz dipole half wavelength is 83 mm. The planar rectangular dipoles are configured with one low band element and two high band elements, one high band element on each side of the low band element as displayed in Figure 3.18. The widths of the dipoles are initially chosen as 10% of their wavelengths, and the spacing between the high band

elements as 60% of the high band wavelength to achieve good radiation performance with low side lobe levels. The values of the parameters are tabulated in Table 3.2.

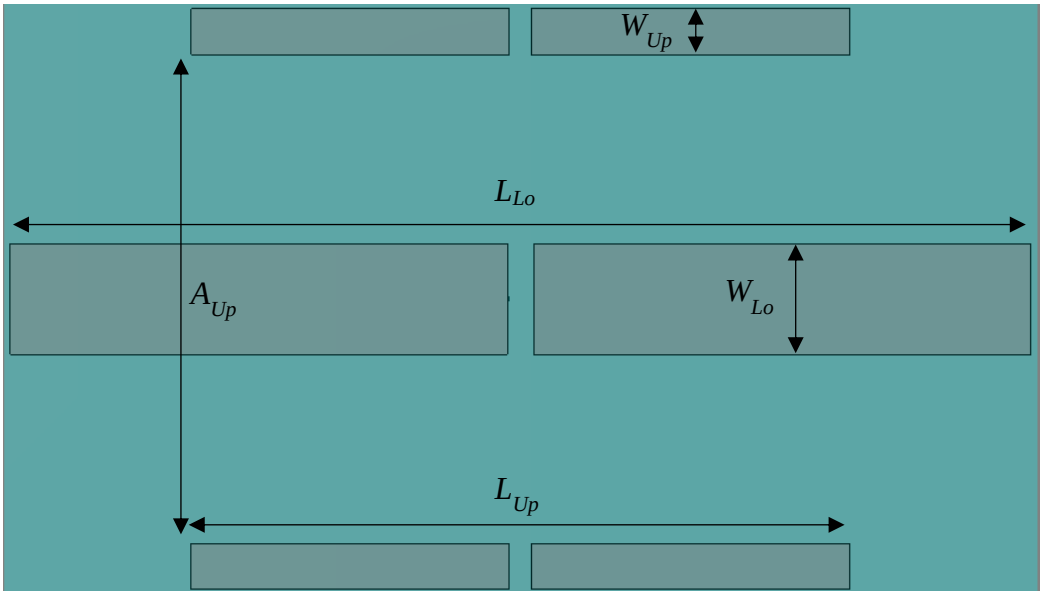

Figure 3.18. Top view layout of the planar dipoles on the substrate.

Table 3.2. Parameters of the dipole layout in Figure 3.18.

Parameter	Dimension	Parameter	Dimension
L_{Lo}	167 mm	W_{Lo}	16.7 mm
L_{Up}	83 mm	W_{Up}	8.3 mm
A_{Up}	90 mm		

3.4.2 Step 2. Connecting the dipoles

The dipoles are connected with a coplanar slot line that would serve as the feed network for the high band dipoles. The connection would combine the dipoles into a single configuration. The width of the slot line ground, W_S, is selected as a quarter of the high band wavelength to ensure that the fields that are excited across the slot line would allow the high band frequency to propagate to the high band elements. The slot line width is 3.22 mm, and is presented with the parameter *S*. The non TEM slot line width is derived from the low relative permittivity (< 9.8) single-sided slot line equation 2.5 for Z_0 = 50 Ω. The addition of the connecting network is displayed in Figure 3.19.

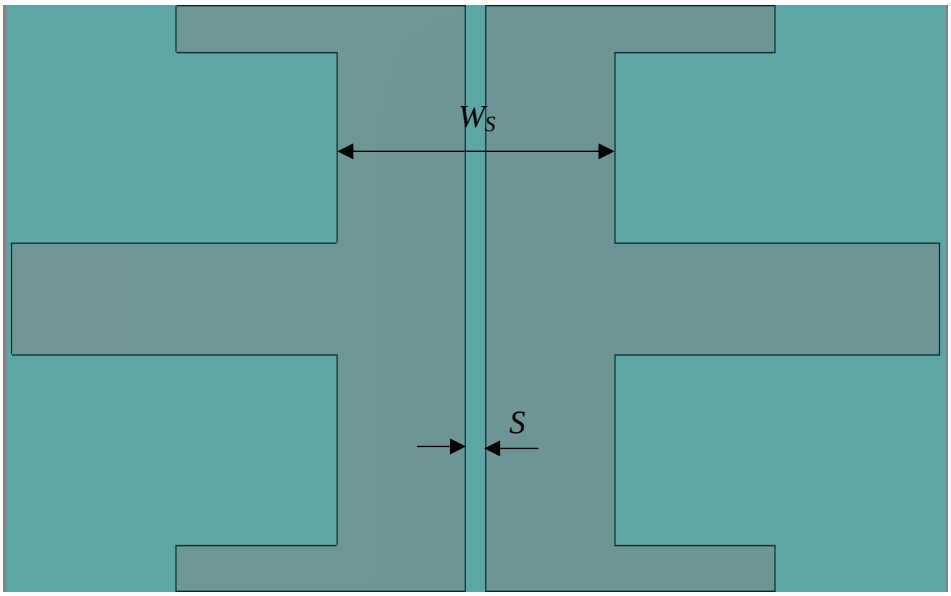

Figure 3.19. Coplanar slot line feed addition to the dipole configuration.

3.4.3 Step 3. Exciting the dipole configuration

The dipole configuration is excited with a microstrip line on the opposite side of the substrate. The microstrip line couples through to the other half of the low band element and excite a field across the slot line to feed the high band elements. The length of the microstrip line, L_m, is initially chosen as a quarter wave of the high band wavelength to be optimised later. The width is chosen as 10% of the high band wavelength also to be optimised for better matching to the coaxial feed. Figure 3.20 displays the top view that includes the microstrip line.

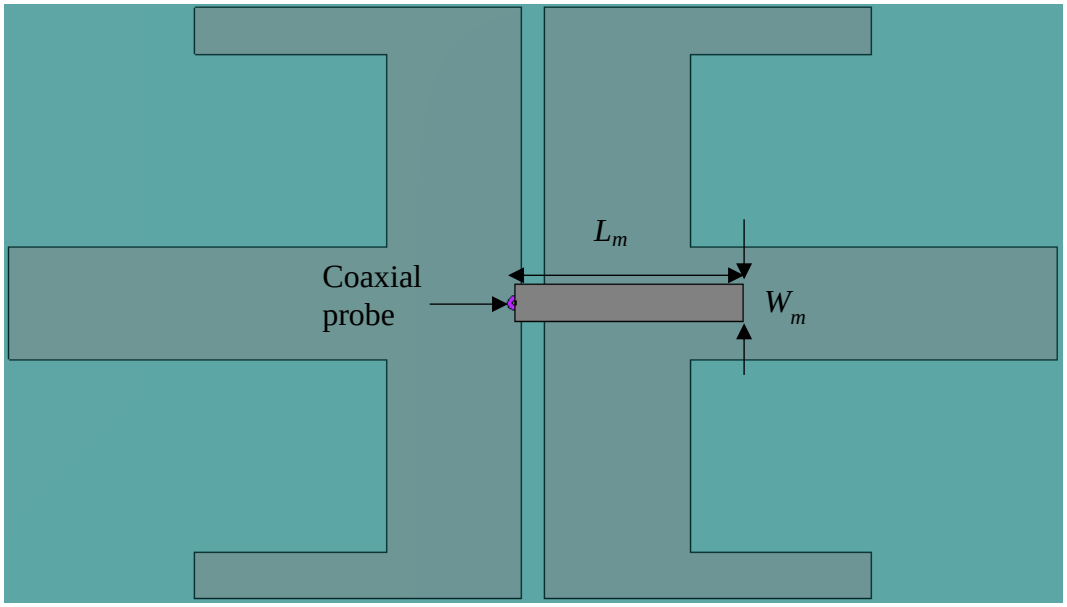

Figure 3.20. Top view of the dual-band dipole configuration.

The dipole configuration is placed above a ground plane to obtain a directional antenna. The height between the antenna element and ground plane should be a balance between the low band and high band dipoles quarter wavelengths. For this example, the height between the dipole configuration and ground plane is chosen as 30% of the high band wavelength that is 50 mm [18].

3.4.4 Design example results

The reflection coefficient of the current design from step 3 is displayed in Figure 3.21. The bandwidth is defined from where the reflection coefficient is below -10 dB to eliminate high reflection levels in the band. Figure 3.21 is the reflection coefficient before any optimisation.

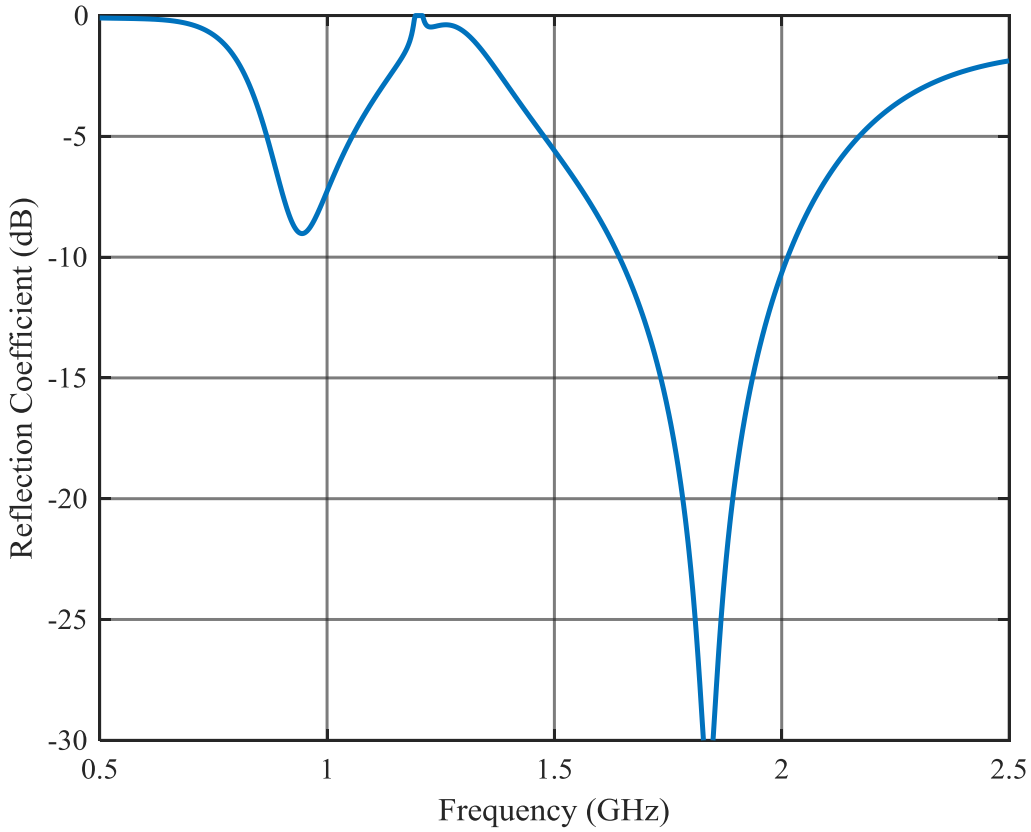

Figure 3.21. Reflection coefficient of the design in Figure 3.20.

From the results of the current dipole configuration, the insight gained from the parametric study should make it clear what parameters should be optimised to obtain the specified results.

The low and high bands are resonating at their desired frequencies. In order to increase the bandwidth at the low band, the low band dipole width, W_{Lo}, should be increased and the width of the slot line ground, W_S, can be increased. The increased slot line ground width, W_S, can change the low band centre frequency and can be countered by increasing the low band length, L_{Lo}.

The high band matching can be improved by optimising the microstrip line length, L_m, and the slot line width, S. The slot line ground width, W_S, can also be optimised to increase the high band matching.

Figure 3.22 is the top view of the optimised design, and Table 3.3 has the parameters of the final model. The reflection coefficient of the new design is displayed in Figure 3.23. Figure 3.24 and 3.25 present the simulated radiation patterns of the optimised design example.

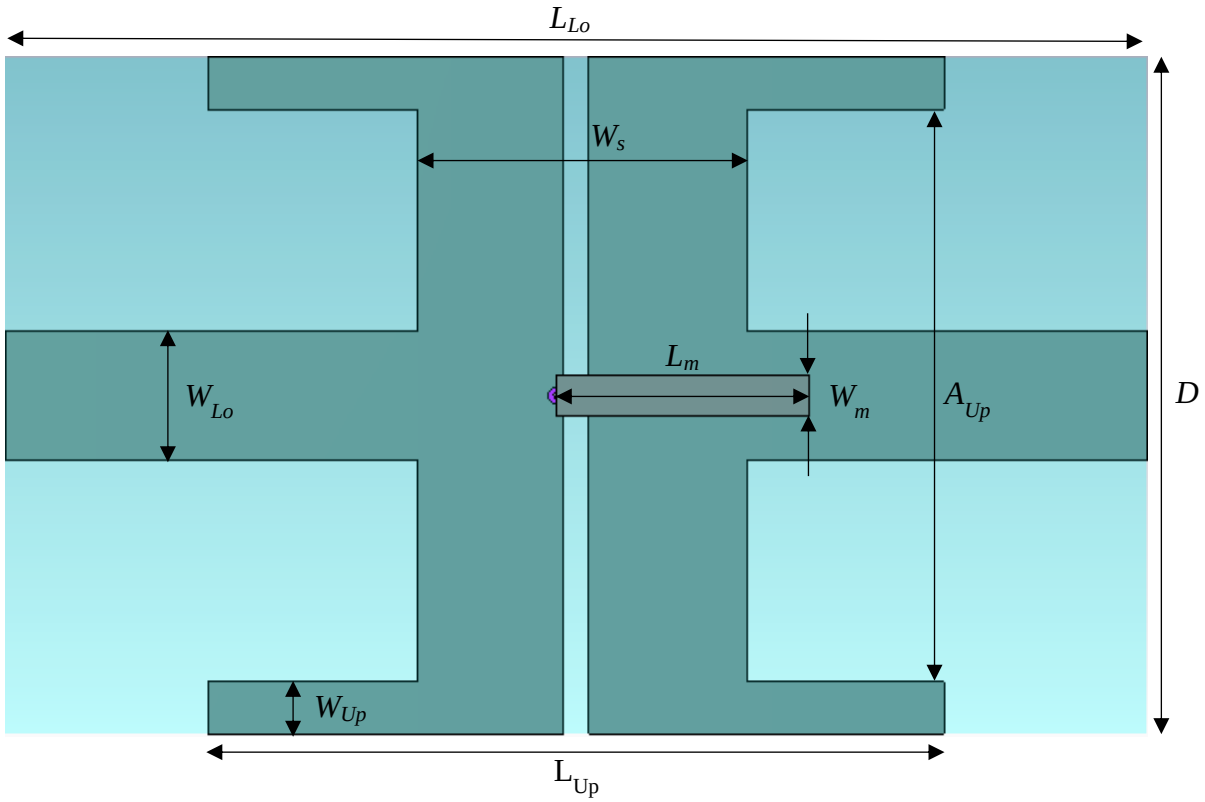

Figure 3.22. Top view of the new design example resonating at 0.9 GHz and 1.8 GHz.

Table 3.3. Parameters of the new design.

Parameter	Dimension (mm)		Parameter	Dimension (mm)	
	Original	Optimised		Original	Optimised
L_{Lo}	167	160	W_s	41.5	40
L_{Up}	83	88	S	3.22	3
L_m	41.5	34.5	W_m	8.3	5.5
D	106.6	89	W_{Lo}	16.7	17
H	50	50	W_{Up}	8.3	7
t	0.5	0.5	A_{Up}	90	75

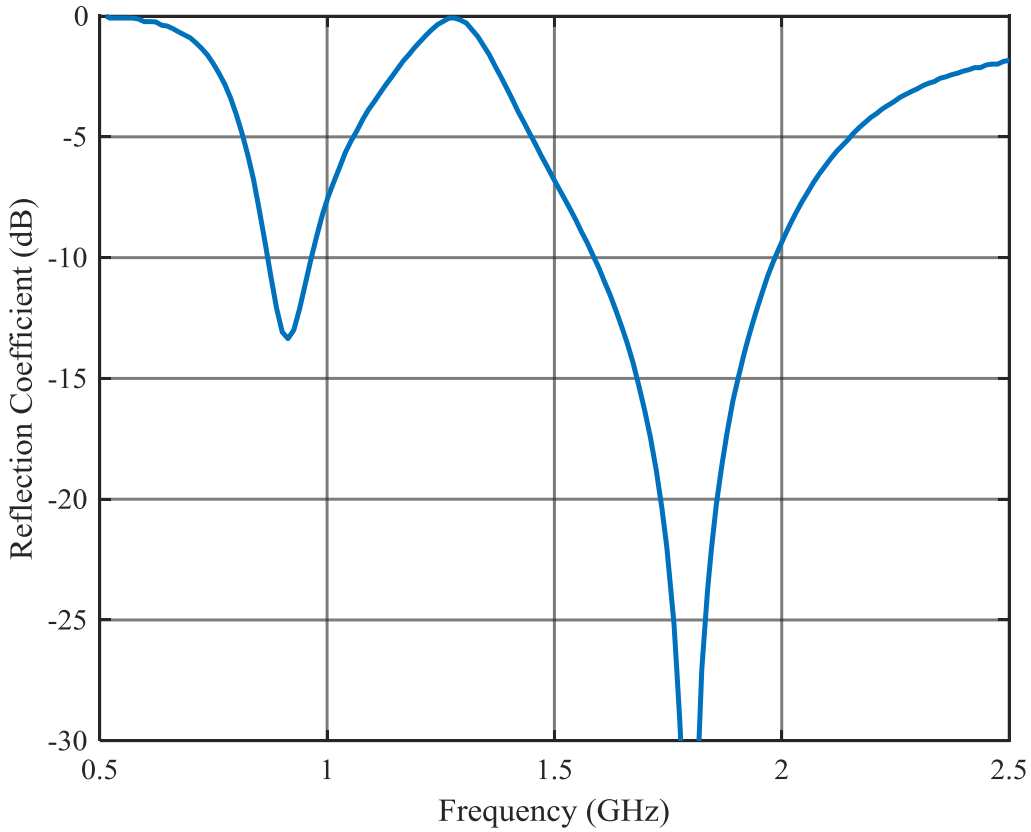

Figure 3.23. Reflection coefficient of the design example antenna.

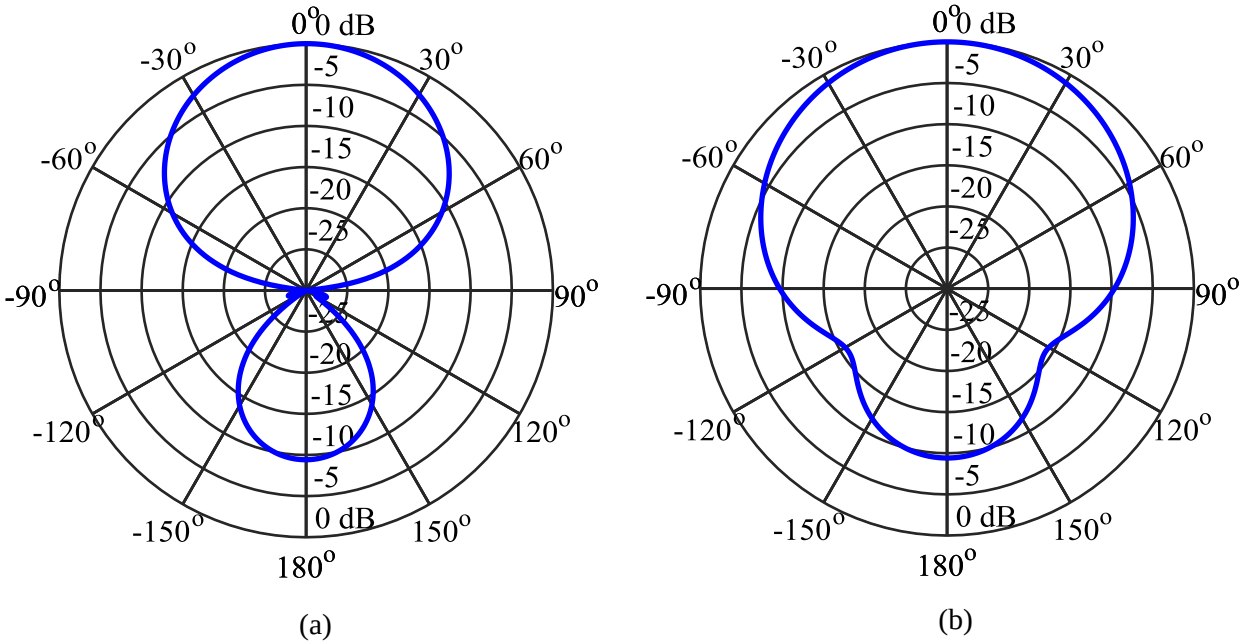

Figure 3.24. The normalised low band radiation pattern at 900 MHz.

(a) *E*-plane (b) *H*-plane

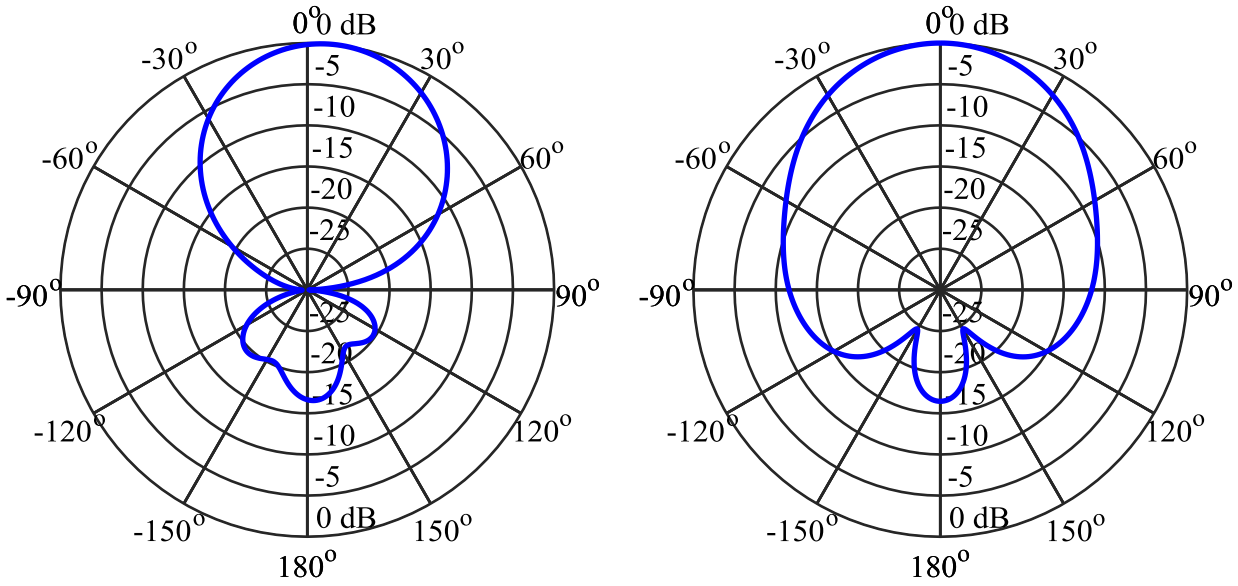

Figure 3.25 The normalised high band radiation pattern at 1.8 GHz.

(a) *E*-plane (b) *H*-plane

Acceptable results were achieved for the design as the low and high frequency bands at the two design frequencies are clearly visible in Figure 3.23, bandwidths of 11% and 22% respectively. The antenna has a gain of 8.4 dBi at 900 MHz with reasonably good radiation performance, except for the somewhat high back lobe level. The gain at 1.8 GHz is 9.6 dBi, with good radiation performance, with low sidelobe levels.

The parametric study made it possible to design a new dual-band antenna with a different frequency ratio and at different frequency bands. The new design example had a frequency ratio of 2 with the low band centred at 900 MHz and the high band centred at 1.8 GHz. From the parametric study, it is straightforward to note what parameters should be changed to reduce the frequency ratio, as well as which parameters should be optimised to improve the bandwidth at the respective frequency bands. The design example geometry changed slightly with the capacitively loaded arms of the low band dipole removed to decrease the frequency ratio. Thus, a single layer dual-band antenna with a large frequency ratio, high gain and good radiation patterns is realisable with the help of the knowledge obtain from the parametric study.

3.5 THE NEW SUB-ARRAY ELEMENT

The dipole configuration is expanded into a new sub-array element to enable the antenna to be configured into an array. The high band elements are expanded to the four corners of the new configuration. The expansion enables the dipole configuration to be incorporated in an array with elements that are set apart in an arrangement for desirable radiation performance. The sub-array element design consists of four high band elements and one low band element. The final array antenna will comprise of four of the sub-array elements and will be arranged in a square 2 × 2 structure.

Figure 3.26 shows the top view of the expanded design. From the figure it is visible that the high band dipoles are fed with the slot transmission line that splits with a T-junction. The low band dipole is fed with the microstrip line. The dimensional parameters of the design are tabulated in Table 3.4. The expanded element results are presented in Figures 3.27 up to Figure 3.29.

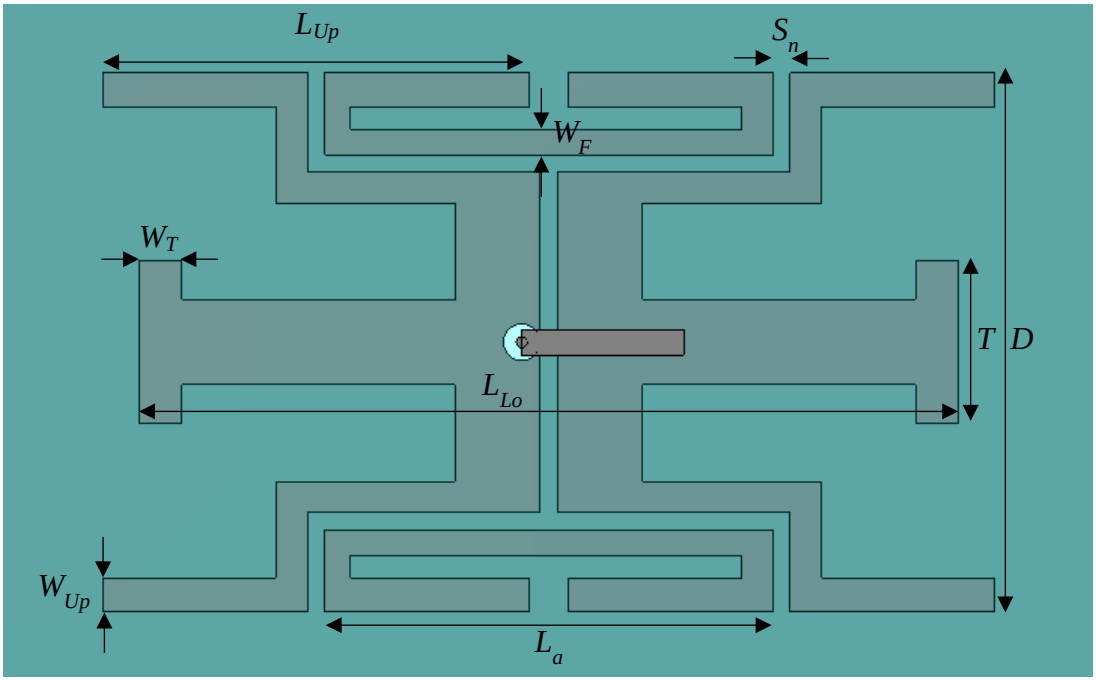

Figure 3.26. Top view of the sub-array element.

The new parameters of the sub-array element L_a, W_F, and S_n are used to define the high band dipole expansion. The *E*-plane spacing between the dipoles are presented with the L_a parameter, W_F presents the slot line feed width, and S_n the extended slot line width.

Table 3.4. The parameters of the new expanded design, the missing parameters are indicated in Figures 3.1 and 3.2.

Parameter	Dimension	Parameter	Dimension
L_{Lo}	52 mm	W_S	10 mm
L_{Up}	25 mm	S	1 mm
L_m	10 mm	W_m	1.5 mm
D	32 mm	W_{Lo}	5 mm
T	10 mm	W_{Up}	2 mm
H	12 mm	W_T	2.5 mm
t	0.5 mm	S_n	1 mm
L_a	26 mm	W_F	1.8 mm

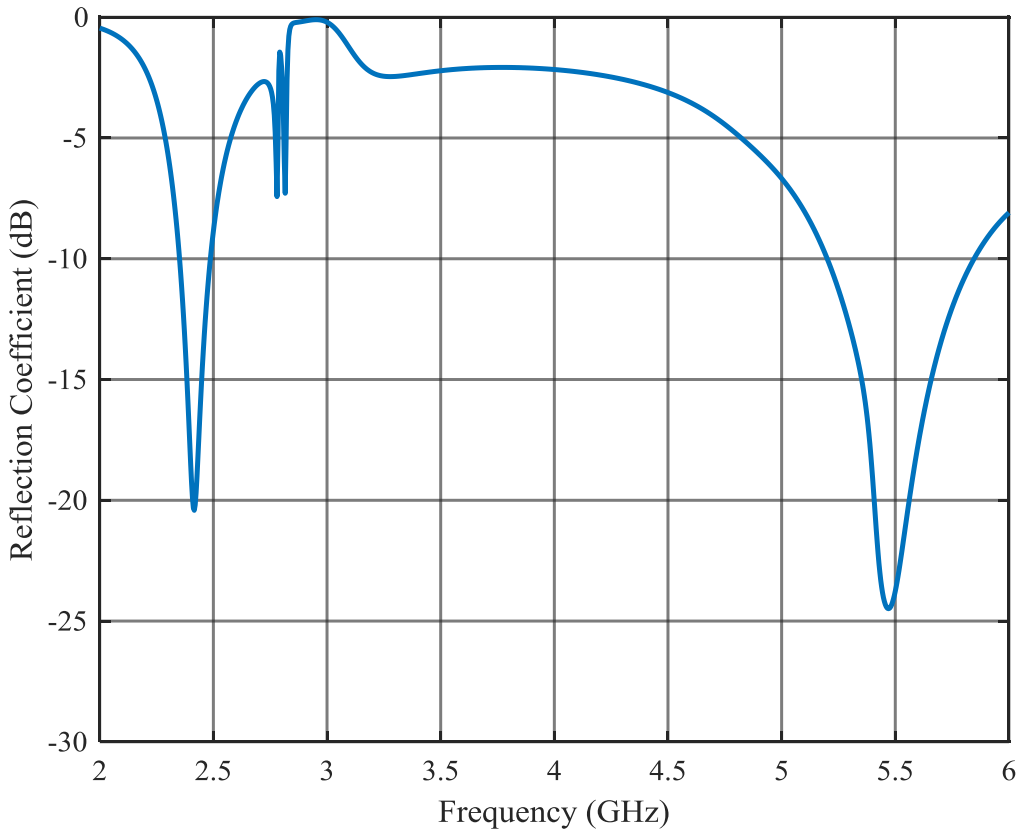

Figure 3.27. Reflection coefficient of the sub-array element.

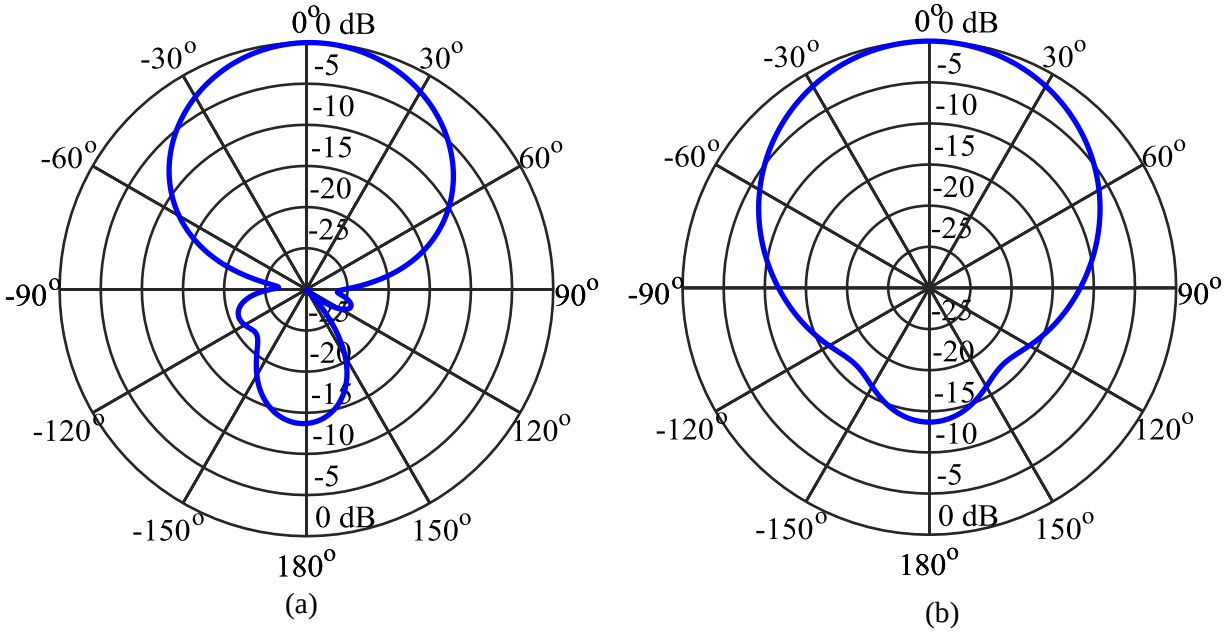

Figure 3.28. The normalised radiation pattern at 2.45 GHz.

(a) *E*-plane. (b) *H*-plane.

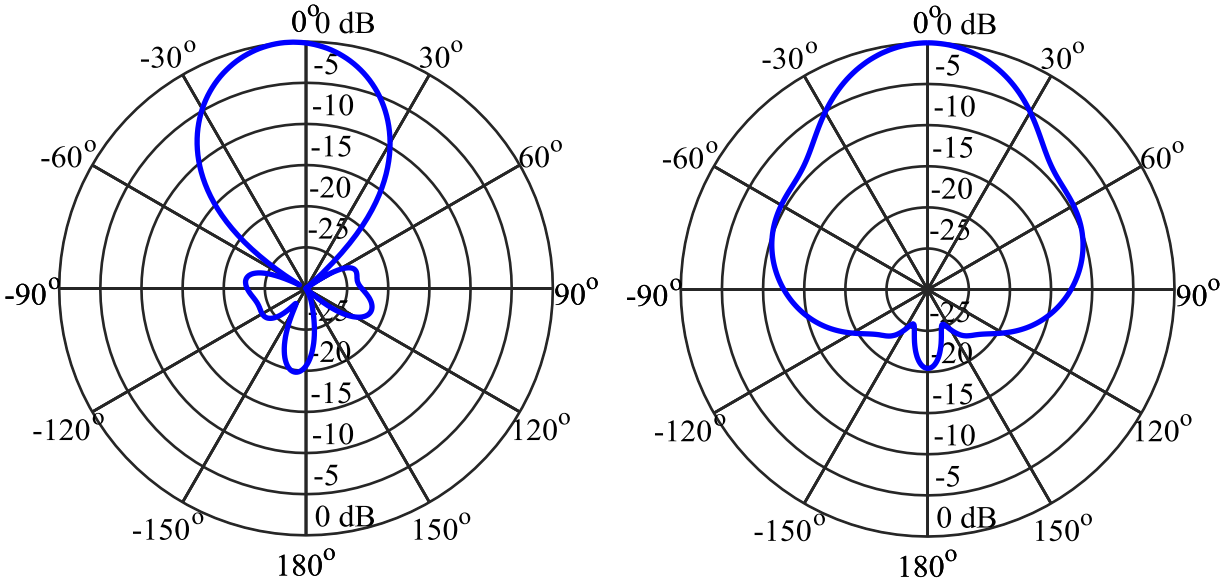

Figure 3.29. The normalised radiation pattern at 5.5 GHz.

(a) *E*-plane. (b) *H*-plane.

The simulated reflection coefficient results of the expanded design are shown in Figure 3.27. The low and high band bandwidths are 5.8% and 11.8% respectively. The sub-array element has a gain of 8.1 dBi in the low band accompanied with good radiation performance. The gain in the high band is 11.8 dBi, also with good radiation performance, with low side lobe levels. The 5º squint in the E-plane of the high band radiation pattern as can be observed in Figure 3.29a is because of the asymmetry of the microstrip feed line structure. The 5º squint does not render the radiation pattern undesirable as the radiation pattern in the E-plane has a wide beamwidth and the power directed at boresight is only 0.4 dB below the peak. The spacing of the four high band dipoles in the new sub-array element is $0.50\lambda_{5.5GHz}$ in the *E*-plane and $0.54\lambda_{5.5GHz}$ in the *H*-plane. The high band element expansion not only opened the possibility to use the element in an array but also doubled the number of high band dipoles per element which increased the gain of the sub-array element, making the sub-array element an already competitive dual-band antenna.

The element can now be integrated into an array where the spacing between the elements is a crucial design parameter as a balance is required between mutual coupling and radiation pattern performance at both frequency bands. If the elements are spaced to close to each other the mutual coupling might affect the array input impedance significantly. When the elements are spaced too far apart from each other the array might have reduced directivity with high side lobe or grating lobe levels.

3.6 ARRAY SPACING

The array spacing investigation is performed too get the maximum spacing limits in the *E*- and *H*-plane to avoid grating lobes in the array arrangement. The spacing limits of 2 × 2 arrays are investigated to determine the effects of the spacing on the radiation pattern. The investigation is conducted with the help of FEKO simulations of four planar dipoles on a substrate with a ground plane reflector. Figure 3.30 shows the top view of the 2 × 2 array structure used in the investigation. The investigation is performed on the high band elements but the results are also applicable to the spacing of the low band elements in the 2 × 2 array configuration. The initial vertical and horizontal spacing parameters are chosen as $0.65\lambda_g$, also listed in Table 3.5. The radiation pattern of the dipole array is displayed in Figure 3.31 as a 3D pattern illustration.

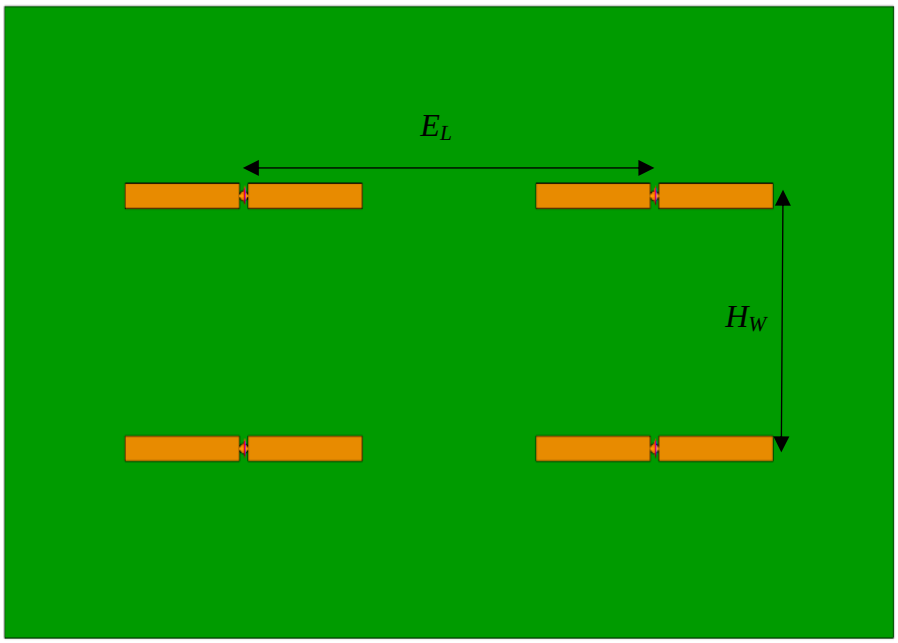

Figure 3.30. Top view of the four-dipole spacing configuration.

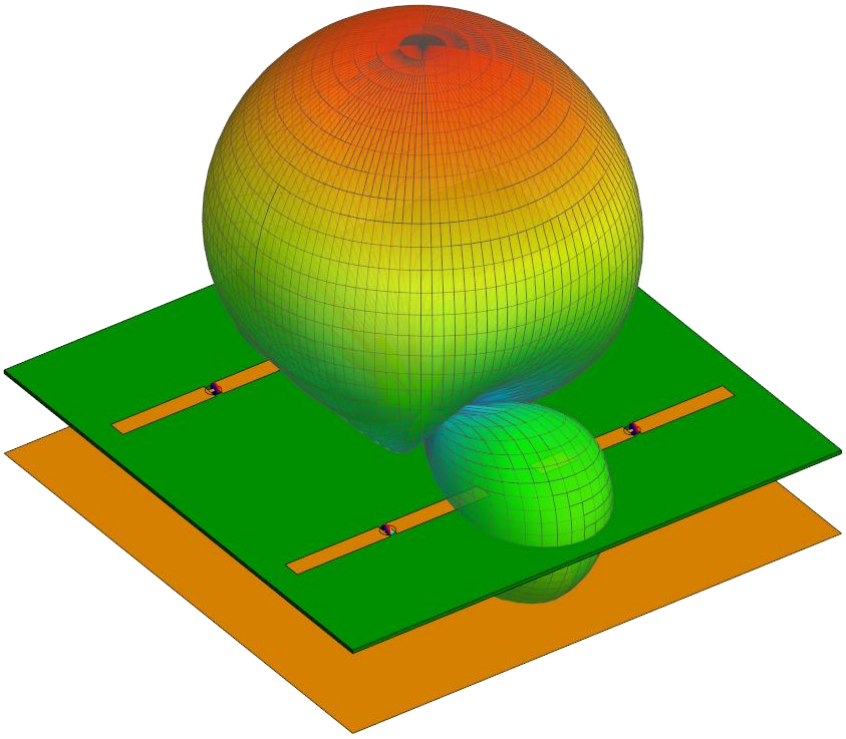

Figure 3.31. 3D far field of the four dipoles at 5.5 GHz.

The four planar high band dipoles are simulated with four independent feeds of equal magnitude and phase. The sidelobe levels of the *E*- and *H*-plane patterns are observed to determine possible radiation pattern degradation. Figure 3.32 shows the *E*- and *H*-plane radiation patterns in polar plot format.

Table 3.5. Initial vertical and horizontal spacing of the array.

Parameter	Dimension	Parameter	Dimension
E_L	$0.65\lambda_g$	H_W	$0.65\lambda_g$

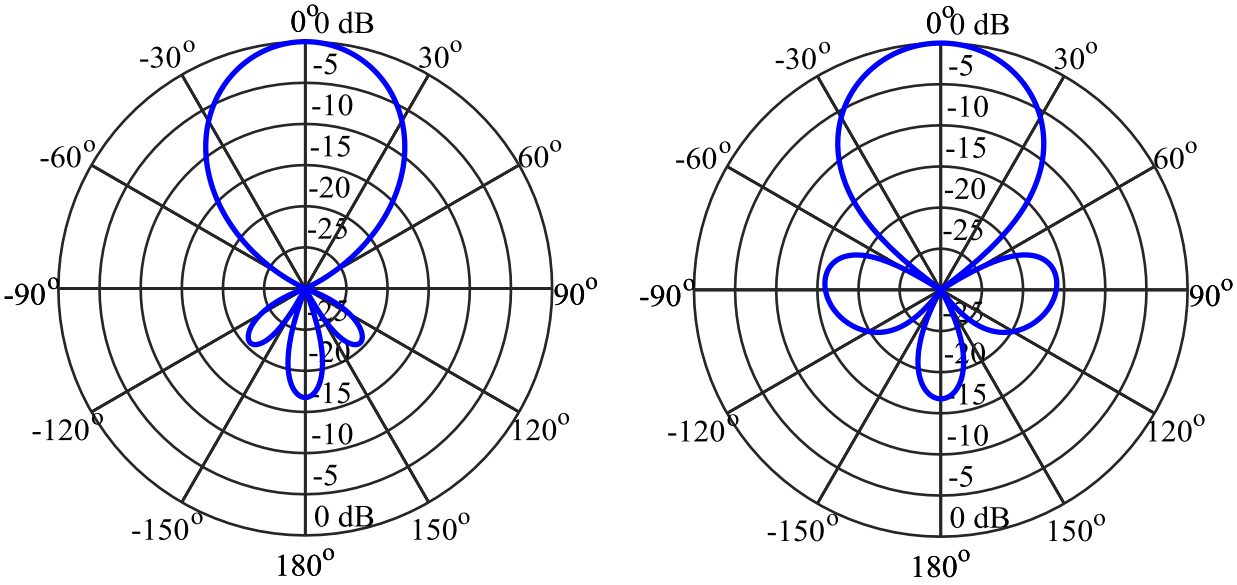

Figure 3.32. The normalised radiation pattern of the 0.65 wavelength spacing.

(a) *E*-plane (b) *H*-plane

The array has a good radiation pattern with a gain of 12.6 dBi directed in the boresight direction. The front to back lobe difference is more than 15 dB with low sidelobe levels. This is a desirable result for the $0.65\lambda_g$ array spacing. Next, the array spacing parameters are increased to monitor the effects of the increasing array dimensions for the array design.

The *E*-plane spacing (E_L) and the *H*-plane spacing (H_W) between the dipoles are increased to $0.75\lambda_g$, $0.875\lambda_g$ and $1.0\lambda_g$ for the next set of figures. According to [3], the elements in an array should ideally be spaced less than a wavelength from each other to avoid grating lobes. The radiation patterns are shown in Figures 3.33 to 3.35.

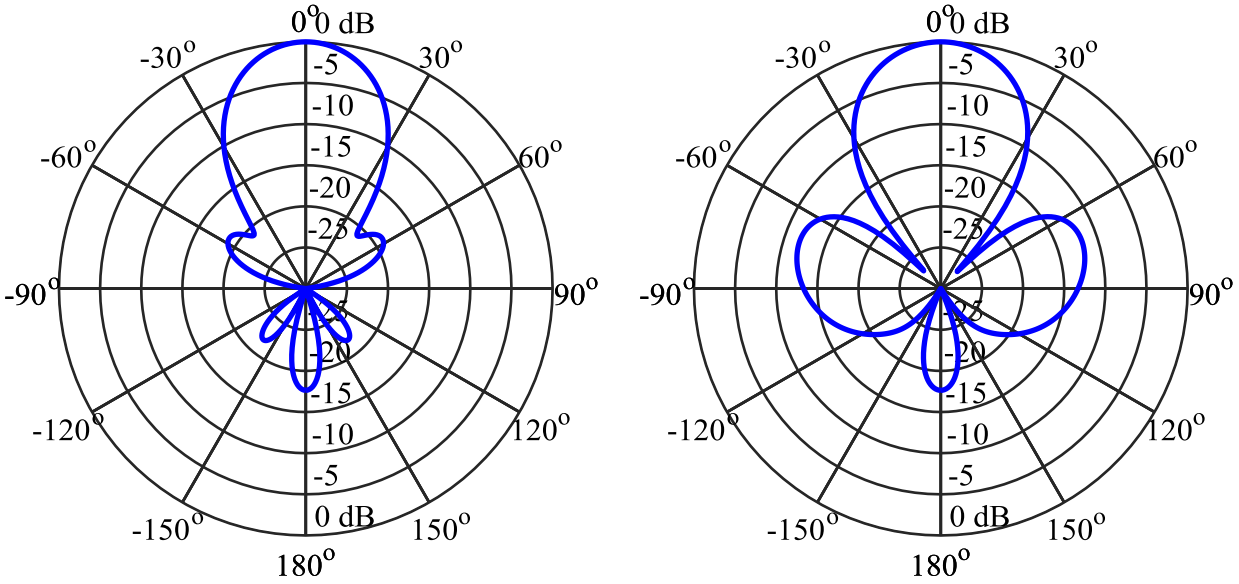

Figure 3.33. The normalised radiation pattern of the 0.75 wavelength spacing.

(a) *E*-plane (b) *H*-plane

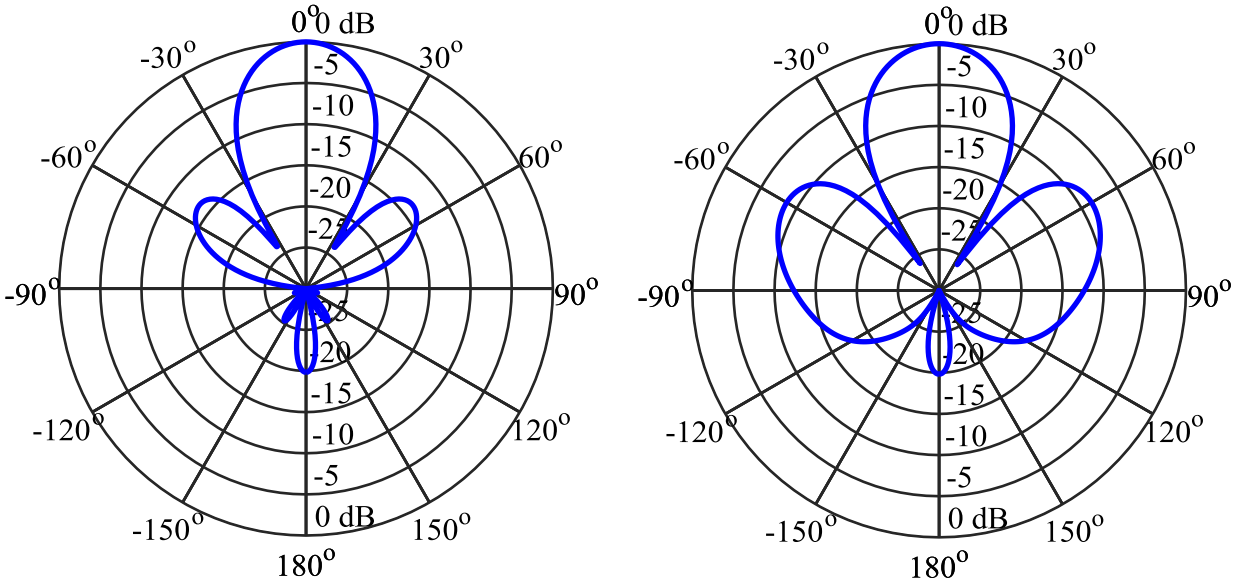

(a) (b)

Figure 3.34. The normalised radiation pattern of the 0.875 wavelength spacing.

(a) *E*-plane (b) *H*-plane

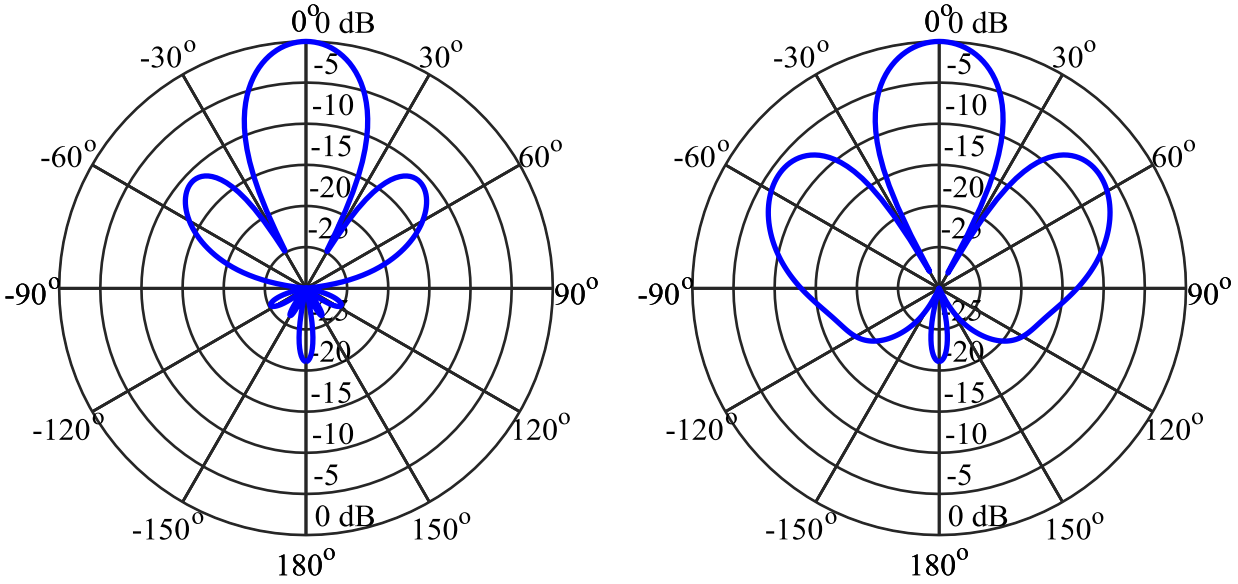

(a) (b)

Figure 3.35. The normalised radiation pattern of the 1.0 wavelength spacing.

(a) *E*-plane (b) *H*-plane

In Figure 3.33 where the dipoles are spaced $0.75\lambda_g$ apart, the array gain is 13.8 dBi, which is higher than the $0.65\lambda_g$ array spacing gain. The front to back lobe difference is 17 dB with sidelobes 18 dB below the main lobe magnitude in the *E*-plane. The *H*-plane has higher sidelobes, 12 dB below the main lobe magnitude.

For the array where the spacing between the elements is $0.875\lambda_g$, the side lobe levels are higher, and the gain is at its maximum, 14.4 dBi. The front to back lobe difference is 19 dB with sidelobes 14 dB below the main lobe magnitude in the *E*-plane. The side lobes in the *H*-plane are 8 dB below the main lobe which is undesirable as significant radiated power is directed into unwanted directions.

The radiation pattern of the array with the full wavelength spacing between the dipole elements, Figure 3.35, has a front to back lobe difference of 21 dB and a maximum gain of 14.3 dBi. The sidelobes in the *E*-plane is 11 dB below the main lobe magnitude. The *H*-plane has higher sidelobes, 6 dB below the main lobe magnitude.

From this investigation the upper spacing limits before the radiation performance becomes undesirable was obtained for a square array. The *E*-plane spacing, E_L, is mainly responsible for the radiation performance in the *E*-plane and the *H*-plane spacing, $H_{W,}$ for the *H*-plane radiation performance. The dipole spacing limit in the *E*-plane is a full wavelength whereas the *H*-plane spacing limit is $0.75\lambda_g$. A combination of the two spacing limits can be considered to see whether a spacing combination is possible to maintain good radiation performance with side lobe levels more than 10 dB below the main beam. The two upper spacing limits in the two respective planes was combined to observe the radiation performance. The radiation patterns of the *E*-plane spacing of a full wavelength and the *H*-plane spacing of $0.75\lambda_g$ is displayed in Figure 3.36.

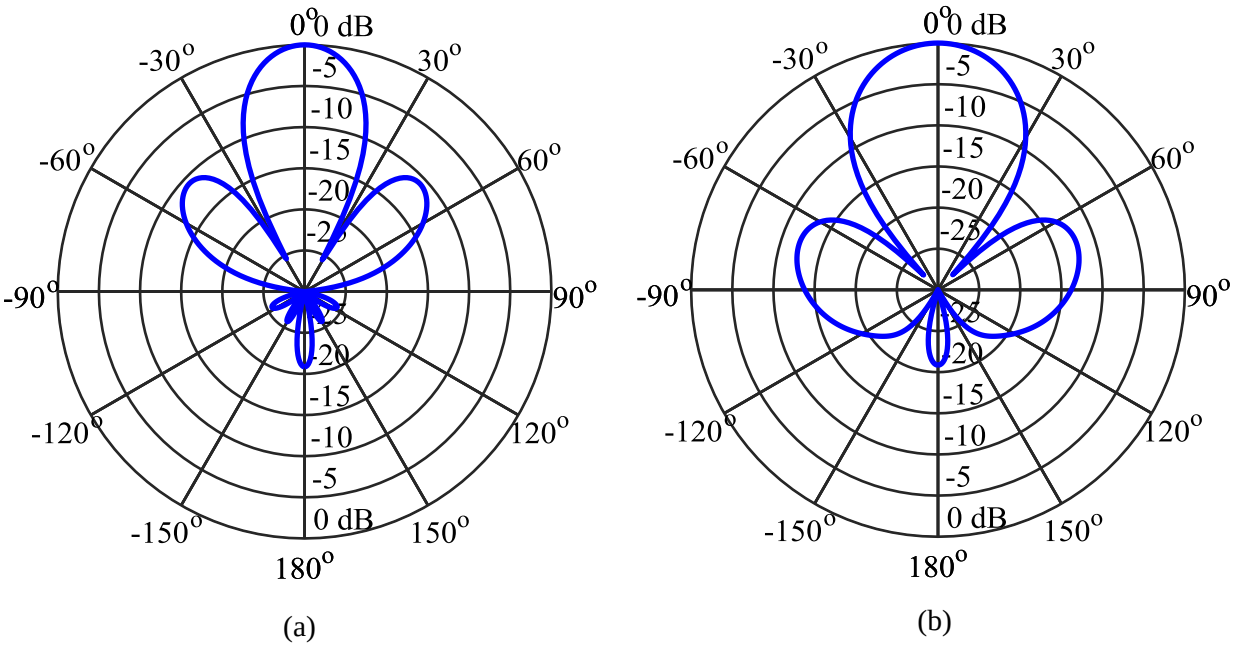

Figure 3.36. The normalised radiation pattern for the spacing combination.

(a) *E*-plane (b) *H*-plane

The maximum gain obtained for the rectangular 2 × 2 array configuration is 14.6 dBi and the side lobes are more than 10 dB below the main beam in both planes. The overall radiation performance for this parameter set is considered good.

The array spacing investigation for the four dipoles was valuable to establish an upper spacing limit for the dipoles. The investigation shows that the dipoles can be spaced further apart in the *E*-plane, up to one wavelength. The *H*-plane spacing limit before grating lobes is $0.75\lambda_g$. A combination of the *E*-plane spacing of one wavelength and *H*-plane spacing of $0.75\lambda_g$ shows that a combination is also possible and has good radiation performance.

3.7 SLOT TRANSMISSION LINE FEED NETWORK

The slot transmission line feed network for the four high band dipoles was also investigated. The investigation was done to confirm that the slot line feed network does not radiate in the frequency bands of interest. In the investigation, the four dipoles at the end of

the slot line configuration are terminated with ports. The substrate from the computer-aided design (CAD) model was changed from a lossy material (tan δ = 0.0009) to a lossless material (tan δ = 0) for this investigation. The change of the substrate material properties in this case is to eliminate any non-radiating losses in the transmission line network. The feed network is designed to divide the input power equally among the four output ports for the high band. In the case of acceptable matching and negligible radiation from the feed network, the transmission coefficients to the four high band antenna ports should be very close to -6 dB, specifically in the high band from 5 to 6 GHz. Figure 3.37 shows the 3D model of the simulated feed network, and Figure 3.38 shows the simulated S-parameters.

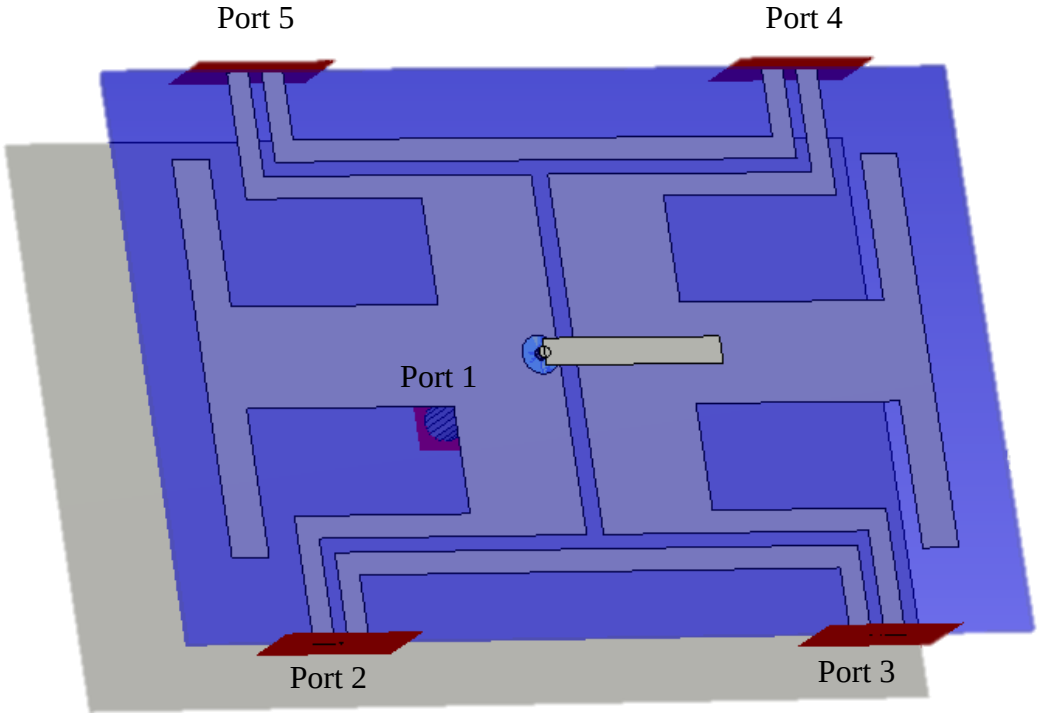

Figure 3.37. Simulation setup to determine whether the slot line feed network radiate in the high band.

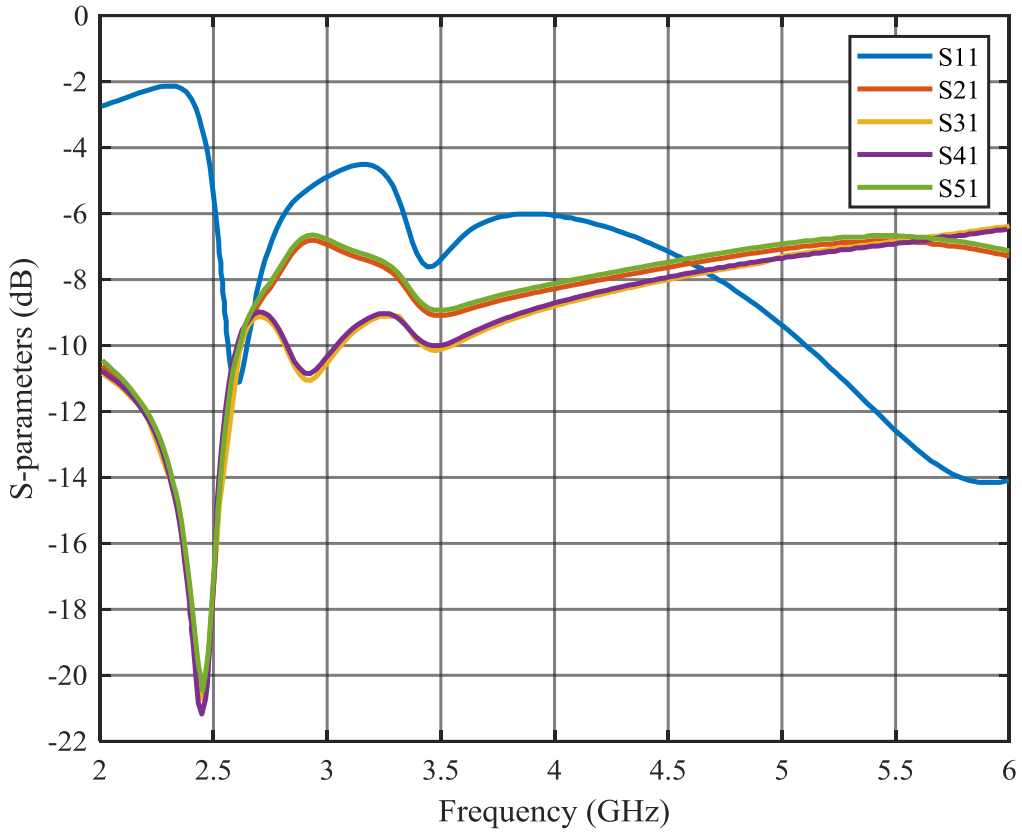

Figure 3.38. S-parameters of the slot line feed network.

The S-parameter results displayed in Figure 3.38 confirm that very little power is radiated in the high band. Power is radiated in the low 2.45 GHz band, which is correct since the capacitively loaded low band dipole is part of the structure on which the investigation was performed. The discrepancy at 3 GHz between the transmission ports is a combination of the unbalanced feed used to excite the antenna and the higher order modes. From 4 to 6 GHz there is not any significant loss in total power. The S21 through to S51 transmission parameters are a little lower than the expected -6 dB, but this is because port 1 is not perfectly matched over the whole band when the four dipoles are removed, and then some reflection of power occurs at port 1. From the results of this experiment, it is safe to say that the slot line feed network does not radiate unwanted power in the high band, and it should successfully transfer the power to the high band dipoles.

3.8 THE 2 × 2 DUAL-BAND ARRAY

The final array design consists of four of the sub-array elements that are configured in a square 2 × 2 array. The array is fed with a microstrip line tapered corporate feed network that divides the input power equally between the four sub-arrays. The feed network is optimised to have an input impedance of 50 Ω. Figure 3.39 shows the top view of the feed network and Figure 3.40 displays the simulated S-parameters of the network while the sub-array ports are terminated in 50 Ω. The sub-arrays are spaced 64 mm from each other in the *E*- and *H*-planes (centre to centre). The 64 mm is $0.52\lambda_{2.45GHz}$, and the high band elements are spaced 35 mm apart and equate to $0.65\lambda_{5.5GHz}$. The *E*- and *H*-plane spacings are below the spacing limits defined in the array spacing investigation. The spacing is optimised for bandwidth at the two respective bands and not gain.

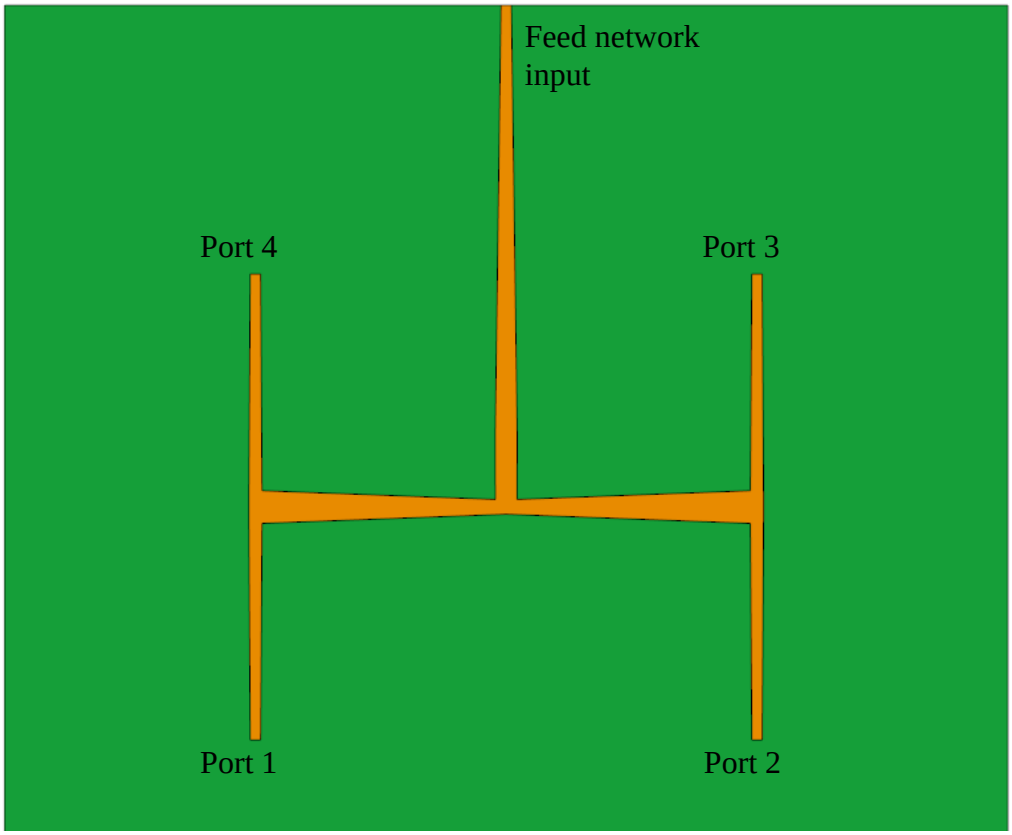

Figure 3.39. Top view of the 50 Ω tapered feed network.

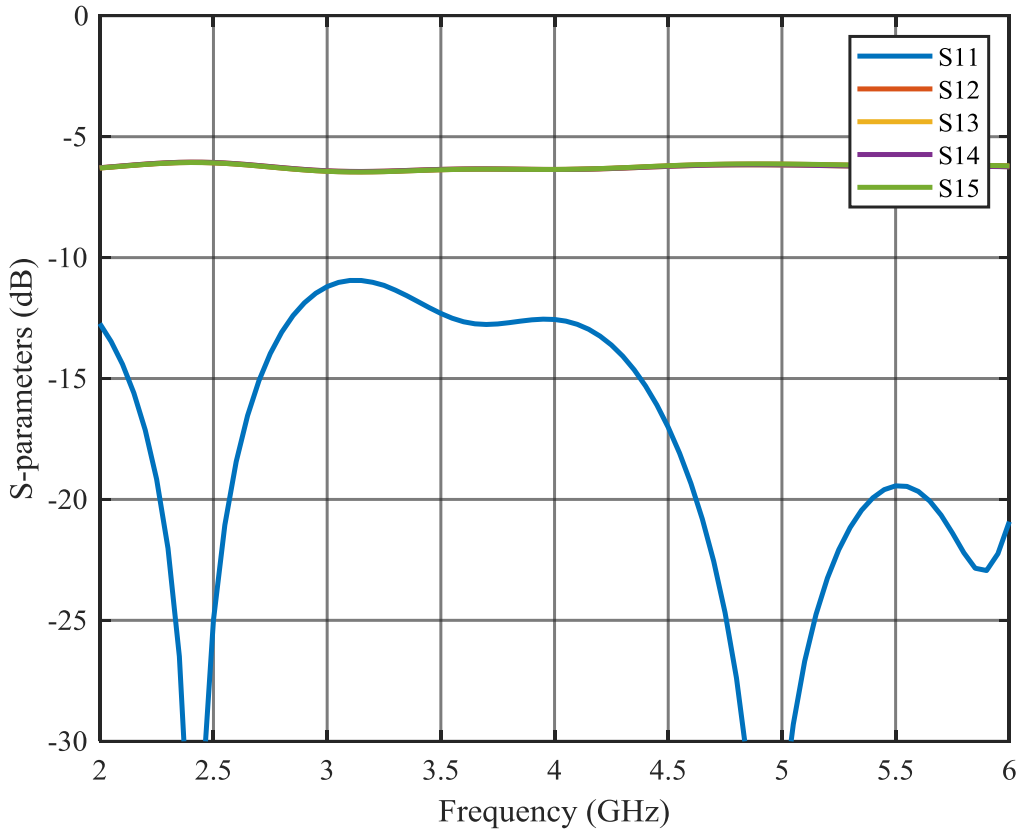

Figure 3.40. Simulated S-parameters of the array feed network.

The spacing between the array elements affects the feed network input impedance. The low band elements are spaced $0.52\lambda_{2.45GHz}$ apart from each other. The $0.52\lambda_{2.45GHz}$ spacing is at the lower theoretical spacing limit in order to avoid high mutual coupling levels. The high band elements are spaced $0.65\lambda_{5.5GHz}$ from each other. The feed network is optimised to have low reflections at the two frequency bands of operation of the array elements. The simulated feed network results also confirm that the input power is divided equally between the four sub-arrays.

Figure 3.41 shows the top view of the dual-band array and the reflection coefficient and gain of the array are displayed in Figures 3.42 and 3.43 respectively. The radiation patterns of the low and high bands are presented in Figures 3.44 up to Figure 3.47.

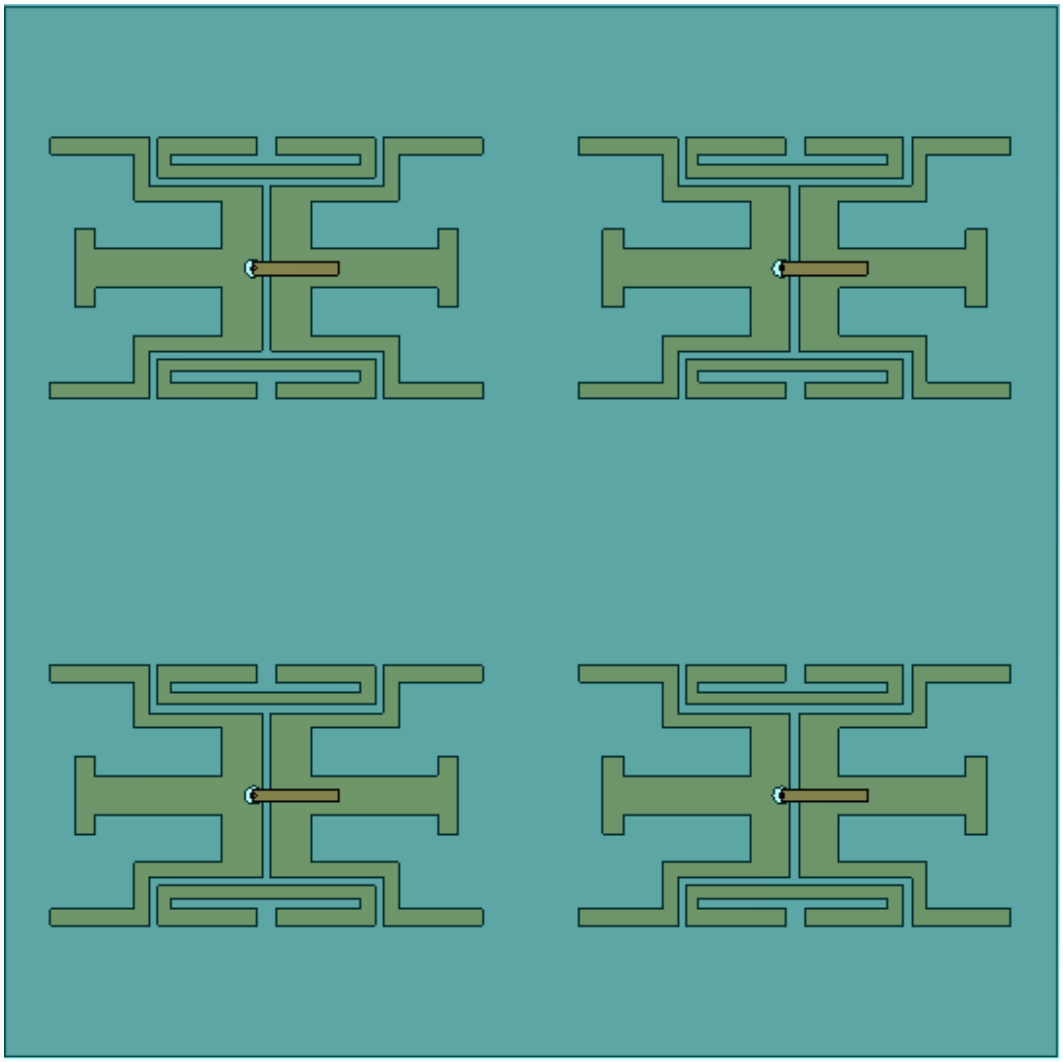

Figure 3.41. Top view of the dual-band array.

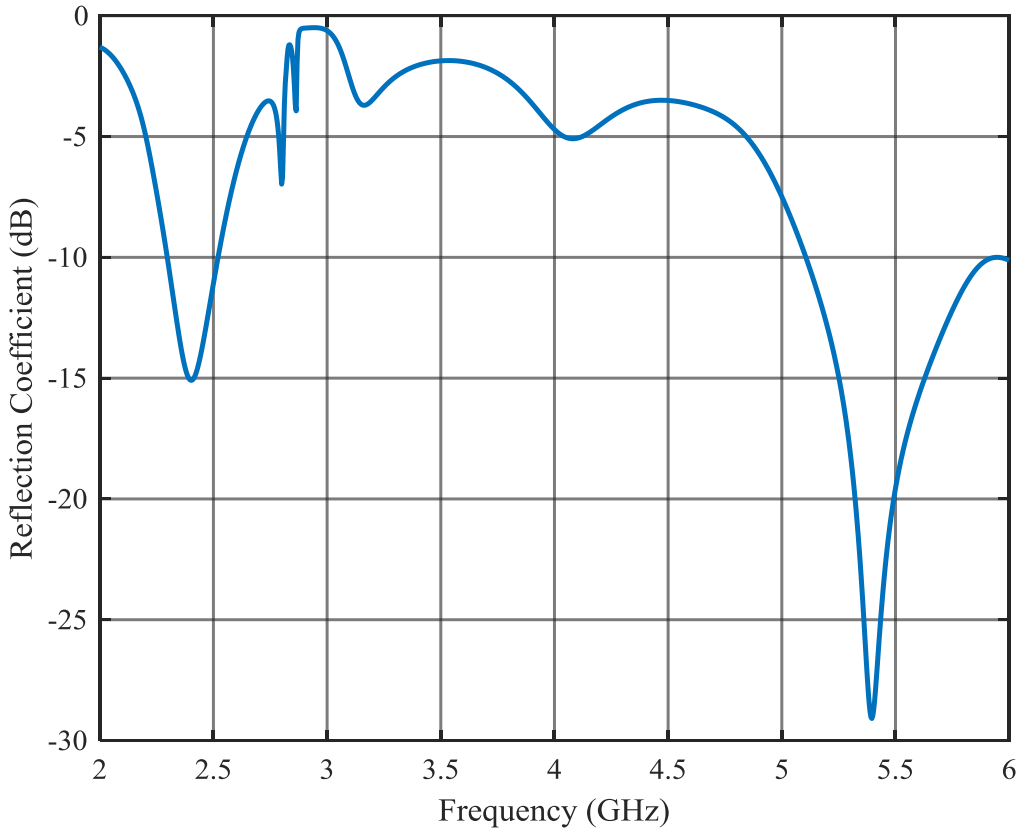

Figure 3.42. Simulated reflection coefficient of the dual-band array.

The low band has a 9% bandwidth centred at 2.41 GHz. The high band centre frequency is at 5.53 GHz and has a 15% bandwidth. The frequency ratio between the two bands is 2.3. The antenna has sufficient bandwidth to be utilised for the WLAN application at both bands.

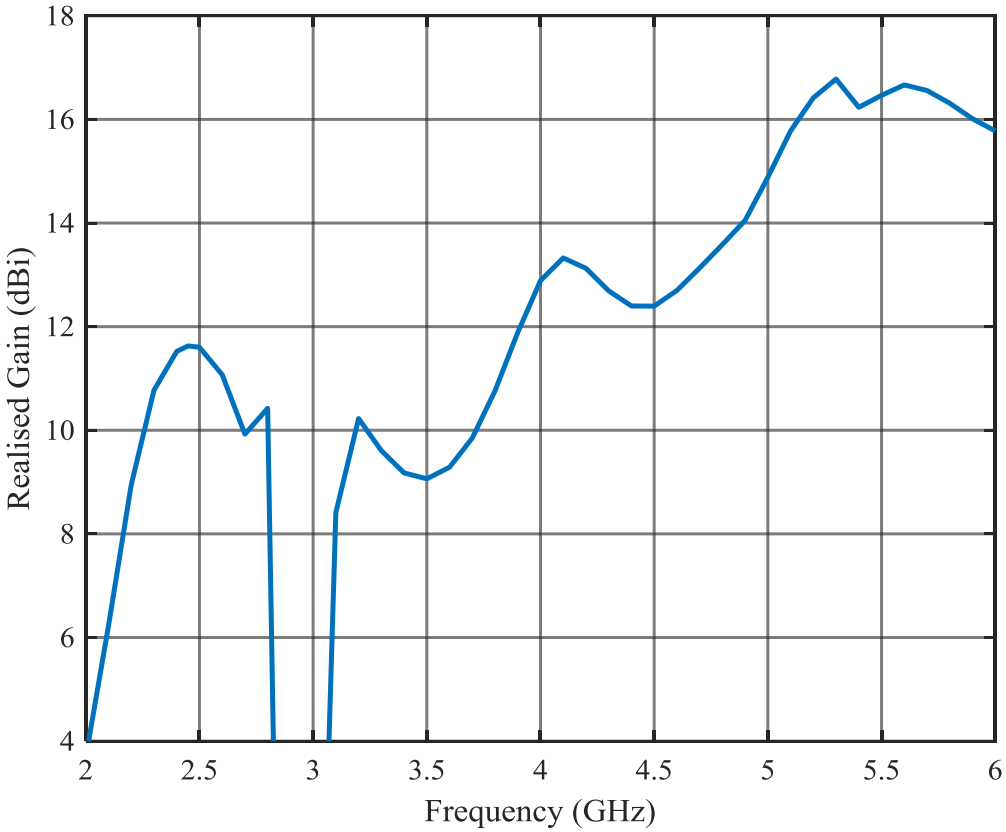

Figure 3.43. The simulated realised gain of the array.

The simulated gain at the 2.45 GHz frequency band is 11.7dBi. The gain at the high frequncy band is above 16 dBi over the specified high band.

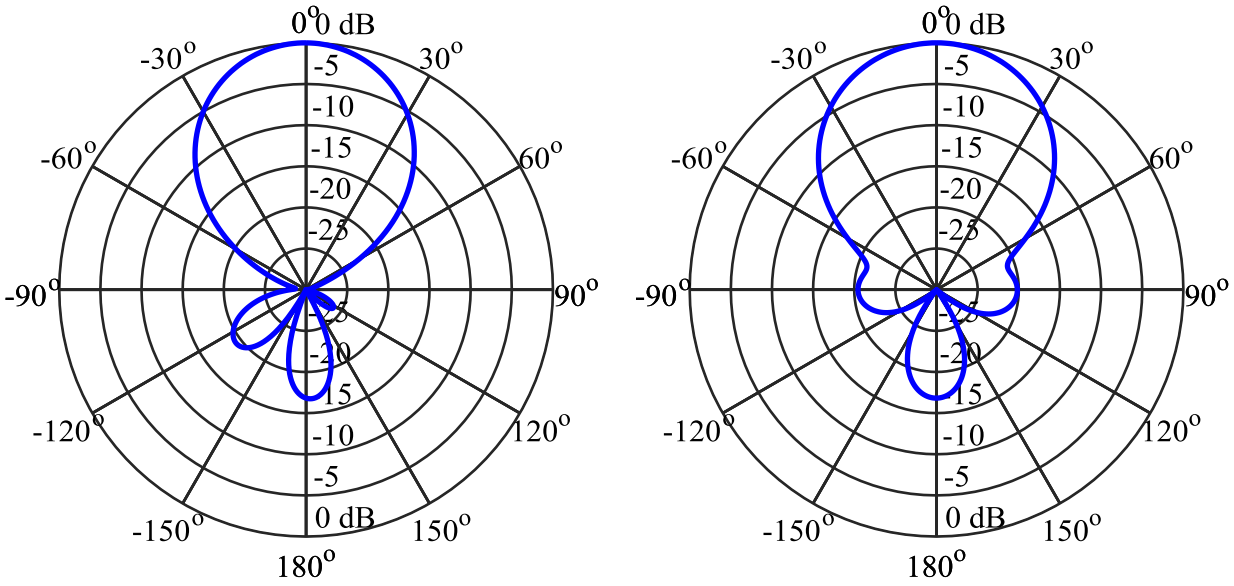

(a) (b)

Figure 3.44. The normalised radiation pattern at 2.45 GHz.

(a) *E*-plane. (b) *H*-plane.

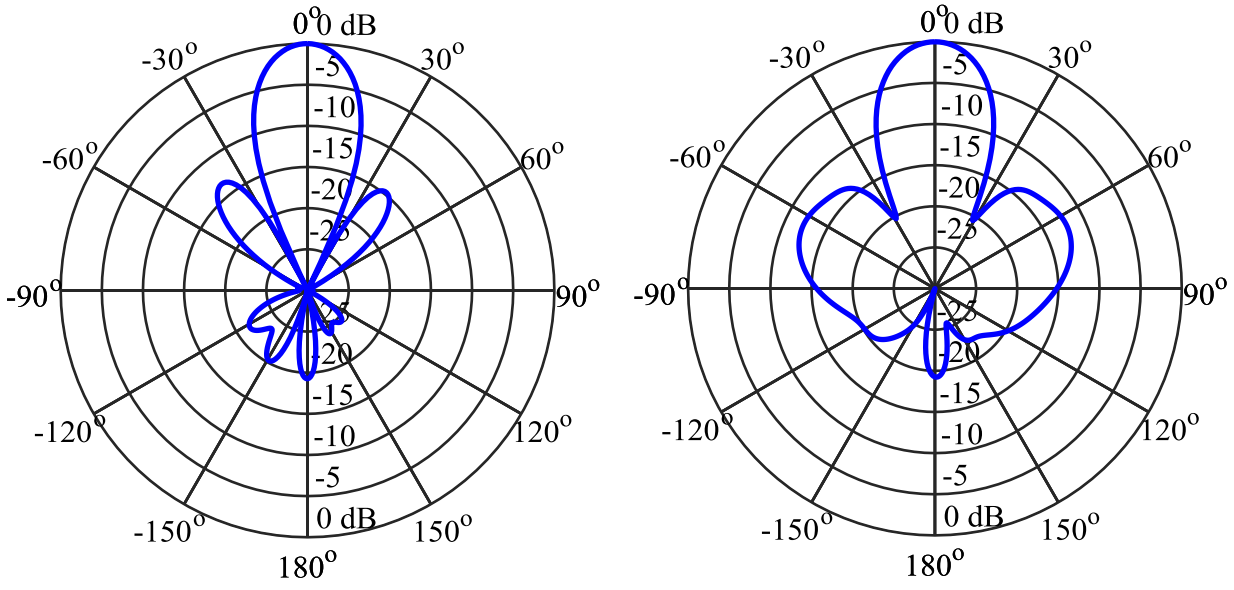

(a) (b)

Figure 3.45. The normalised radiation patterns at 5.25 GHz.

(a) *E*-plane. (b) *H*-plane.

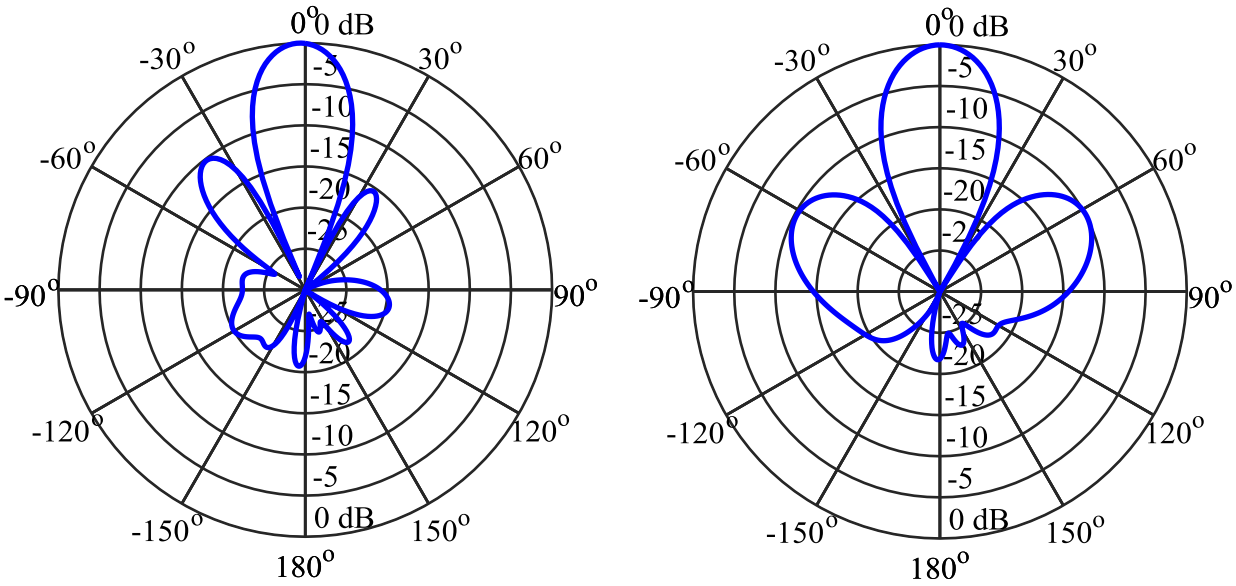

(a) (b)

Figure 3.46. The normalised radiation pattern at 5.5 GHz.

(b) *E*-plane. (b) *H*-plane.

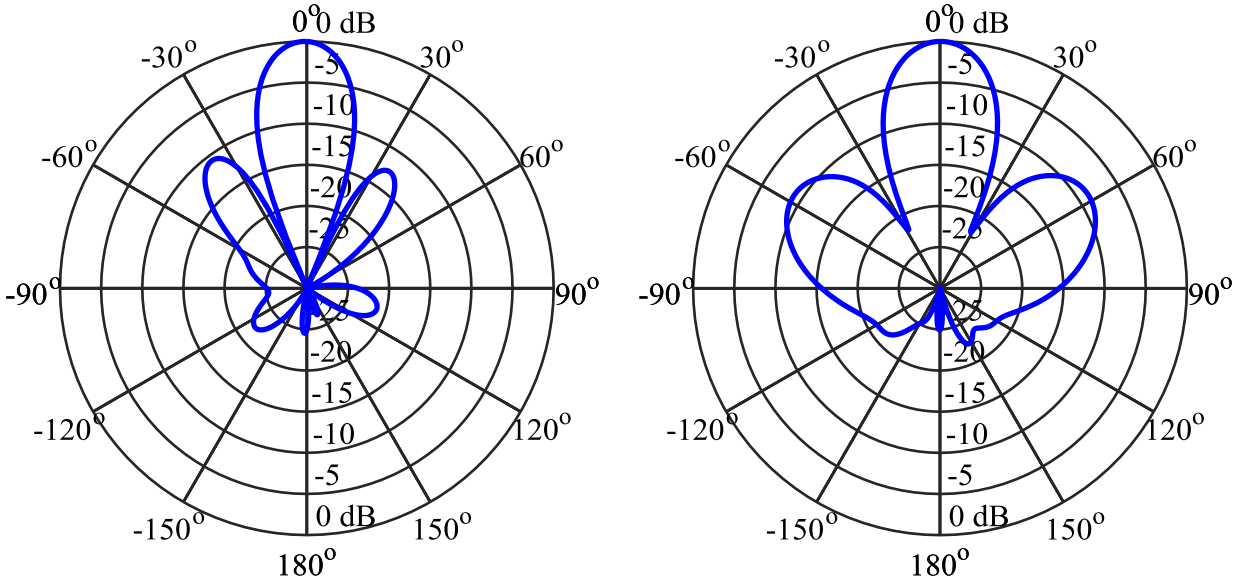

(a) (b)

Figure 3.47. The normalised radiation pattern at 5.75 GHz.

(b) *E*-plane. (b) *H*-plane.

The radiation pattern in the low band have side lobe levels 18 dB below the main beam and the back lobe is 16 dB below the main beam magnitude. The high band radiation pattern is displayed at three frequency intervals because of the broad high band. The side lobe levels are nominally 10 dB below the main beam over the high band, although the side lobe levels are higher at the high band compared to the low band. The asymmetry in the E-plane radiation pattern is due to the asymmetry of the structure. The microstrip feed is the cause for the asymmetry in the antenna structure and leads to the slight squint.

The radiated power in both bands is effectively directed in the boresight direction to make this antenna array a directional dual-band antenna suitable for WLAN. The final size of the antenna array is $128 \times 128 \times 13$ mm^3.

3.9 SUMMARY

The parametric study on the dipole configuration from [18] gave valuable insight into what parameters of the configuration are responsible for which of the antenna performance properties. The insight gained from the parametric study was used to formulate a design approach for a general dual-band antenna configuration. The insight from the parametric study was also used to increase the number of high band dipoles to form a new sub-array arrangement which can be used in a larger array. The simulated results of the expanded sub-array element indicated good dual-band performance. The simulated results of the array consisting out of four of the sub-arrays fed with a tapered corporate feed network have high gain and acceptable radiation patterns in the two bands.

CHAPTER 4 EXPERIMENTAL VERIFICATION

4.1 CHAPTER OBJECTIVES

This chapter presents the measured results of the 2 × 2 dual-band antenna array. Four sub-arrays are assembled into a 2 × 2 array with a tapered corporate feed network to feed the four sub-arrays in phase and with equal magnitude. The simulated and measured results of the array are compared with each other to verify the design.

4.2 MEASURED DESIGN AND RESULTS

The dual-band antenna array was manufactured on two 128 × 128 mm^2, 0.5 mm thick Taconics TLY 5 substrate sheets. The electrical properties of the Taconic TLY 5 are equivalent to the Rogers 5880 substrate that was used in [18] with a relative permittivity of 2.2 and loss tangent of 0.0009. The four coaxial lines used to feed the four antenna elements from the corporate feed network are 0.085" coaxial cables cut to the desired length of 12 mm for the design. Figure 4.1 shows a photograph of the compact dual-band antenna and Figure 4.2 a photograph of the dual-band antenna measured at the compact antenna range of the University of Pretoria.

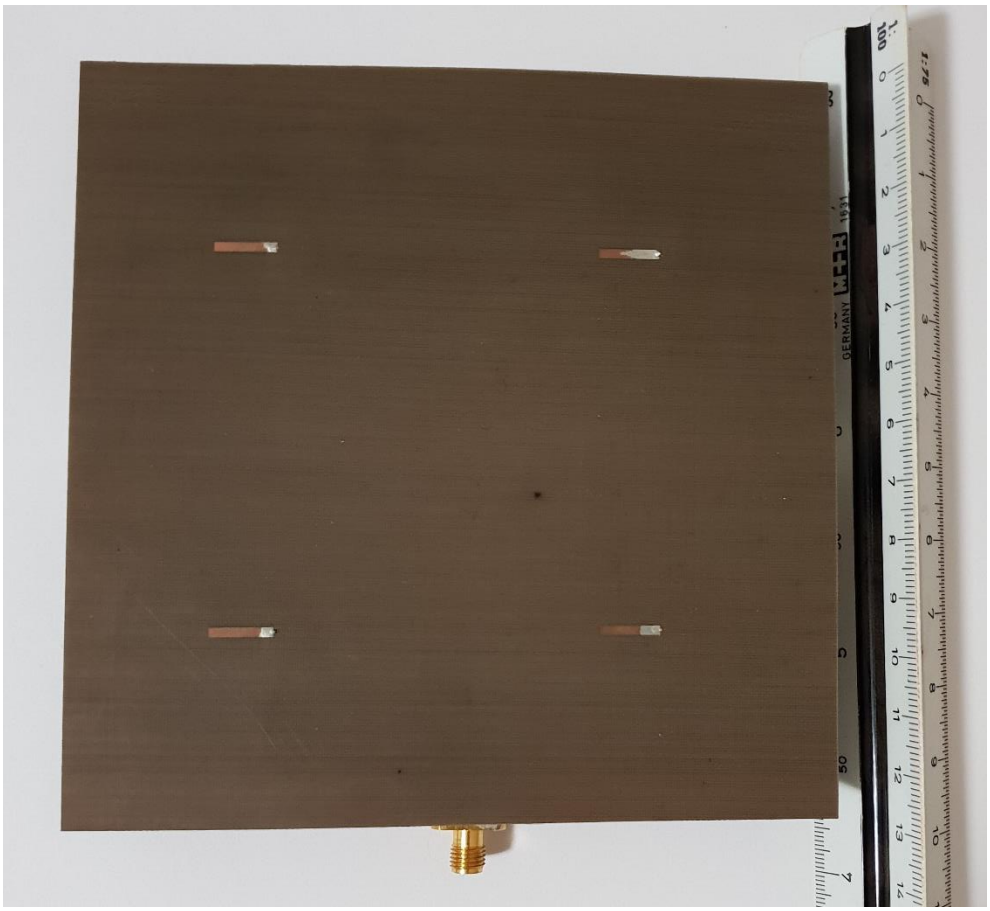

Figure 4.1. Top view of the measured antenna.

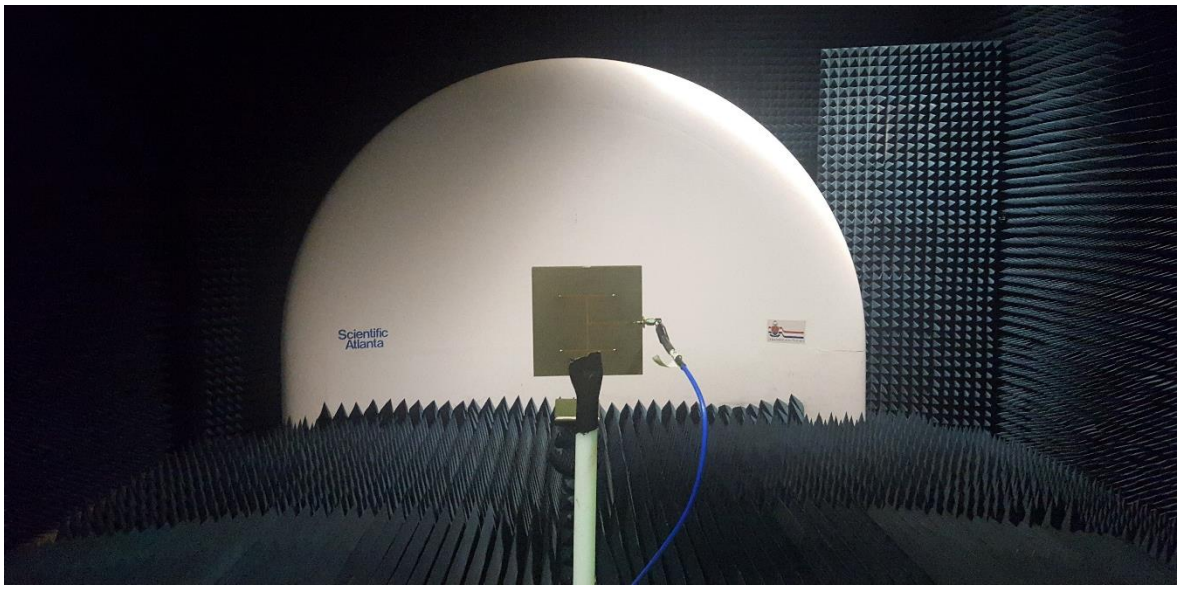

Figure 4.2. The compact, high gain, dual-band antenna during the measurement.

Figure 4.3 is an overlay of the simulated and measured reflection coefficient of the final design, and Figure 4.4 compares the simulated and measured gain.

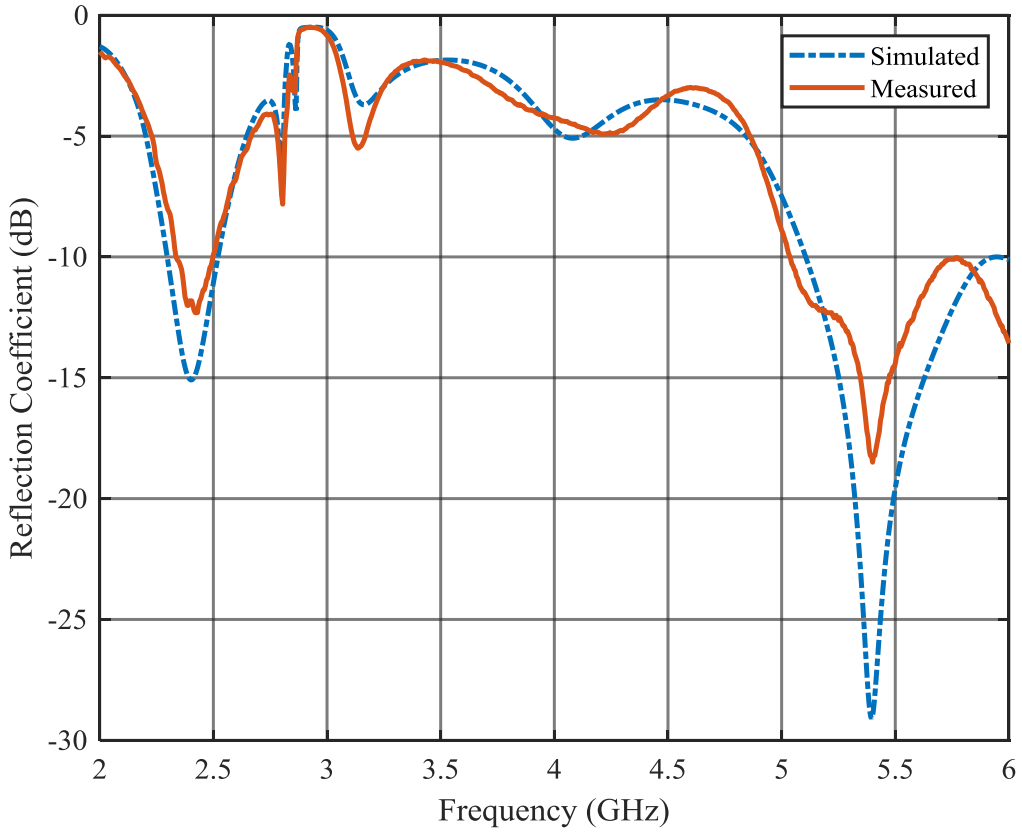

Figure 4.3. Simulated and measured reflection coefficient of the dual-band array.

The measurements showed a low band with acceptable matching in the frequency range 2.33 – 2.50 GHz, which represents a 7% bandwidth. The requirement for a WLAN antenna is 2.4 – 2.484 GHz. The high band was measured as 5.03 – 6.00 GHz, which represents an 18% bandwidth. The required high band for WLAN applications is 5.15 – 5.825 GHz.

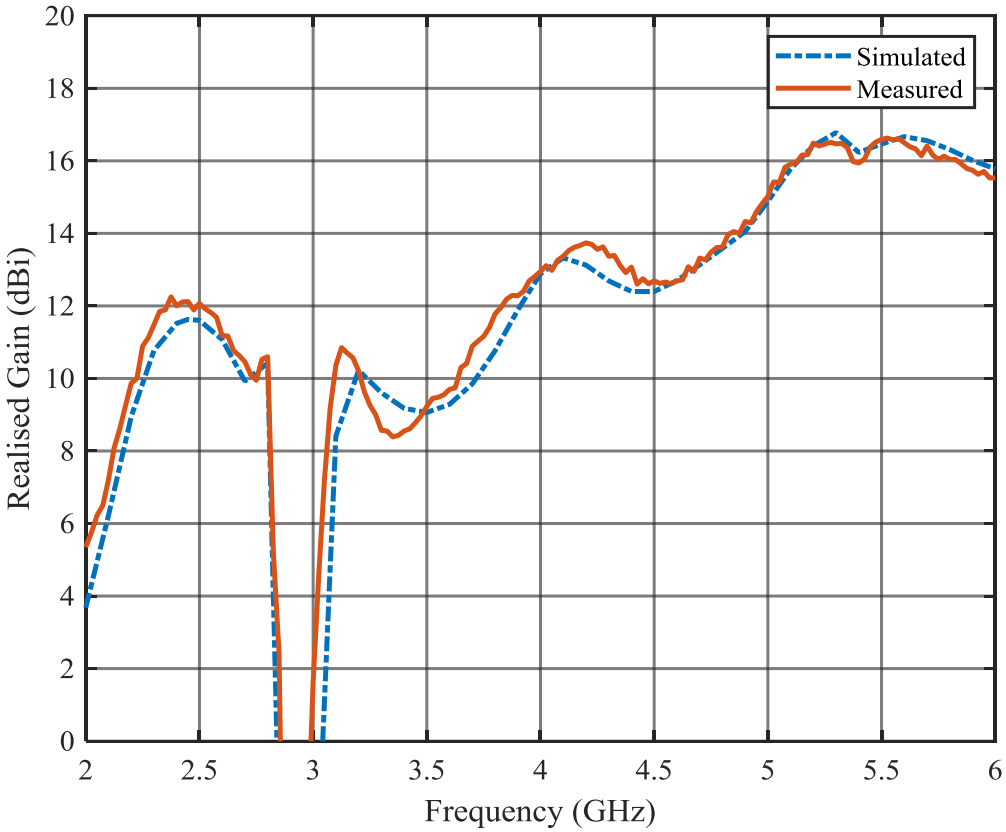

Figure 4.4. Simulated and measured boresight gain of the final design.

The maximum simulated gain in the 2.45 GHz band is 11.8 dBi, while the measured gain at 2.45 GHz is 12.1 dBi. The simulated gain at the high band is above 16 dBi over the specified high band. The maximum measured gain at the high band was at 5.5 GHz with a value of 16.6 dBi.

The simulated and measured antenna radiation patterns are presented in Figures 4.5 to 4.12. Figures 4.13 to 4.16 show both the measured co- and cross-polarisation radiation patterns.

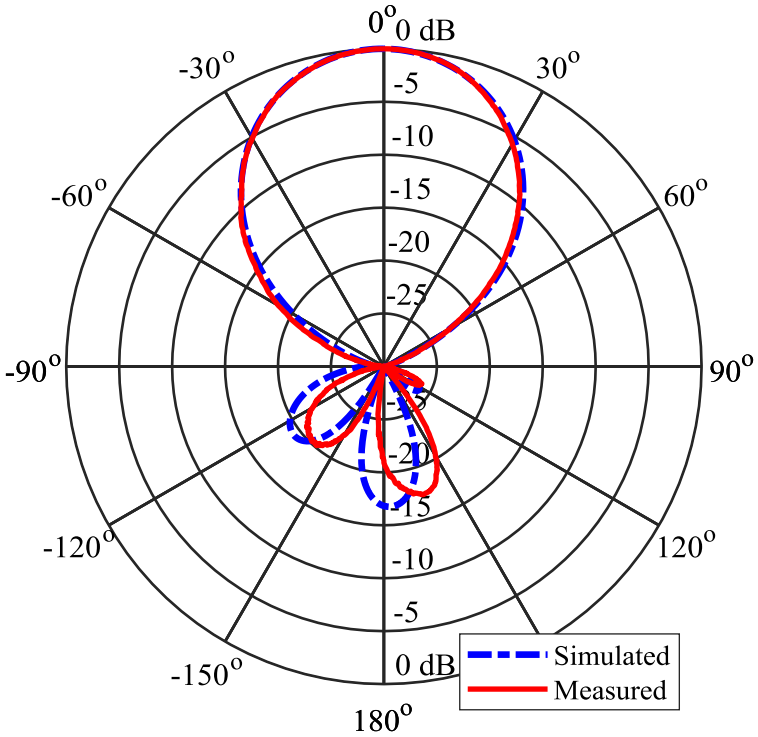

Figure 4.5. Simulated and measured *E*-plane pattern at 2.45 GHz.

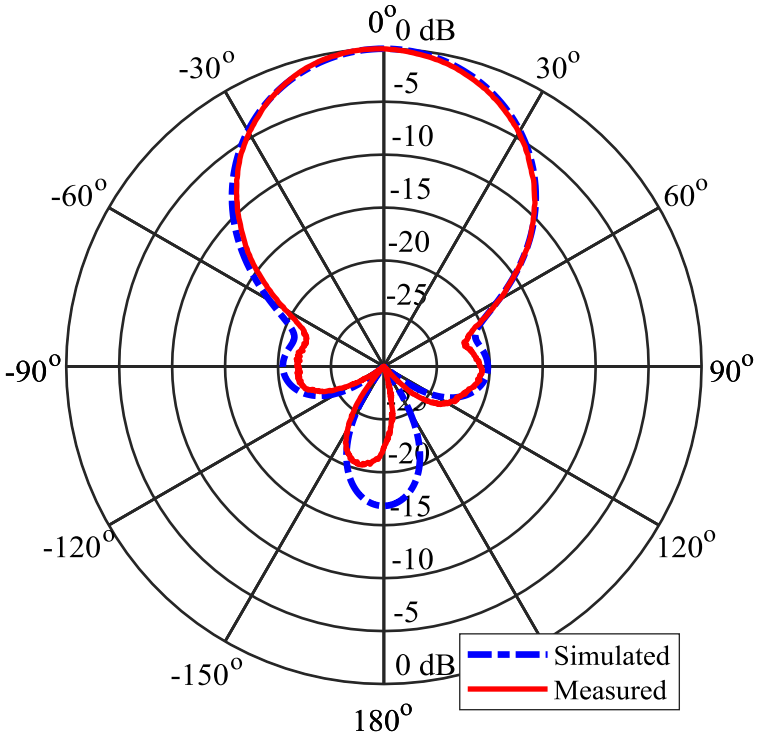

Figure 4.6. Simulated and measured *H*-plane pattern at 2.45 GHz.

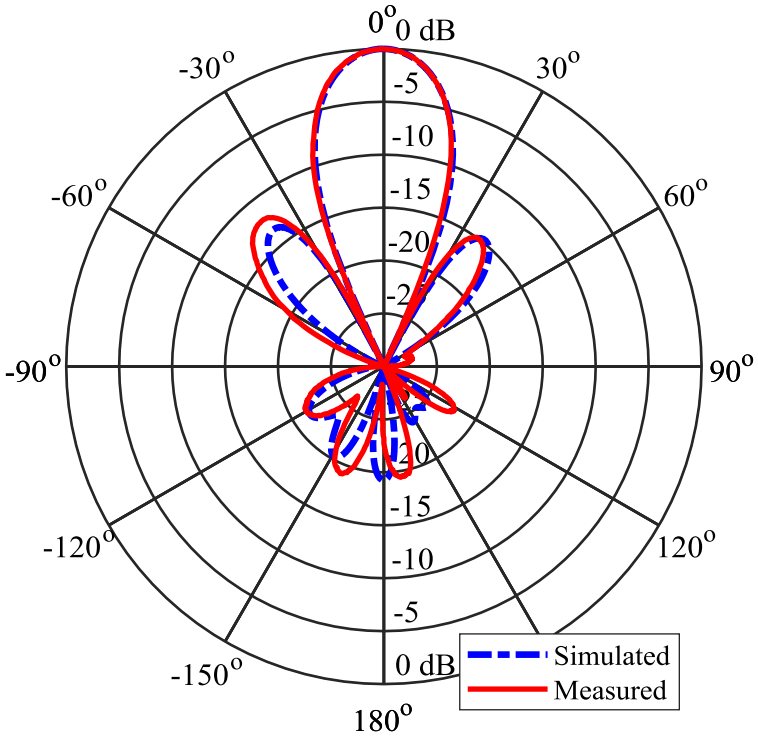

Figure 4.7. Simulated and measured *E*-plane pattern at 5.25 GHz.

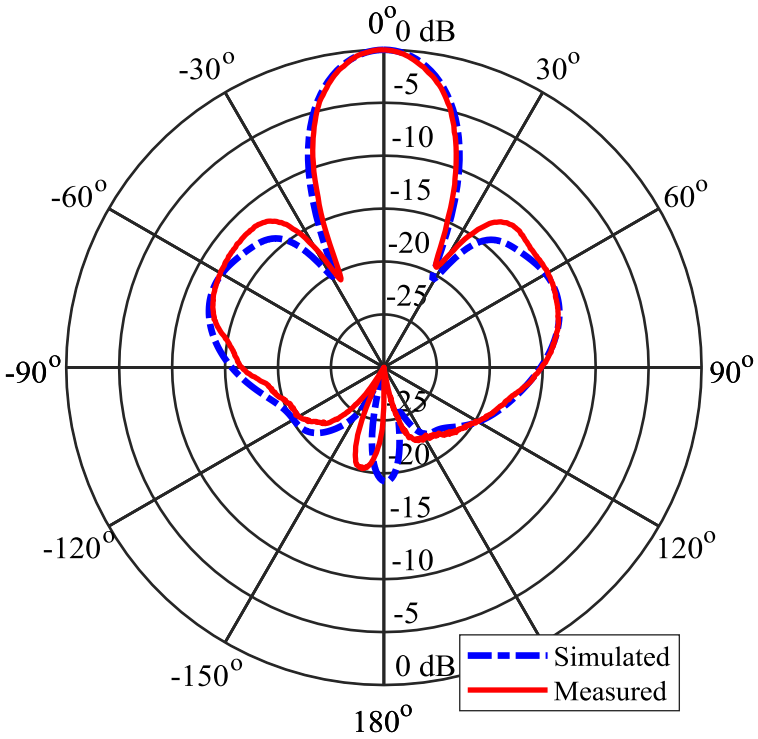

Figure 4.8. Simulated and measured *H*-plane pattern at 5.25 GHz.

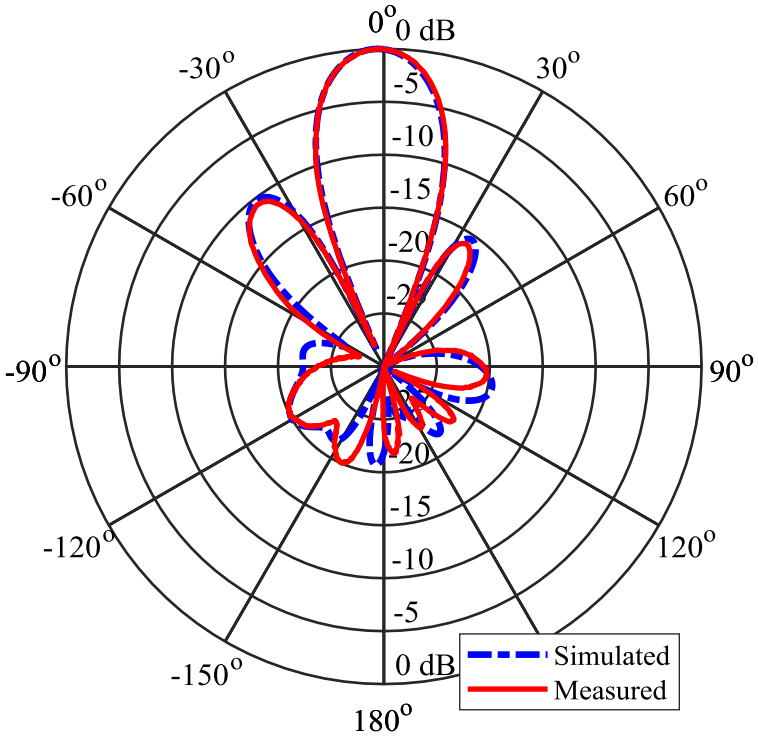

Figure 4.9. Simulated and measured *E*-plane pattern at 5.5 GHz.

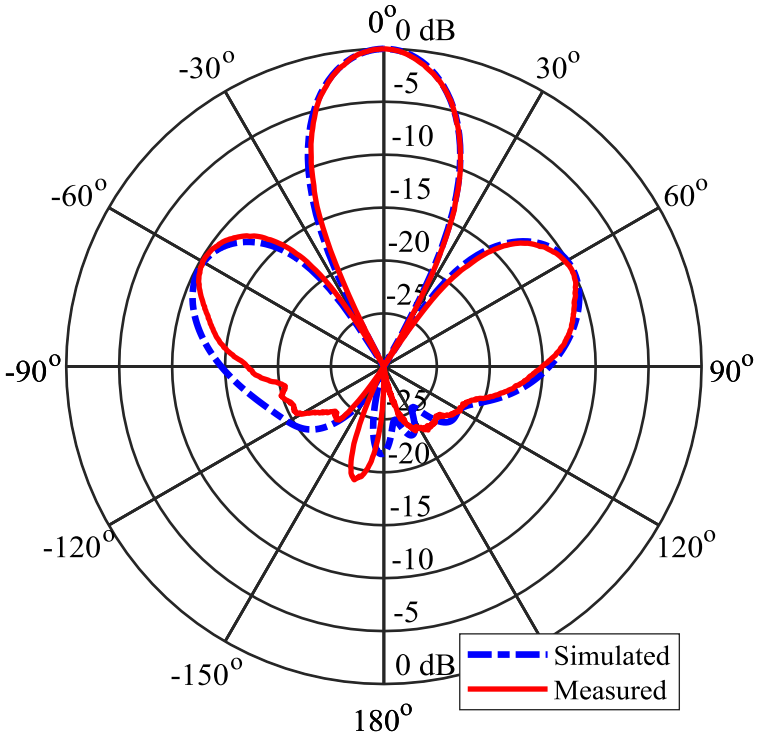

Figure 4.10. Simulated and measured *H*-plane pattern at 5.5 GHz.

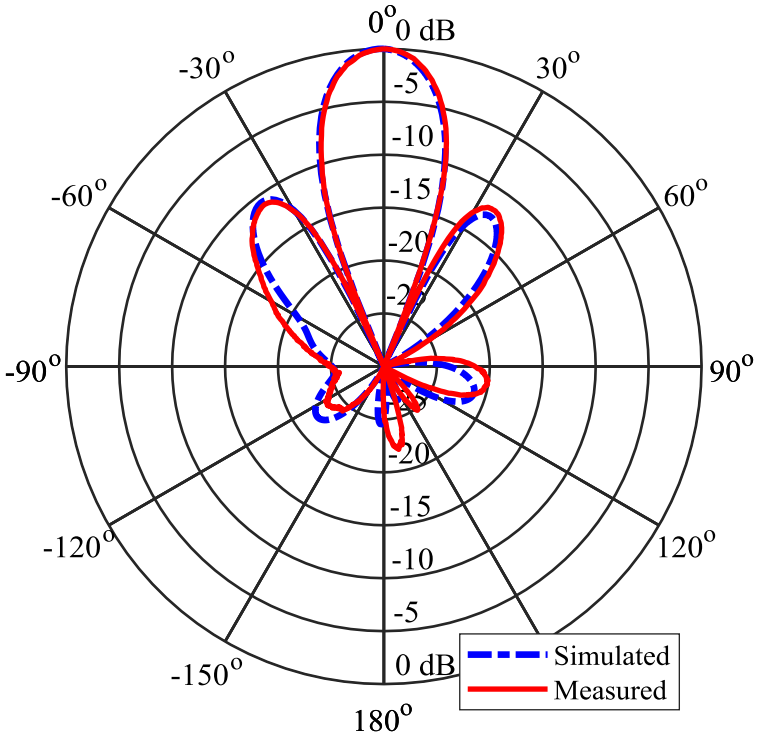

Figure 4.11. Simulated and measured *E*-plane pattern at 5.75 GHz.

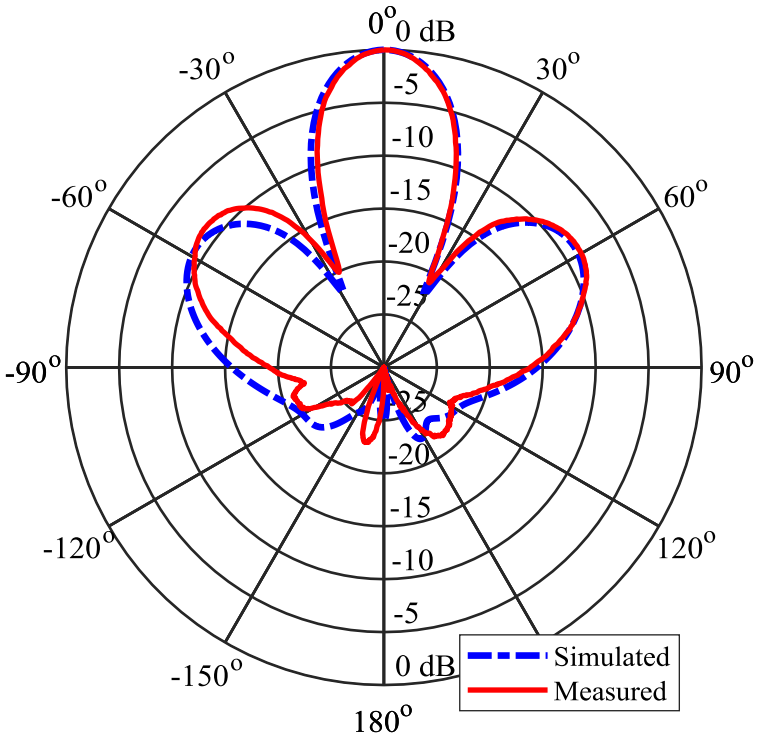

Figure 4.12. Simulated and measured *H*-plane pattern at 5.75 GHz.

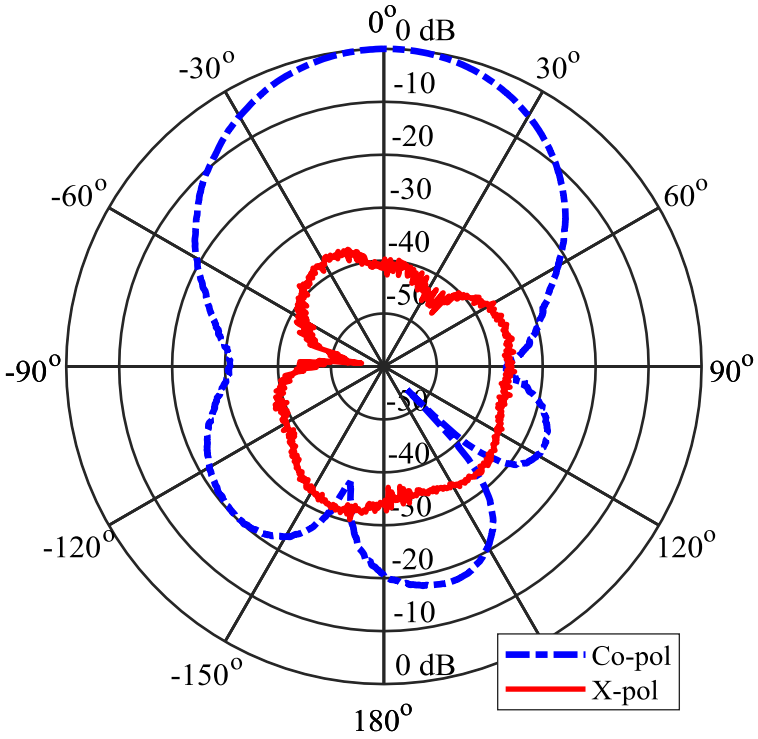

Figure 4.13. Measured co- and cross-polarisations of the low band in the *E*-plane.

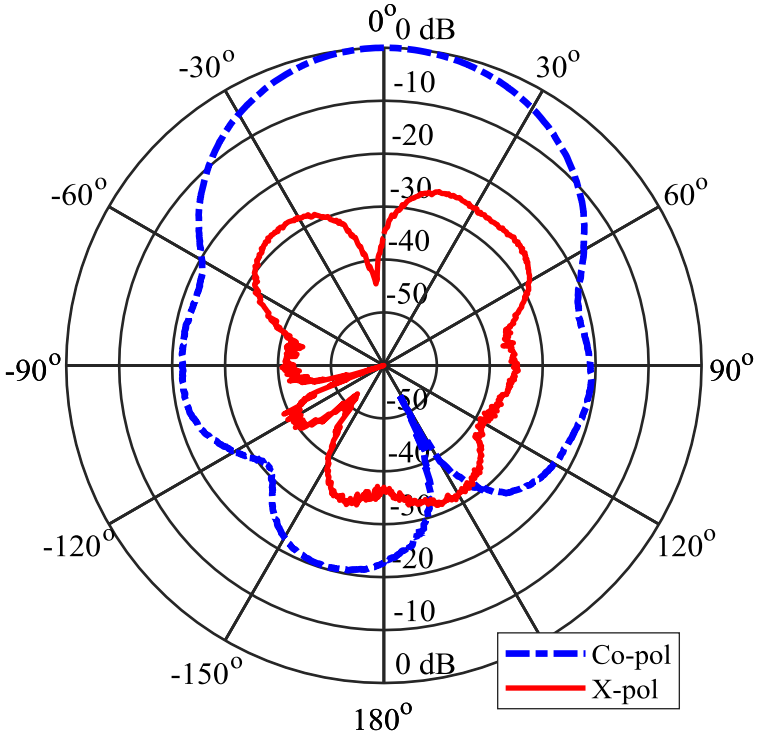

Figure 4.14. Measured co- and cross-polarisations of the low band in the *H*-plane.

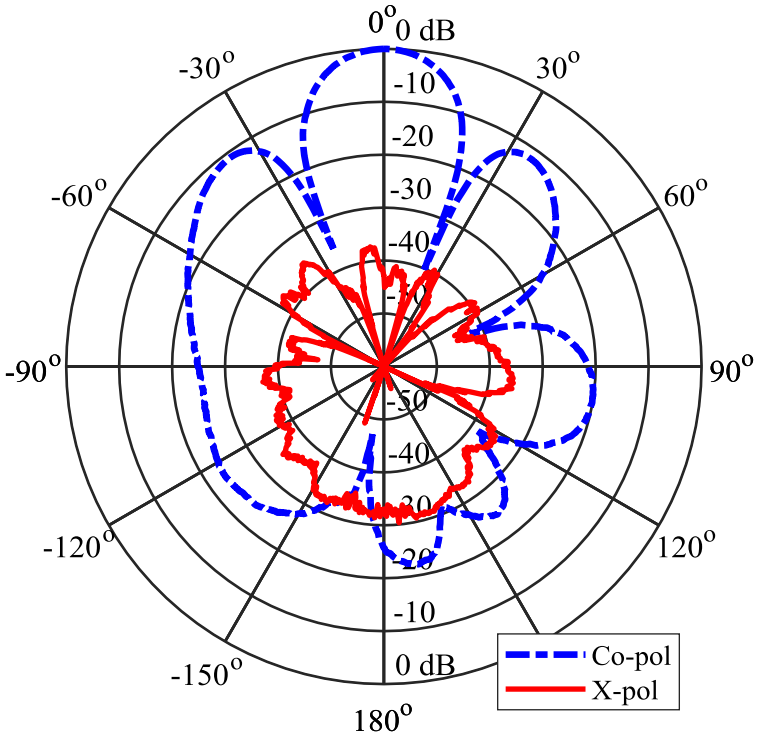

Figure 4.15. Measured co- and cross-polarisations of the high band in the *E*-plane.

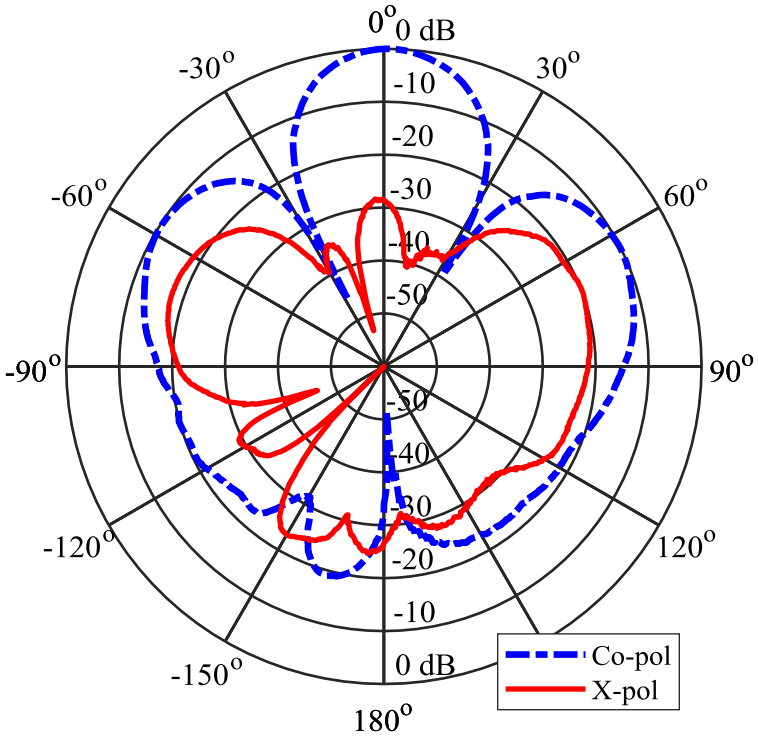

Figure 4.16. Measured co- and cross-polarisations of the high band in the *H*-plane.

The measured radiation patterns correspond well with the simulated radiation patterns of the final antenna array. The cross-polarisation level at boresight for the low and the high bands is more than 25 dB below the co-polarisation level.

4.3 SUMMARY

The measured reflection coefficient is below -10dB in both the low and high WLAN frequency bands and corresponds well with the simulated data.

The measured gain shows good correlation with the simulated gain at the two desired bandwidths. The gain dip between 2.8 GHz and 3.1 GHz is visible in both the simulated and the measured data. The gain dip may be caused by a mode that is excited in the frequency range from 2.8 GHz to 3.1 GHz. The correlation between the simulated and measured antenna radiation patterns is very good. The measured main lobe is identical in beamwidth and shape to the simulated main lobe. The measured levels and positions of the back and side lobes also correlate well with the simulated data. The measured polarisation purity is good with the cross-polarisation at least 25 dB below the co-polarisation at boresight in the two respective planes and frequency bands.

The antenna design is adequately verified by the experimental results. A compact, high gain, dual-band antenna array was successfully designed and manufactured for WLAN applications.

CHAPTER 5 CONCLUSION

A literature study was conducted to compare different dual-band antennas, which operate with a large frequency ratio between the bands, with respect to their radiation performance and size. The dual-band antenna from Quan et al. [18] was identified as an antenna with potential for further development to be suitable for WLAN communication applications where relatively high gain is required. The compact dual-band dipole configuration from Quan et al. [18] is a combination of single resonance elements and was used as the basic starting point to develop and design a high gain dual-band antenna array. A background study was also performed on the basic building blocks of the antenna from [18].

A parametric study of the antenna configuration in [18] was performed to obtain a better understanding of the various dimensional parameters of the antenna and what affect they have on the performance of the antenna. The insight gained from the parametric study was used to formulate a design approach which was illustrated with a design example. The antenna design from [18] was then modified to contain four high band elements and one low band element. The new sub-array element had improved gain in the high band as compared to [18], without really increasing the size of the antenna. Four of these sub-arrays were configured into a square 2 × 2 array with 4 low band elements and 16 high band elements. The array was fed with a microstrip line tapered corporate feed network. The design was optimised to achieve radiation bandwidths sufficient for WLAN applications. The antenna array design was verified by comparing the simulated results to measured results of an experimental antenna array that was manufactured. Radiation measurements were performed in a compact antenna range. The simulated and measured antenna performance was found to correlate well.

5.1 CONTRIBUTIONS

A compact, high gain, dual-band antenna array was successfully designed and manufactured for WLAN applications. A step by step design approach for dual-band printed dipole antennas with a large frequency ratio between the bands was also formulated and illustrated with an example. The measured dual-band antenna array performance is summarised in Table 5.1.

Table 5.1. Measured results of the compact high gain dual-band antenna.

	Low frequency band	High frequency band
Standard	IEEE 802.11b	IEEE 802.11a
Required bandwidth	2.4 – 2.484 GHz (3%)	5.15 – 5.85 GHz (13%)
Measured bandwidth	2.33 – 2.50 GHz (7%)	5.03 – 6 GHz (18%)
Gain	12.1 dBi	16.6 dBi
Side lobe level	20.7 dB	10.0 dB
Front to back lobe ratio	17.6 dB	19.5 dB
Half power beamwidth	51º	24º

The volume of the proposed antenna array is 128 × 128 × 12 = 196 608 mm^3, which is compact when compared to alternative antennas tabulated in Table 2.1. The gain of the antenna array is also large when compared to alternative antennas in Table 2.1. The proposed antenna is relatively easy to design and manufacture, and suitable for wall-mounted WLAN applications where high gain is a requirement.

5.2 FUTURE WORK

In future the gain of the dual-band array can be further increased by the addition of more elements to the array, which will then require a larger and possibly more complicated feed network. The number of elements can also be increased in one the planes, e.g. a 1 × 4

array, or in both planes, e.g. a 3 × 3 array. The sub-array element is suitable for both these expansion options.

The sub-array element can be configured to accommodate an additional frequency band to realise a tri-band antenna. This would be advantageous as the antenna would be able to also function within the WiMAX standards to increase the functionality of the antenna.

REFERENCES

[1] J. M. Steyn, J. Joubert and J. W. Odendaal, "A polarization diverse antenna for dual-band WLAN applications", *2009 European Microwave Conference (EuMC)*, Rome, 2009, pp. 540-543.

[2] S. Liu, S. S. Qi, W. Wu, and D. G. Fang, "Single-Layer Single-Patch Four-Band Asymmetrical U-Slot Patch Antenna", *IEEE Transaction on Antennas and Propagation*, vol. 62, no. 9, pp. 4895 – 4899, Sep. 2014.

[3] C. A Balanis, *Antenna theory analysis and design*, New York: John Wiley and Sons Inc, 1997.

[4] K. F. Lee, S. L. S. Yang, and A. A. Kishk, "Dual- and Multiband U-Slot Patch Antennas" *IEEE Antennas and Wireless Propagation Letters*, vol. 7, pp. 645 – 647, Jan. 2008.

[5] K. F. Lee, S. L. S. Yang, A. A. Kishk, and K. M. Luk, "The Versatile U-Slot Patch Antenna", *IEEE Antennas and Propagation Magazine*, vol. 52, no. 1, pp. 71 – 88, Feb. 2010.

[6] G. Mayhew-Ridgers, J. W. Odendaal, and J. Joubert, "Single-Layer Capacitive Feed for Wideband Probe-Fed Microstrip Antenna Elements", *IEEE Trans. Antennas and Propagation*, vol. 51, no. 6, pp. 1405 – 1407, Jun. 2003.

[7] L. Guo, Y. Wang, and Z. Du,"A Compact Uniplanar Printed Dual-Antenna Operating at the 2.4/5.2/5.8 GHz WLAN Bands for Laptop Computers", *IEEE Antennas and Wireless Propagation Letters*, vol. 13, pp. 229 – 232, Jan. 2014.

[8] S. Chebolu, S. Dey, R. Mittra and M. Itoh, "A dual-band stacked microstrip antenna array for mobile satellite applications,"*IEEE Antennas and Propagation Society International Symposium. 1995 Digest*, Newport Beach, CA, USA, 1995, pp. 598-601 vol.1.

[9] W. Ahmad and D. Budimir, "Dual-band WLAN antenna array with integrated bandpass filters for harmonic suppression,"*2015 IEEE International Symposium on Antennas and Propagation & USNC/URSI National Radio Science Meeting*, Vancouver, BC, 2015, pp. 619-620

[10] M. van Rooyen, J. W. Odendaal and J. Joubert, "High-Gain Directional Antenna for WLAN and WiMAX Applications," *IEEE Antennas and Wireless Propagation Letters*, vol. 16, pp. 286-289, 2017.

[11] W. Chen, J. Yin, J. Yang and M. Li, "A directional dual-band rectangular inverted-F antenna with Eleven slots for WLAN applications", *2015 IEEE 6th International Symposium on Microwave, Antenna, Propagation, and EMC Technologies (MAPE)*, Shanghai, 2015, pp. 107-110.

[12] L. M. Si, W. Zhu and H. J. Sun, "A Compact, Planar, and CPW-Fed Metamaterial-Inspired Dual-Band Antenna", in *IEEE Antennas and Wireless Propagation Letters*, vol. 12, pp. 305-308, 2013.

[13] R. S. Daniel, R. Pandeeswari and S. Deivalakshmi, "A CPW-fed dual band antenna based on metamaterial inspired split ring structure", *2017 IEEE 2nd International Conference on Signal and Image Processing (ICSIP)*, Singapore, 2017, pp. 437-440.

[14] S. K. Sharma, R. K. Chaudhary and C. W. Park, "A compact wideband concentric SRR-based metamaterial antenna with dual-band characteristics",*2016 URSI Asia-Pacific Radio Science Conference (URSI AP-RASC)*, Seoul, 2016, pp. 1223-1226.

[15] R. Jasmine Banu, R. Rajkumar, P. Thiruvalar Selvan and C. Elavarasi, "A compact CPW fed metamaterial staircase planar antenna", *2014 International Conference on Communication and Signal Processing*, Melmaruvathur, 2014, pp. 242-245.

[16] L. M. Si, Q. L. Zhang, W. D. Hu, W. H. Yu, Y. M. Wu, L. Xin and W. Zhu, "A Uniplanar Triple-Band Dipole Antenna Using Complementary Capacitively Loaded Loop", in *IEEE Antennas and Wireless Propagation Letters*, vol. 14, pp. 743-746, 2015.

[17] S. He and J. Xie, "Analysis and Design of a Novel Dual-Band Array Antenna with a Low Profile for 2400/5800-MHz WLAN Systems", in *IEEE Transactions on Antennas and Propagation*, vol. 58, no. 2, pp. 391-396, Feb. 2010.

[18] X. L. Quan, R. L. Li, Y. H. Cui, M. M. Tentzeris, “Analysis and design of a compact dual-band directional antenna”, *IEEE Antennas and wireless propagation letters*, vol. 11, pp. 547 – 550, 2012.

[19] K. D. Katore, M. B. Kadu, R. P. Labade and S. S. Dongare, "2.4/5.2 GHz dual band rectangular microstrip antenna with orthogonal polarization for bluetooth and WLAN applications," *2017 International Conference on Communication and Signal Processing (ICCSP)*, Chennai, 2017, pp. 2031-2035.

[20] F. T. Ulaby, E. Michielssen and U. Ravaioli, *Fundamentals of applied electromagnetic*, New Jersey: Pearson, 2010.

[21] S. Maci, G. B. Gentili, "Dual-Frequency Patch Antennas", *IEEE Antennas and Propagation Magazine*, vol. 39, no. 6, pp. 13 – 20, Dec. 1997.

[22] W. C. Mok, S. H. Wong, K. M. Luk and K. F. Lee, "Single-Layer Single-Patch Dual-Band and Triple-Band Patch Antennas," *in IEEE Transactions on Antennas and Propagation*, vol. 61, no. 8, pp. 4341-4344, Aug. 2013.

[23] J. Baviskar, A. Mulla, A. Baviskar, S. Kamat, Z. Z. Mulla and R. Waghmare, "Metamaterial lens incorporated dual band U-slot patch antenna for WLAN application", *2017 IEEE Aerospace Conference*, Big Sky, MT, 2017, pp. 1-8.

[24] T. Y. Liao, I. F. Chen, C. M. Peng and H. Cheng, "Dual-band patch antenna for WLAN applications",*2016 IEEE 5th Asia-Pacific Conference on Antennas and Propagation (APCAP)*, Kaohsiung, 2016, pp. 31-32.

[25] W. Ren, Z. G. Shi and K. S. Chen, "Compact dual-band slot antenna for WLAN applications", *2006 IET International Conference on Wireless, Mobile and Multimedia Networks*, hangzhou, China, 2006, pp. 1-4.

[26] T. Shanmuganantham, "CPW-fed Temple Tower Kalasam shaped monopole antenna for dual band applications", *2015 IEEE Applied Electromagnetics Conference (AEMC)*, Guwahati, 2015, pp. 1-2.

[27] H. Zhang, L. Chang, J. Zhang and Z. Chen, "Dual band directional bowtie antenna loaded with a square loop," *2016 11th International Symposium on Antennas, Propagation and EM Theory (ISAPE)*, Guilin, 2016, pp. 35-38.

[28] T. G. Vasiliadis, E. G. Vaitsopoulos, and G. D. Sergiadis, "A wideband printed dipole antenna with optimized tapered feeding balun for ISM and FWA bands*", Microwave and Optical Technology Letters*, vol. 48, no. 3, pp 444 – 449, Mar. 2006.

[29] G. A. Evtioushkine, J. W. Kim, K. S. Han, "Very wideband printed dipole antenna array", *Electronic letters*, vol. 34, no. 24, pp. 2292 – 2293, 1998.

[30] E. Levine, S. Shtrikman, D. Treves, “Double sided printed arrays with large bandwidth” *IEE Proceedings*, vol. 135, no. 1, pp. 54 – 59, 1988.

[31] T. A. Milligan, *Modern antenna design*. Hoboken, N.J.: IEEE Press, 2005, pp. 102-135, 223-231.

[32] E. Mariani, C. Heinzman, J. Agrios and S. Cohn, 'Slot Line Characteristics', *IEEE Transactions on Microwave Theory and Techniques*, vol. 17, no. 12, pp. 1091-1096, 1969.

[33] Cohn, 'Slot Line on a Dielectric Substrate', *IEEE Transactions on Microwave Theory and Techniques*, vol. 17, no. 10, pp. 768-778, 1969.

[34] Yong Seok, S. (1990). Comparison of slot line characteristics. Masters Thesis. Monterey, California.

[35] B. Shuppert, "Microstrip/slotline transitions: modeling and experimental investigation," *in IEEE Transactions on Microwave Theory and Techniques*, vol. 36, no. 8, pp. 1272-1282, Aug. 1988.

[36] "*CST MICROWAVE STUDIO 3D EM Simulation Software* [Online]", Cst.com, 2018. [Online]. Available: https://www.cst.com/products/cstmws. [Accessed: 07- Oct- 2018].

[37] "*Electromagnetic Simulation Software | Altair FEKO* [Online]", Altairhyperworks.com, 2018. [Online]. Available: https://altairhyperworks.com/product/FEKO. [Accessed: 07- Oct- 2018].